Order Number 9209700

Simulation of the recurrence probability of ice islands in the Arctic Ocean

Li, Fu-cheng, Ph.D.

University of Alaska Fairbanks, 1991

U·M·I
300 N. Zeeb Rd.
Ann Arbor, MI 48106

SIMULATION OF THE RECURRENCE PROBABILITY OF ICE ISLANDS IN THE ARCTIC OCEAN

A

THESIS

Presented to the Faculty of the University of Alaska Fairbanks

in Partial Fulfillment of the Requirements

for the Degree of

DOCTOR OF PHILOSOPHY

By

Fu-cheng Li, M.S.

Fairbanks, Alaska

May 1991

SIMULATION OF THE RECURRENCE PROBABILITY OF ICE ISLANDS IN THE ARCTIC OCEAN

by

Fu-Cheng Li

RECOMMENDED:

Chairman, Advisory Committee.

Dept. Head, Geology and Geophysics

APPROVED:

Dean, College of Natural Sciences

Dean, The Graduate School

5/1/91

Date

ABSTRACT

Ice islands, the most extreme ice features in the Arctic Ocean, are hazards to offshore structures. To determine the probability of ice island trajectories in coastal areas of the Arctic Ocean, a random simulation model has been established. The model consists of the random ice island generation, the ice island dynamic model, and the Monte Carlo model for random geostrophic wind generation.

Based on statistics of observation data, the generation location was assumed as uniformly distributed along the northern side of Ellesmere Island from Clements Markham Inlet west to the mouth of Nansen Sound. Channel. A 4 year interval of generation event is considered in the simulation. The number of new ice islands calved from ice shelves in one calving event is automatically produced by deducting each ice island area from the random area of ice shelf calved in one time. The ice island area is calculated with length and length-width ratio which are randomly generated from their distributions.

As a driving force source, geostrophic wind field was calculated from monthly-averaged pressure charts. Water form drag and pack ice force were considered in the dynamic equation of an ice island. Comparison showed that the water form drag is greater than the water skin friction. As a significant force, the pack ice force was formulated by theoretical analysis combined with an existing empirical formula for each case.

The results of probabilities of simulated ice island trajectories show that there are two zones of highest recurrence of ice islands, one near the Canadian Beaufort Sea, and another near the Chukchi Sea. There is a broad area of 1 to 10 year recurrence interval in the central ocean, and a high probability zone near the north end of Greenland. The simulation also yielded the frequencies of ice island ejection, the lifetime of ice islands, and the number of live ice islands in the Arctic Ocean. Two basic drift patterns of ice islands have been displayed by the simulation: short drift patterns in which ice islands move directly out of the ocean after generation, and the large-scale circulation pattern in which ice islands circulate around the Beaufort Sea from one to four times.

TO

MY PARENTS

TABLE OF CONTENTS

LIST OF FIGURES

LIST OF TABLES

ACKNOWLEDGEMENTS

I would like to express my sincere appreciation to Dr. William M. Sackinger, my advisor and chairman of the thesis advisory committee, for his advice, encouragement and support. My special thanks to the advisory committee members, Dr. Lewis H. Shapiro, Dr. David C. Fritts, Dr. John J. Kelley and Dr. Gary A. Gislason, for their advice and encouragement. I offer my sincere thanks to Dr. Martin O. Jeffries for his valuable comments and suggestions concerning the ice island generation and drift, and for his drawing of computer program flow charts on the Macintosh. The suggestions and information including the arctic pressure charts from Dr. Wilford F. Weeks are gratefully acknowledged. Thanks are given to Dr. R. Colony, for his permission to use the sea level pressure charts over the Arctic Ocean.

To the memory of my father, and to my mother, to whom this thesis is dedicated, my heartfelt thanks are given for a lifetime of love and support. To my family and friends, thanks are given for their encouragement and support throughout my Ph.D. study. A special thanks is reserved for my wife, Hong, for her constant patient help and understanding during this study.

Thanks are also given to the staff of the Geophysical Institute, University of Alaska Fairbanks, for their kind assistance.

The research described herein was funded by the U.S. Department of Energy, and the Geophysical Institute, University of Alaska Fairbanks, which was gratefully appreciated.

CHAPTER 1

INTRODUCTION

1.1 Topography Features of Ice Islands

The tabular icebergs of the Arctic Ocean are termed "ice islands", and they are the most massive ice features that have been discovered in the Arctic Ocean. These ice features are normally characterized by a large surface area and often by a deep keel depth. Their dimensions range from a few meters across to several kilometers long and wide, and as much as 50 meters thick. The largest ice island presently known to exist in the Arctic Ocean, Hobson's Choice Ice Island, had a mass of approximately 700×10^6 tonnes, an area of about $26km^2$ and a mean thickness of 42.5 meters over 64% of its area during its early drift period (Jeffries et al., 1988).

Significant topographic features of ice islands are the undulating ridges and troughs of the upper surface, which are commonly referred to as "rolls", which develop on the parent ice shelves (Hattersley-Smith, 1957). Several ice shelves of this kind are located on the north coast of Ellesmere Island. The rolls offer a good way to identify an ice island visually, particularly in the summer when the depressions contain meltwater lakes. Some such lakes have been observed to drain catastrophically over the edge of the ice island, leaving relatively dry depressions, each with an irregular topography (M. Schmidt, unpublished data, 1988). On Hobson's Choice Ice Island, for example, the undulating ridges extend for thousands of meters, and are spaced about 200 meters apart (a mean value); the relative relief from ridge to trough-bottom is 1 to 2 meters (Figure 1) (Jeffries and Sackinger, 1990).

Figure 1: Oblique aerial photograph of Hobson's Choice Ice Island, August 11, 1987. Numbered features are (1) the main shelf ice section, (2) multiyear landfast sea ice previously attached to the front of the Ward Hunt Ice Shelf, and (3) multiyear pack ice that has become attached to the ice island since it calved. (Photo credit: Michael Schmidt, Geological Survey of Canada) (source: Jeffries and Sackinger, 1990).

The shape of ice islands is generally long and thin, and more angular than the surrouding pack ice floes. In both visible band and active microwave imagery, the surface of the pack ice looks rougher because of deformation and ridge building of the pack ice. These topographic features allow one to distinguish Arctic ice islands from large sea ice floes, especially when searching for ice islands over a large scale area by remote-sensing techniques (Jeffries and Sackinger, 1990).

1.2 Historical Background of Ice Islands

By distinguishing the topographic features, possible drifting ice islands were noted early in 1886 by Greely, in 1918 by Storkerson, and by other early explorers as well (Peary, 1907; Stefansson, 1922; Zubov, 1945). A thorough search of aerial photos by Greenaway in 1952 yielded 59 possible ice islands at that time, as well as many more small fragments (Greenaway, 1952).

In 1946, an ice island measuring approximately $28 \times 33km$ was discovered on a U.S. Air Force reconnaissance flight less than $556km$ north of Point Barrow, and was designated "Target X" or "T-1". From 1946 to 1949, T-1 travelled over $2600km$ across the Arctic Ocean towards Ellesmere Island and Greenland before it moved farther from the reconnaissance routine flight paths (Koenig et al., 1952). In 1950, during a thorough search for ice islands north of Alaska by the U.S. Air Force, T-2, measuring $31 \times 33km$, was discovered at $86°40'N$, $167°00'W$. The ice island T-3 was discovered in 1950 at $75°24'N$, $173°00'W$, and was estimated to be $8 \times 17km$ (Koenig et al, 1952). It was used as a research camp base for many scientific studies of the ice island itself, and of the Arctic Ocean generally, from 1952 until the late 1970's. It travelled in the Arctic Ocean for at least 35 years, completing at least 3 circuits of the Beaufort Gyre from 1950 to 1979. By 1983-84, it was drifting out of the Arctic

Ocean via the Trans-Polar Drift Stream and was sighted twice near the southern tip of Greenland in summer 1984 (Sackinger et al., 1990). In 1961, ice island Arlis II was sighted at $73°N$, $156°W$; it was approximately $3 \times 6km$ in size with a thickness of 12 to 25 meters (LeSchack, 1961; Smith, 1964).

In early 1962, a massive calving event from the Ward Hunt Ice Shelf off the north coast of Ellesmere Island was discovered. Five large ice islands (WH-1, WH-2, WH-3, WH-4, WH-5) and 14 smaller fragments were created (Hattersley-Smith, 1963). This particular calving event may have been related to abnormal tidal excursions and a small seismic event (Holdsworth, 1971) but detailed mechanisms of calving remain unclear.

From 1972 to 1976, a five-year program of the A.P.O.A. (Arctic Petroleum Operator's Association) was conducted to record the number and size of ice islands in the southern Beaufort Sea. By using reconnaissance flights, a total of 433 ice islands or ice island fragments were observed in 1972. Most of them were between 30 meters and 76 meters in maximum dimension. The largest ice island was about 1.6 km long. In 1973, a total number of 299 was observed and the sizes were smaller than those observed during the 1972 flights. From 1974 to 1976, the total number of ice islands counted decreased from 27 to zero (Spedding, 1977).

In April 1974, scientists involved in the Arctic Ice Dynamics Joint Experiment (AIDJEX) reported an ice island located about 160 km north of the MacKenzie River delta in the southern Beaufort Sea (Martin and Thorndike, 1974). This ice island was 7 km long and 3 km wide with a thickness of about 9 meters.

A recent, substantial calving of ice islands occurred in 1982-83, when at least eight ice islands were produced from the Ward Hunt Ice Shelf (Jeffries and Serson,

1983). Since then, an additional 26 ice islands have been observed in the pack ice near the northern coasts of Ellesmere and Axel Heiberg Islands (Jeffries et al., 1988). Some of those produced at the Ward Hunt Ice Shelf in 1982-83 were named, and were instrumented and tracked on a daily basis using both the system Argos buoys/beacons and satellite navigation systems (Yan, 1986; Lu, 1988)

The largest ice island of the cluster, Hobson's Choice Ice Island, originally had an area of about $26km^2$ and a mean thickness of 42.5 meters over 64% of its area. It comprised two ice components: 1) shelf ice with a mean thickness of 42.5 meters; 2) multiyear landfast sea ice, believed to be as much as 10 meters thick in places, which was attached to the ice shelf at the time of calving and which has since remained attached to the shelf ice component (Jeffries et al., 1988). Since the time of the calving and during the drift parallel to the northernmost coasts of Ellesmere Island and Axel Heiberg Island, newly-formed multiyear pack ice presumed to be 5 to 6 meters thick has become attached to Hobson's Choice Ice Island (Jeffries and Sackinger, 1989). The Hobson's Choice Ice Island has been the major research object since the calving. An Argos satellite beacon was first placed on the ice island in August 1983 and a permanent field station of the Polar Continental Shelf Project (PCSP) was established in autumn 1984 (Hobson, 1989). This ice island was tracked on a daily basis using the System Argos buoys until 1989. A substantial amount of hourly data has been obtained from these stations including ice island position (latitude, longitude), surface air pressure variations, and surface air temperatures, which may be useful in future studies; it is archived at the Geophysical Institute, University of Alaska Fairbanks.

1.3 Characteristics of Ice Island Movements

There are few records of ice island paths available at the present time. Based on these data, one can infer that an ice island may start to drift in either of two general directions after its creation by calving from the ice shelves of north Ellesmere Island. One direction is towards the east, e.g. ice island WH-5 drifted to the east shortly after its creation in 1961-62 from the Ward Hunt Shelf (Hattersley-Smith, 1963; Nutt, 1966). Another is towards the southwest, the direction in which most ice islands have been observed to start to move. Often, early in their path in this direction, ice islands drift along the edge of the Canadian Arctic Islands and have been observed along the coast of the Beaufort Sea (Spedding, 1977). Some may enter the channels between the Queen Elizabeth Islands (Greenaway, 1952). For example, Hobson's Choice Ice Island began drift from Ward Hunt Ice Shelf in 1982-83. It drifted towards the southwest along the northern edges of Ellesmere Island, Axel Heiberg Island and Meighen Island, entered the Peary Channel between Meighen Island and Ellef Ringnes Island in summer 1989, and it has since remained locked in fast-ice there.

Most ice islands, however, historically have been carried into the Beaufort Gyre (the clockwise circulation system of the pack ice in the Beaufort Sea). Once they enter the Beaufort Gyre, ice islands then experience two major drift systems in the Arctic Ocean : 1) the Beaufort Gyre in which ice islands can drift for many years around the ocean, and, 2) the adjacent Trans-Polar drift by which many ice islands drift out of the ocean into the Greenland Sea. In the latter case, they then move around the southern tip of Greenland and disappear in the warmer waters of the Labrador Sea (Figure 2).

Figure 2: Scheme of Beaufort Gyre and Trans-Polar drift systems (from Thorndike, 1986).

In the Beaufort Gyre system, when ice islands reach the region near the North Pole, there is a probability that the ice islands join the Trans-Polar drift system, an average drift of sea ice towards the Fram Strait. If the ice islands are subject to one of several possible sequences of wind conditions near the pole (as yet to be determined) they rejoin the mass of low-average-drift-velocity multi-year ice north of Ellesmere Island, and begin another circuit of the Beaufort Gyre. From Figure 3, one can see that the ice island Arlis II experienced the Trans-Polar drift system and was ejected into the North Atlantic. The ice island T-3 executed at least three circuits of the Beaufort Gyre from 1950 until 1979 and was finally ejected into the Greenland Sea in June 1984.

Ice islands also become grounded in the coastal waters of the Beaufort and Chukchi Seas. The industry study reported by Spedding (1977) found 433 such fragments in 1972, 299 fragments in 1973, and 27 ice island fragments in 1974. Ice island fragments have also been observed in the channels between the Queen Elizabeth Islands. Meanwhile, a quite opposite phenomenon has been observed, i.e., multiyear pack ice has become attached to ice islands after they calved from ice shelves, thereby increasing their size. In the case of Hobson's Choice Ice Island, the addtion of multiyear pack ice has increased the ice island area by almost 30% to $34km^2$ and the mass by 6% to $7.4 \times 10^{11}kg$ (Jeffries and Sackinger, 1989). As long as both the multiyear pack ice (MYPI) and multiyear land-fast sea ice (MLSI) remain attached to the ice-island shelf ice component, they can be considered as integral parts of the ice island (Jeffries and Sackinger, 1989).

Ice islands can escape from the Arctic Ocean by a number of different routes. According to the observations, the most common routes are 1) the Trans-Polar drift which carries the ice islands past the east coast of Greenland, 2) the Archipelago

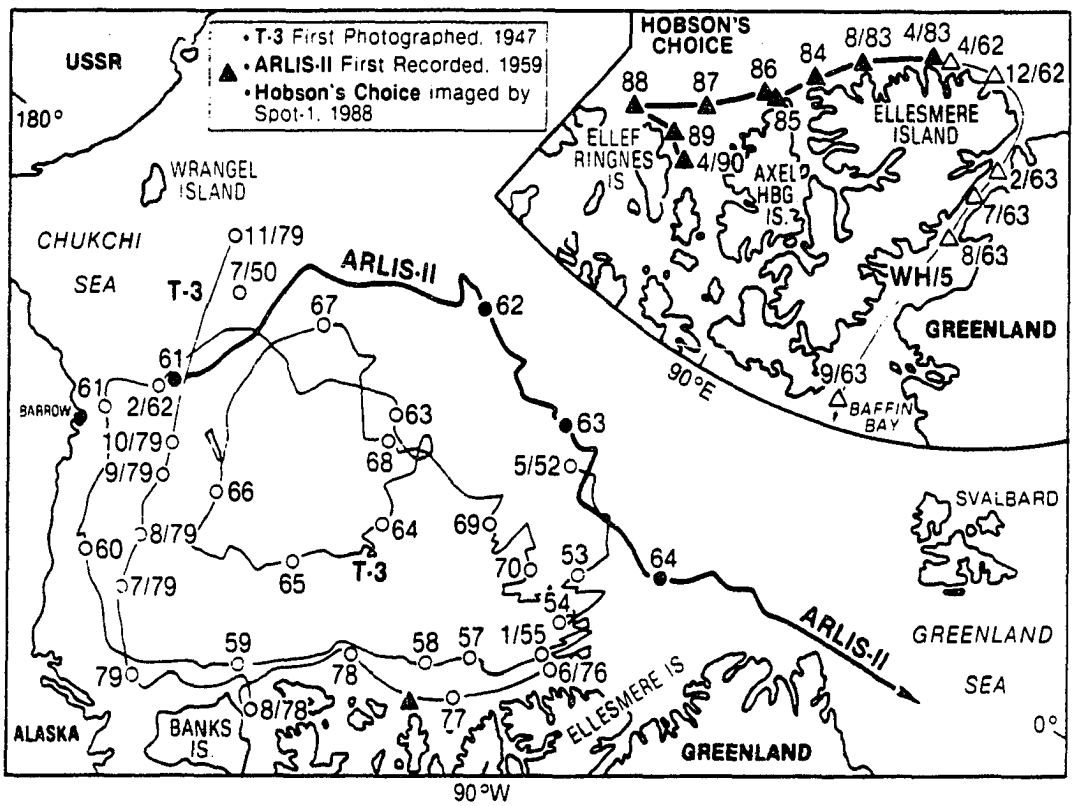

Figure 3: Drift records of Arlis II and T-3 ice islands. o66 – Location in the year of 1966. ▲88 – Location in the year of 1988. △12/62 – Location in December, 1962. (source: Sackinger et al., 1990).

escape route where the ice island passes through one of the straits between the Queen Elizabeth Islands, and 3) the Robeson Channel exit where the ice island drifts between Ellesmere Island and Western Greenland, into Baffin Bay.

1.4 Research Emphases

These massive ice features, ice islands, drifting in open water or within the pack ice zones with appreciable longevity, may approach the sites where offshore oil platforms or vessels are in operation in the Beaufort and Chukchi Seas, and in the Canadian Arctic Archipelago. With regard to the design of such installations, it is important to estimate the risk of ice island interaction with offshore structures or stationary vessels.

One important objective in quantitative estimates of the risk to offshore structures is to determine the recurrence interval for ice islands in a given area in the Arctic Ocean. The recurrence intervals are dependent upon the probability of ice island trajectories, as well as upon the rate of ice island generation, the probability of natural fragmentation of ice islands, and upon the ice island dimensions.

One may directly observe the statistics of ice island trajectories. Although many ice islands have been found during the past four decades, the search and subsequent tracking has not been systematic , and even the total number and location of ice islands presently in the Beaufort Gyre alone is not known. Thus, this approach is constrained because of the very limited data at the present time. Many years are needed to gather such data. De Paoli et al. (1982) presented an analysis of interaction probabilities between large ice features and offshore structures in the Canadian Beaufort Sea. The basic assumption was made that the Beaufort Gyre is that mecha-

nism whereby large ice features (ice islands and multi-year hummock fields) drift into the Southern Beaufort Sea, i.e., the large ice features are transported by multi-year ice into the Southern Beaufort Sea. Furthermore, he considered that the probability of large ice features entering an area of concern is the same as the probability of multi-year ice intrusion. He then calculated the probability of multi-year ice (for an averaged concentration of 5%) entering the area of concern based on the statistical data of multi-year ice. De Paoli et al. (1982) also calculated the probabilities of pack ice edge intrusion and the intrusion of the edge of 1/10 concentration of multi-year ice in summer, and took these as the probabilities of intrusion of large ice features, to compare with the probabilities of an average concentration of 5% of multi-year ice. In fact, as shown by Lu (1988), the ice islands move in a different trajectory pattern from that for pack ice or multi-year ice. Therefore, the assumption of application of multi-year ice statistics of occurrence to ice islands has a poor underlying foundation.

De Paoli's study also was only focussed on areas of the Canadian Beaufort Sea, and the probability of ice island trajectories in the Alaskan Beaufort Sea and the Chukchi Sea still remained unstudied. To understand the recurrence probability of ice island trajectories over a wide area in the Arctic Ocean, one has to search for a method in which one can overcome the limitation of observed data on ice island trajectories and obtain the recurrence probability of ice island trajectories.

An alternative approach to analyse the probability of ice island trajectories is a computer simulation by the Monte Carlo method. This approach needs to make use of a dynamic model of ice island movement, and the statistical distributions of related driving forces, ice island generation and the natural fragmentation of ice islands. To the author's knowledge, the present study is the first published attempt to use such an approach in the study of long-term recurrence probability of ice islands in the

Arctic Ocean.

As for the dynamics of ice island movement, the most detailed study has taken place only since 1983. Worthy of mention, however, is the analysis of some aspects of the drift of ice island T-3 (Browne and Crary, 1958; Hunkins, 1967) between 1952 and 1963. Since April 1985 several satellite positioning buoys have been deployed on a number of different ice islands, which have delivered data by both the Argos system and satellite navigation systems (Sackinger et al., 1990). These data provide a basis for the dynamic analysis of ice island movement. A comprehensive work by Yan (1986) gave details of three types of ice island movement for the period 1983-85. The first type is the large movement (10 km/day typically) in the southwest direction along the coastline; the second one is medium movements (1 - 10 km/day) in two sequentially opposite directions along the coastline; and the third is small (< 1 km/day) random movements in any direction, which may have been random fluctuations in the Argos positioning system as well as possible small tidally-driven movements. Yan indicated that the speed ratio between Hobson's Choice Ice Island and the geostrophic wind ranged from 1.0% to 1.5% for large movements, and the average angle of the geostrophic wind ranged from 20 to 26 degrees counterclockwise from the ice island motion direction. More detailed analysis of ice island movement (Lu, 1988) has resulted in more accurate relationships between ice island movement, surface wind velocities and geostrophic wind velocities, and evidence of a mountain barrier effect. A relationship between residual force and the speed of Hobson's Choice Ice Island was also obtained.

Regarding the generation of ice islands, several ice shelf calving events have occured at the Ward Hunt Ice Shelf on the north coast of Ellesmere Island (Hattersley-Smith, 1963; Jeffries and Serson, 1983). A report (Sackinger et al., 1985) of ice island

generation rate gave a statistical review of calving area of the ice shelves and the calving event time intervals. A statistical analysis of ice island dimensions was presented by Jeffries et al. (1988). All of this provides a good basis for understanding the statistical distributions of ice island generation.

Because of meteorological studies which have investigated the Arctic, there are sources of information available which enable one to make reasonable assumptions on the statistical characteristics of the wind field in the Arctic Ocean. The wind force is commonly considered as the dominant driving force on an ice island, and realistic winds should be used. Moreover, it has not been observed that ice islands break into fragments as they circulate in the Arctic Ocean. The observed ice island fragmentation events have occurred only in shallow water areas after the ice islands have become grounded. Ice islands T-3 and WH-4, for example, grounded a short distance north of Pt. Barrow, Alaska and disintegrated into several smaller pieces (Spedding, 1977). The sizes of most of these pieces were less than 1 km. Considering the many uncertainties on ice island fragmentation, and particularly the small sizes of ice island fragments, relative to ice island sizes, the decision was made to neglect the fragmenting of drifting ice islands.

The basic factors affecting the probability of ice island occurrence in an area of interest, considered in this study, are ice island generation and ice island movement. The spatial and temporal distributions of ice shelf calving events are to be explained. Thereafter, the methods for generating random ice island dimensions and the numbers of random ice islands existing in the Arctic Ocean are illustrated. An explanation will be given of the governing equation of ice island movement, involving wind driving force, comparision of water form drag and ice island bottom frictional drag, and extension of Lu's (1988) empirical formula for pack ice force calculation.

The development of a Monte Carlo model for generating random geostrophic wind will be explained, as will the domain, mesh and flow chart of the computer simulation. Simulation results and comparisions are then illustrated, and conclusions and recommendations given.

CHAPTER 2

RANDOM ICE ISLAND GENERATION

One important factor affecting the probability of ice island occurrences is the population statistics of ice islands in the Arctic Ocean. The population is directly related to ice island calving or generation rates. The generation in this study includes the spatial and temporal distribution of ice island generation, the ice island dimensions, and appropriately-generated numbers of ice islands.

2.1 Spatial and Temporal Probability Distributions

Because ice islands are generated by calving from the ice shelves, the spatial and temporal distributions of probability for such ice island generation are equivalent to that for the calving event of ice shelves, which can be quantified by historical statistics, assuming a time-invariant statistical process. Considering that the main purpose of this study was to provide a reference for Arctic Ocean oil development, in which the design of structures is usually for withstanding natural hazards with recurrence intervals of one hundred years, this assumption is acceptable. Thus, long term global change and possible depletions of ice-shelf ice are neglected. Many observations on ice shelf calving have been made, and many ice islands related to ice shelf calving have been observed and recorded since the early 1940's (Sackinger et al., 1985). A thorough review of this, especially on the systematic traverses of the ice shelves for the past two decades, (Sackinger et al., 1985) have revealed that calving events occur at ice shelves along the northern coast of Ellesmere Island, from Clements Markham Inlet west to the mouth of Nansen Sound (Figure 4 and 5).

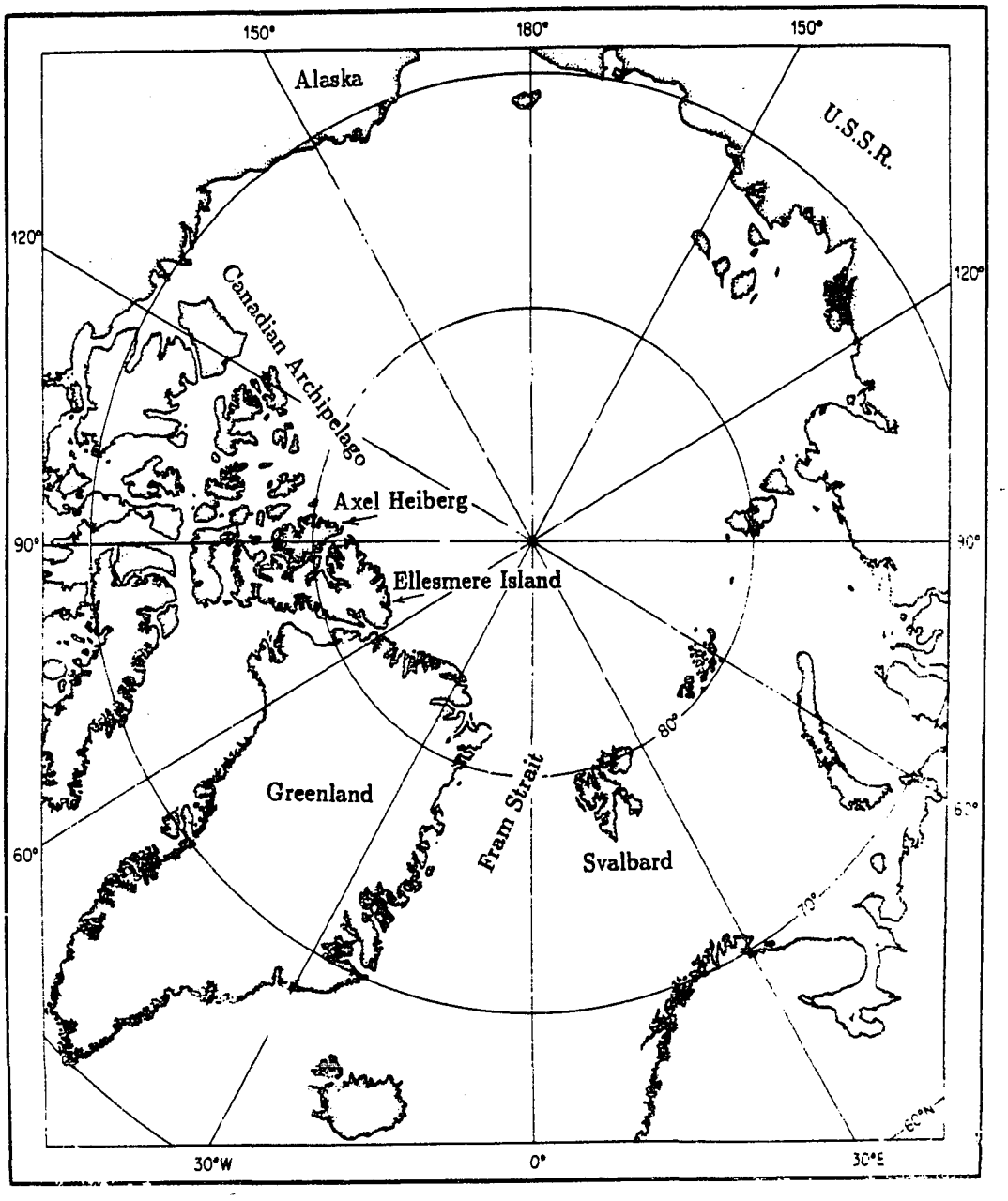

Figure 4: Ellesmere Island location in the Arctic Ocean.

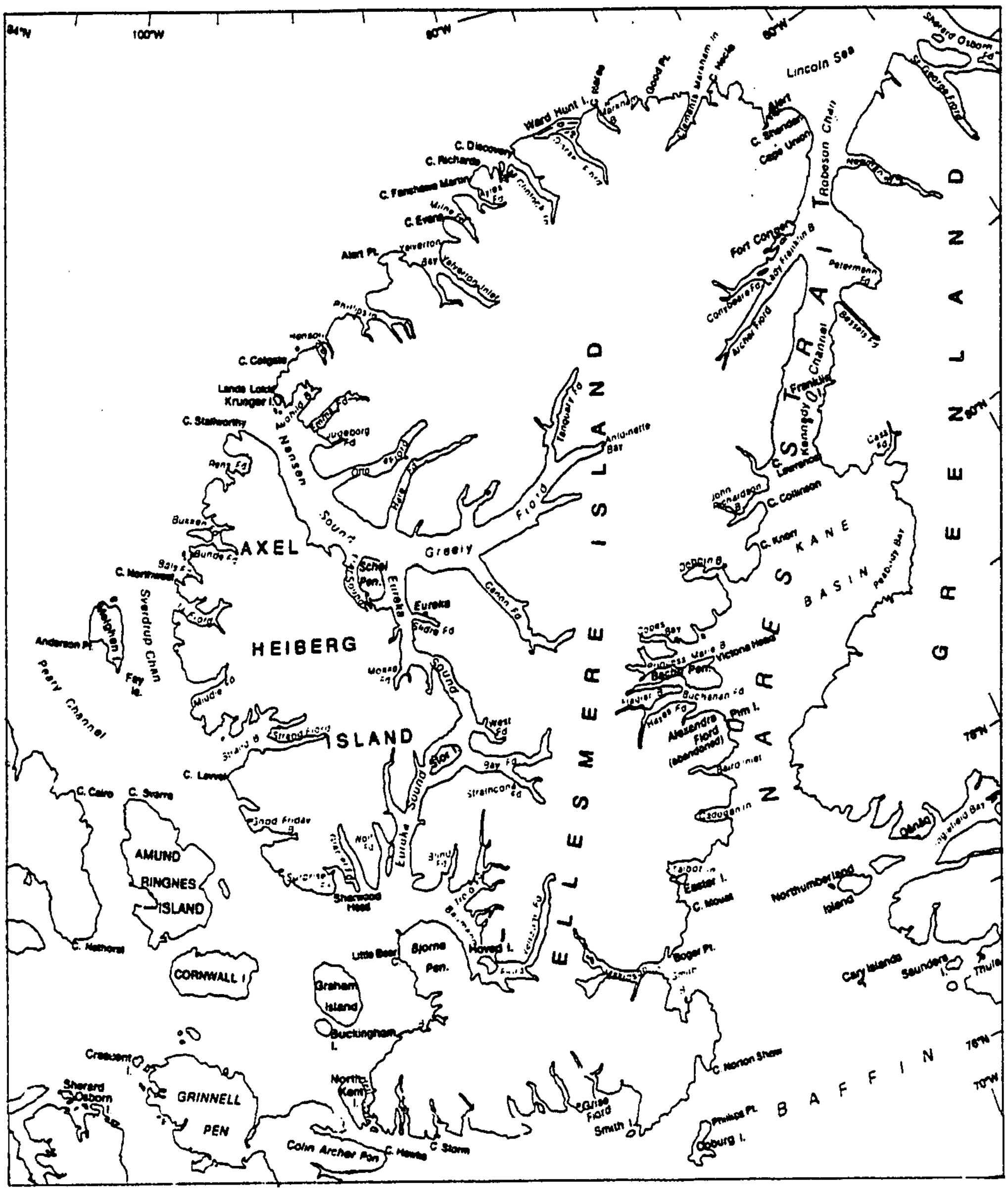

Figure 5. Map of ice shelf area along Ellesmere Island.

The statistics of calving events should not be considered as an annual stochastic process, but rather, calving takes place apparently every third or fourth year, at seemingly pseudo-random intervals, as shown in the review summary for the period 1963 to 1983(Table 1).

Table 1: Ice lost (gain) in km^2 since previous observation along north coast of Ellesmere Island (source: Sackinger et al., 1985; Jeffries, 1989).

Year	W.Hunt	M'Clintock	Nansen	Milne	Ayles	Other	Total
1963	569						569
1964							
1965							
1966		95			15		110
1967				35	(25)	$10_a(15_c)$	45 (40)
1968							
1969							
1970							
1971	4.5		240				244.5
1972	1.5						1.5
1973							
1974	10						10
1975		(no observations were made)					
1976							
1977-79		(no observations were made)					
1980	(1)					3_b	3 (1)
1982-83	40						40
Totals	625(1)	95	240	35	15 (25)	13 (15)	1023 (41)

a) West of Bromley Island

b) Cape Fanshawe Martin

c) East of Hansen Point

On the other hand, ice shelves can regenerate by seaward growth of glaciers, by sea ice accumulation, ridge-building, and pressure ridge ablation along the seaward edges of ice shelves. Due to such growth, the ice shelves do not tend to vanish totally by calving. In the period of 1963 to 1980, actually a total of $41 km^2$ of ice was gained by ice shelves, mainly in Ayles Fiord and other areas. The ice shelf regeneration process and calving process is a virtually continual one when considered over time intervals of centuries (Sackinger et al., 1985).

In the computer simulation, a uniform spatial distribution of probability of an ice shelf calving event was assumed along the northern coast of Ellesmere Island, from Clements Markham Inlet west to the mouth of Nansen Sound, as shown in Figure 6. This uniform assumption in this small distance scale should not have an obvious influence on the simulation results of probability of ice island trajectories in the relatively large spatial scale of the entire Arctic Ocean. For the temporal distribution, one calving event occurring every fourth year was assumed in the simulation. This is an approximation at the present time, based on limited data. As more data on ice shelf calving become available, this assumption can be easily adjusted in the simulation, and several simulation runs with 3-year and 5-year intervals have been run to test the sensitivity of the results to this assumption. Results show no large differences between these different assumed intervals. Details on this will be explained in a later chapter.

2.2 Random Ice Island Dimensions

Ice island dimensions affect movement, and therefore affect the trajectories; they

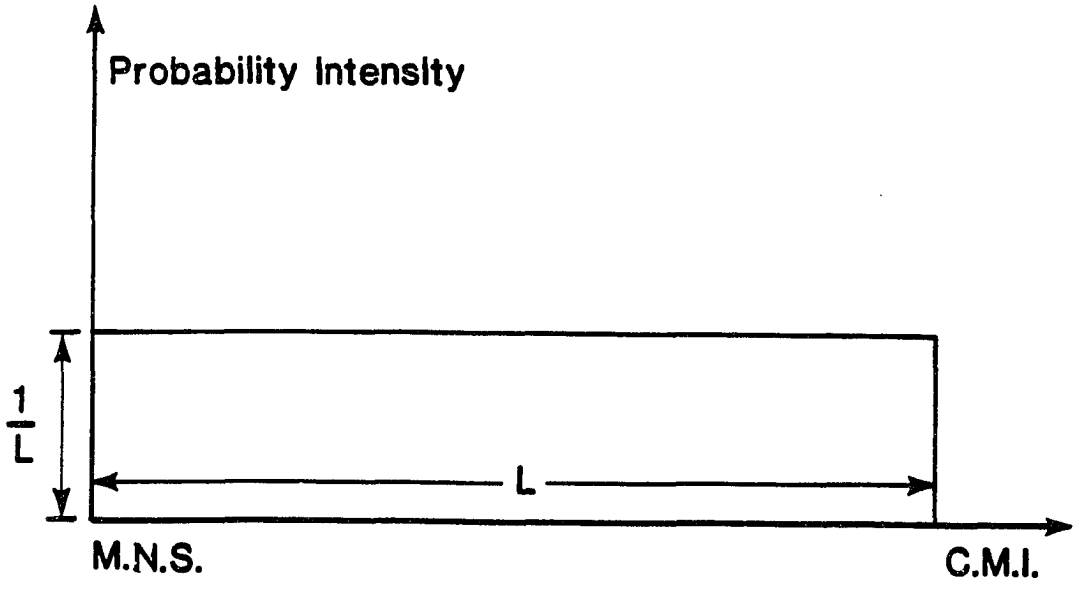

Figure 6: Spatial distribution of probability of ice shelf calving event. M.N.S. – mouth of Nansen Sound. C.M.I. – Clements Markham Inlet. L – distance between M.N.S. and C.M.I.

are important random variables. The statistical characteristics of these variables used in this study are based on observational data analyzed mainly by Jeffries et al.(1988), which is believed to be the most complete summary at the present time. During the past 40 years, a total of 52 ice islands have been recorded with dimension estimates, including new ice islands which are completing their first full Beaufort Gyre drift, and old ice islands completing a second or greater drift circuit. The length and width of each of the ice islands are plotted in Figure 7 (Jeffries et al., 1988). The dimensions of concern in this study are for newly-calved ice islands, so only the dimensions for categories of "new" and "other" ice islands in Figure 7 are considered for distribution calculations. The reason for including "others" is that those which were found freely floating in the Arctic Ocean in the 1960s and 1970s were all large, which suggests that they may have been relatively young when first sighted because they had perhaps not undergone grounding and fragmention (Jeffries et al., 1988). The range of dimensions for these ice islands was from a minimum of $0.5 \times 1.48 km$ to a maximum of $27.0 \times 29.0 km$. For the random dimension generation of the ice islands the length distribution is of interest, and according to these data, the corresponding length distribution assumed for the simulation was as shown in Figure 8. The length range is quite wide, but the distribution is positively skewed; 60% of the data occurs in class $1 - 10 km$ length alone and almost 92% of the data is in class $1 - 10 km$ and $10.1 - 20.0 km$ combined. Only 7.2% of ice islands have a length greater than 20 km when calved, according to the data.

Observations have shown that ice islands are sometimes irregular in shape, but are frequently almost rectangular with quite straight edges. Thus, it is convenient and plausible to assume that they are rectangles, which may be expressed in terms of standardized length-width ratios(Jeffries, et al., 1988). These length-width ratios

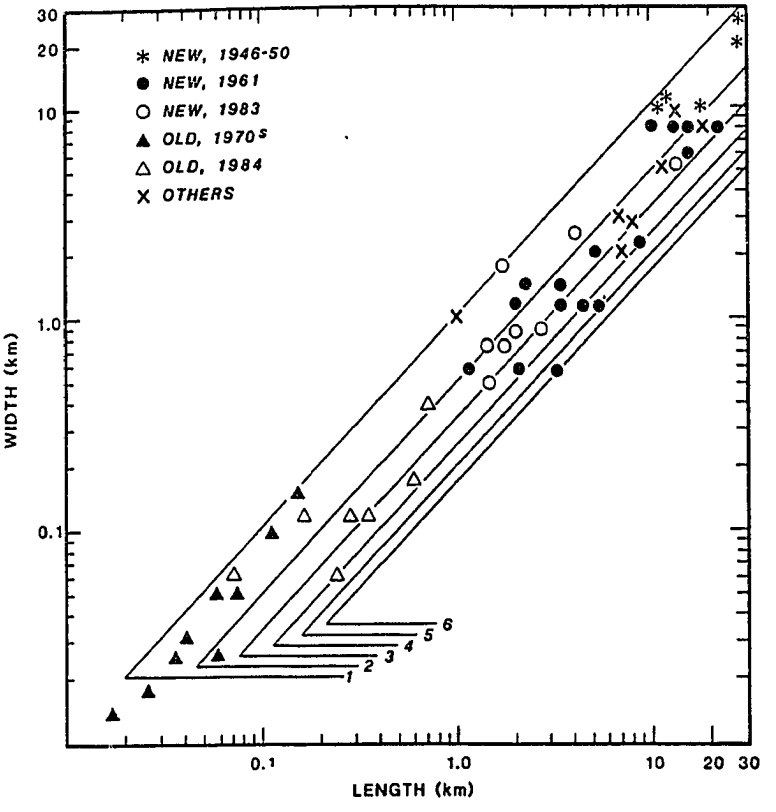

Figure 7: Scatter diagram of the length and width of ice islands. The parallel diagonal lines are for length-width ratios of 1 to 6 (from Jeffries et al., 1988).

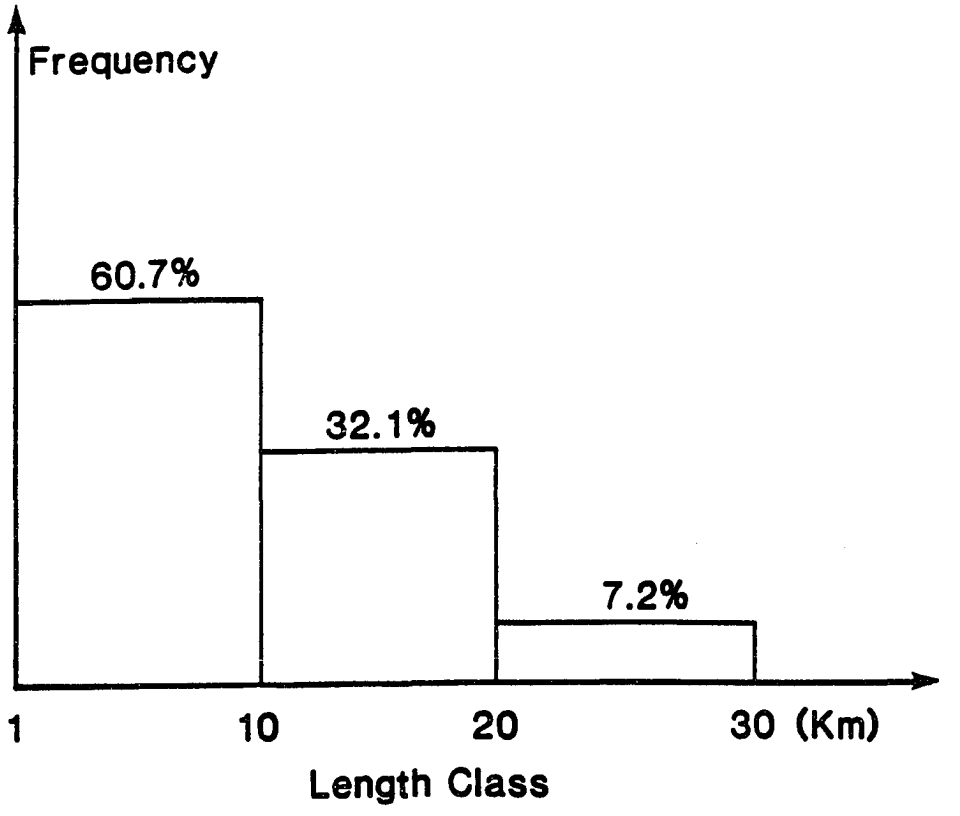

Figure 8: Assumed length distribution of ice islands newly calved from ice shelves.

of ice islands sighted in the past 40 years have a frequency distribution as shown in Figure 9. The highest frequency, almost 50%, is for the ratio from 1.0 to 1.99 and 80% are in the ratio classes from 1.00 to 2.99. This distribution was used in the simulation to generate a random length-width ratio, which was used in combination with the random length, for calculation of the random area of ice islands generated.

For the new ice island thickness, the only data from observation on Hobson's Choice Ice Island shows 42.5m (Jeffries et al., 1988), and this was assumed to be the mean thickness for all new ice islands in the simulation. The ice island thickness may decrease at a variable rate in different latitude areas due to ablation during its drift in the Arctic Ocean. One of the data to quantify this thinning rate is from ice island T-3. T-3 had a mean thickness of about 48m in 1952, as measured by a seismic method (Crary, 1958), and a thickness of about 30m in 1973 (Holdsworth and Traetteberg, 1973). This means that it might have thinned by as much as 18m in 21 years, and the average thinning rate was about 0.82m per year. According to such a rate, a newly-calved ice island with thickness of 42.5m could only drift for at most about 50 years before it melted completely. The drift time in the Arctic Ocean may be less than this, due to grounding, fragmenting, or to ejection out of the ocean boundaries. Since no other data were available at this point in time, it was decided that the average thinning rate from T-3 should be used in this simulation.

2.3 Numbers of Random Generated Ice Islands

Few observations are available on the numbers of new ice islands calved from ice shelves in one calving event. Therefore, it was decided to use an indirect method to obtain the numbers of ice islands randomly-generated in one calving event. One statistical data source available is the areas of calved ice lost from the ice shelves

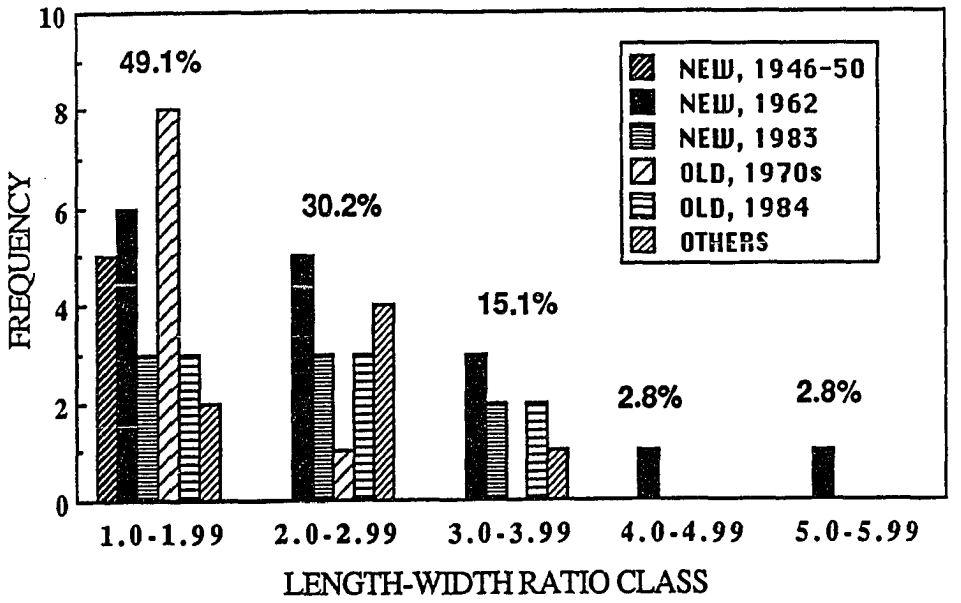

Figure 9: Frequency distribution of ice island length-width ratios (from Jeffries et al., 1988)

along the northern coast of Ellesmere Island, as shown in Table 1. The data listed in Table 1 cover a period of 20 years, from 1963 to 1983. Observing this data, a distribution of calved area of ice was then assumed for the simulation, as shown in Figure 10. The random area of calved ice in one calving event can then be generated in the computer simulation according to this distribution. By deducting each random ice island area from this randomly-calved ice shelf area, until the remaining ice shelf area is less than the last ice island area, the number of randomly-generated ice islands in one calving event was an automatic result. If the last ice island area is greater than the remaining ice shelf calved area, the last ice island area is set equal to the remaining area.

One may consider a possible decreasing trend in ice shelf area calved over time, as seen in Table 1. This decreasing trend may be related to the decreasing trend of ice island sizes observed from 1946 to 1983 (Jeffries et al., 1988). The reason for this decrease in ice shelf area may be that as the total area of ice shelf decreases over time, the smaller individual ice shelves occupy only fiords and bays and do not extend far offshore (Jeffries, et al., 1988). However, ice shelves will not vanish in the near future, due to regeneration by multi-year ice attaching to the seaward edge of existing shelves, followed by accumulation of iced firn from above and also accretion from below. In fact the ice shelves of Ellesmere Island have been producing ice islands sporadically for many decades, and calving processes are still taking place (Sackinger et al..1985). Since there is not enough data to quantify these long-term statistics, this decreasing trend of ice shelf area was neglected in this simulation, and left for future research.

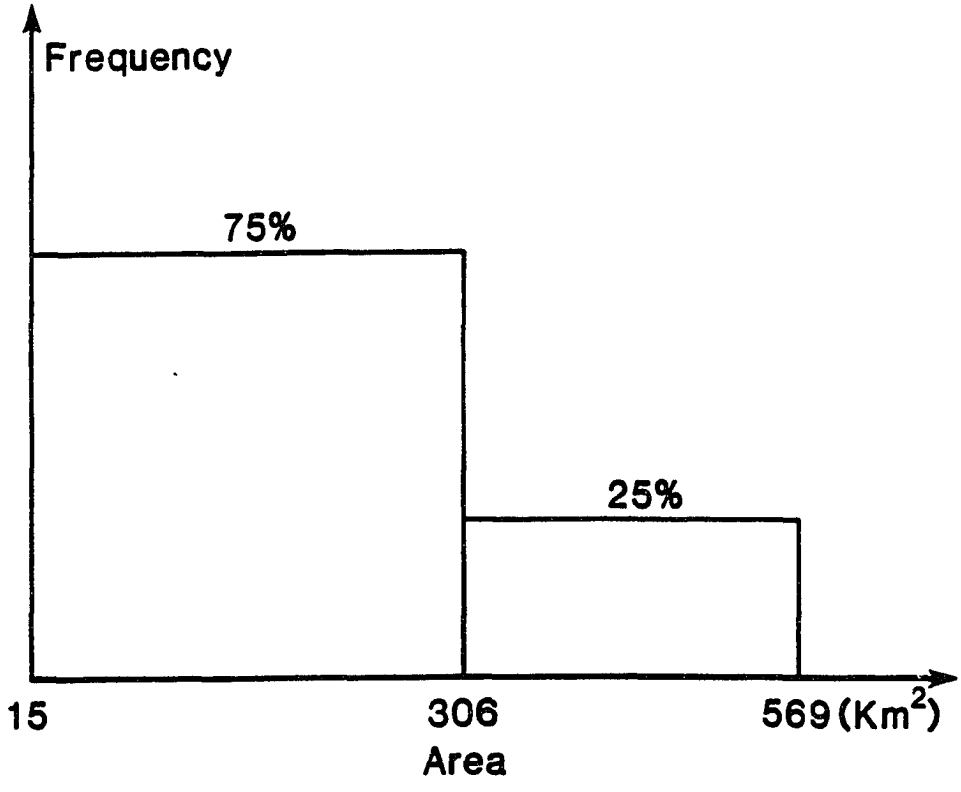

Figure 10: Assumed distribution of calved area of ice shelves.

CHAPTER 3

DYNAMIC MODEL OF ICE ISLAND MOVEMENT

A dynamic model for the simulation of ice island drift is presented in this chapter. This part of the simulation process model deals with the way ice islands drift under various geophysical forces. Basically, the essential causes of ice island drift can be thought of as the geostrophic wind above the ice-atmosphere boundary layer, and the ocean current beneath the ice-ocean boundary layer. The forces acting on ice islands are transmitted from the geostrophic wind and the ocean current via simple integral boundary layers. One important aspect in establishing the dynamic model of ice island drift is understanding how these forces are transmitted, and how to express them in a practical and useful manner. Fortunately a large amount of information on this aspect, originally derived for sea ice dynamics, can be applied to ice island dynamics. In addition, the rotation of the earth also deflects the drift of ice islands. A steady ocean current introduces a tilt of the sea surface height (or alternatively a net transverse pressure across the ice island), which also affects the ice island motion. With respect to the dominant components of the ice island dynamic balance, attention should be given to the forces which differ from those for common sea ice dynamic models, e.g. pack ice force and water form drag force on an ice island.

3.1 Governing Equation of Ice Island Motion

Because each individual ice island can be considered as a rigid body, its essential dynamic features may be characterized by a momentum equation which describes

the forces that determine it's drift. Observations of ice island movement show a strong correlation between ice island motion and wind velocity, even in pack ice zones(Sackinger et al., 1989). Ice island movement was therefore considered as wind-driven motion, as is commonly assumed for sea ice movement models. Geostrophic-scale winds over the whole Arctic Ocean were used in this study. Therefore, the wind drag force acting on an ice island was considered as the unique primary driving force. The secondary forces, which are caused by ice island motion, may include water skin friction, Coriolis force, and sea surface tilt pressure, as commonly considered in sea ice dynamic models. Instead of an internal stress as is assumed for sea ice dynamic models, a lateral pack ice force acting on the ice island edges is significant (Lu, 1988) and was considered in this ice island dynamic model. Another force acting on an ice island, which differs from that for sea ice models, is the water form drag resulting from the great keel depth. This force is usually larger than water skin friction acting on the bottom surface, as will be shown. These two forces acting on an ice island make an ice island motion pattern different from that of a similiar area of sea ice. For example, trajectory data show that the ratio of ice island speed to wind speed is from 0.86% to 1.40% (Lu, 1988), while a ratio of 2% for the ratio of sea ice speed to wind speed is generally found (McPhee, 1980).

For dynamic balance, the ice island is considered to move in a two-dimensional plane with forcing fields. In Cartesian coordinates in the plane of motion of ice islands, the dynamic equation which describes the movement of ice islands in the presence of pack ice can be written as

$$M\frac{d\vec{V}_i}{dt} = \vec{F}_a + \left(\vec{F}_{ws} + \vec{F}_{wf}\right) + \vec{F}_c + \vec{F}_p + \vec{F}_t \tag{3.1}$$

where M is ice island mass, $\vec{V}_i$ is ice island velocity, t is time, $\vec{F}_a$ is wind shear force, $\vec{F}_{ws}$ is water skin friction acting on the lower surface of the ice island, $\vec{F}_{wf}$ is water

form drag due to the frontal and rear areas of the submerged portion of the ice island, $\vec{F}_c$ is Coriolis force, and $\vec{F}_p$ is the pack ice force acting on the boundary of the ice island. $\vec{F}_t$ is the force due to sea surface tilt. There is a high incidence of transient processes in observed experimental data and in the simulations of ice island motion sequences, so the acceleration term is maintained in the dynamic equation. In Figure 11 a schematic illustration of the various forces acting on an ice island is presented.

3.2 Wind Shear Force

To determine the wind shear force on an ice island it is useful to understand how the force is transmitted via the atmospheric boundary layer (ABL). The ABL is that part of the atmosphere for which the presence and characteristics of the earth's surface (land, water, ice, vegetation,etc.) are directly important. In some circumstances the boundary layer might then extend to the top of a towering thunderstorm whereas for a windless polar night the depth may be only tens of meters. Most typically, the ABL is of the order of hundreds of meters to a few kilometers in depth (McBean, 1986).

The most important characteristic of the ABL is turbulence, continuously in space and time. This turbulent nature is responsible for the complexity of the ABL processes and makes them much more difficult to observe and understand. It is observed that the turbulence is very dependent upon the surface conditions, or surface roughness, and upon the surface temperature relative to the air above. An evidence of this is the turbulence over a patchy ice-water surface. The states of the ABL can be classified as stable, unstable, and neutral depending on the vertical gradient of air potential temperature. The potential temperature is defined as the temperature a parcel of air would attain if brought adiabatically to a reference pressure (usu-

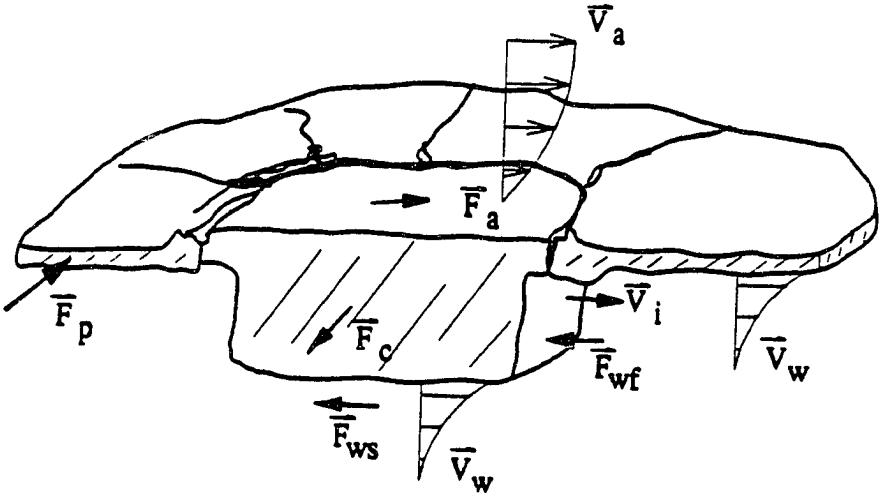

Figure 11: Scheme of forces acting on ice island.

ally 1000 mb). The neutral ABL has a constant potential temperature throughout and turbulence is entirely due to wind shear (no buoyancy effects). Because of its simplicity, in the sense of no buoyancy effects, it has been extensively considered theoretically (McBean, 1986).

Because of the complexity of the atmospheric boundary layer under general conditions, both modellers and experimentalists have looked for and investigated idealized ABL's. The most common idealization is that of horizontally-homogeneous flow over a uniform surface. Monin and Obukhov (1954) postulated for a time-stationary, horizontally-homogeneous surface layer that the structure of the layer and characteristics of turbulence should depend on relatively few scaling parameters. Their theory provides a framework for indirect estimates of the momentum flux. The Monin-Obukhov stability parameter (Z/L) is introduced from their similarity theory; here Z is measuring height, and L is the Monin-Obukhov length scale. A detailed definition can be found in Monin and Obukhov (1954). For the ABL over snow and ice-covered surfaces, (Z/L) is usually near zero or greater than zero, i.e. is usually near neutrally or stably stratified (McBean, 1986).

For many purposes it is useful to think about the ABL as being divided into sub-layers. First, adjacent to the surface and very thin (typically about 0.1 mm thick) is the molecular sub-layer where the vertical transfers or fluxes are dominated by molecular processes. Above the molecular sub-layer and extending upward a few tens of meters is the surface boundary layer. This is the most-studied and best-understood part of the ABL. The processes are dominated by turbulence. The idea of a surface layer arises naturally from numerous observations which show that under typical conditions the mean wind profile may vary dramatically in the first few meters, but that shear stress changes by only a few percent over the lower tens of

meters. Between the surface layer and the top of the ABL is a region sometimes called the Ekman layer, because the wind profile in certain circumstances approximates an Ekman spiral. This layer is characterized by a changing wind direction with height, and has a more complicated structure than does the surface layer (McBean, 1986).

From the point of view of ice dynamics, the most important atmospheric effect is the wind drag on the surface. To derive methods of estimating the surface wind stress from easily-measured variables, such as from the surface pressure field, a model is needed to relate the momentum flux at the surface to the synoptic-scale flow field. Since a general analytic solution to the governing equations for a turbulent flow in a rotating frame of reference does not exist, various approximate methods have been explored to obtain simple empirical or semi-empirical drag laws. The driving force for the ice-ocean motion is from the synoptic free-stream flow above the ABL. Since this flow arises from the large-scale pressure differences, it can be related to the large-scale pressure field. There generally exists good horizontal pressure gradient coherency vertically through the ABL, so that the geostrophic flow determined from the surface pressure gradient/Coriolis force balance is a good approximation to the flow immediately above the ABL (Brown, 1980).

Furthermore, to provide the basic parameter for wind stress calculation in the sea ice dynamic model in the AIDJEX experiment, surface pressure maps were constructed four times daily for one year over local Beaufort Sea (Albright, 1980). The geostrophic winds calculated from the pressure maps were estimated to be accurate to ± 0.7 m/sec in speed and $\pm 5°$ in direction. Statistics of the calculated geostrophic winds and the observed 10 meter surface winds showed a speed ratio of 0.585 for surface wind to geostrophic wind, and 25.9° of cross-isobar turning angle for the surface wind, expressed as an annual mean value. The correlation coefficient is 0.9.

The seasonal ratio of magnitudes of surface wind to geostrophic wind was 0.60 in summer and 0.55 in winter. The angle between surface and geostrophic wind was 24° in summer and 30° in winter (Albright, 1980). This behavior is consistant with greater stable stratification during winter than during summer (Paulson, 1980). It appears, therefore, that even without the application of a sophisticated model of the planetary boundary layer, surface winds can be derived from the pressure field.

Schlichting (1979) presented theoretical calculations for the turbulent skin friction at a flat plate based on the momentum integral equation of boundary-layer theory. With the fundamental assumption that the velocity distribution in the boundary layer on a plate is identical with that inside a circular pipe, he used many results obtained earlier for the turbulent flow in a pipe and obtained the skin friction drag D(x) of a flat plate of length x, with fluid on one side, as

$$D(x) = b\rho U^2 \delta_2 \tag{3.2}$$

here b is plate width, ρ is fluid density, U is the constant free-stream velocity, and δ_2 is related to the velocity distribution $u(y)$ in the boundary layer, and is defined as

$$\delta_2 = \frac{1}{U^2} \int_0^\infty u(y)(U - u(y))dy \tag{3.3}$$

Using an empirical equation for velocity distribution in smooth pipes of radius R, of the form

$$\frac{u}{U} = (\frac{y}{R})^{\frac{1}{n}}, \tag{3.4}$$

with n=7, he obtained the drag on a plate of width b and length l as

$$D = 0.036\rho b l U^2 (\frac{Ul}{\nu})^{-\frac{1}{5}}, \tag{3.5}$$

ν being the kinematic viscosity. For practical purposes he introduced the dimensionless drag coefficient C_s, defined as

$$C_s = \frac{D}{\frac{1}{2}\rho U^2 b l} \tag{3.6}$$

and obtained

$$C_s = 0.074(\frac{Ul}{\nu})^{-\frac{1}{5}} = 0.074(R_l)^{-\frac{1}{5}} \quad (3.7),$$

which is valid for the Reynolds number R_l in the range of 5×10^5 to 10^7. Thus the drag force

$$D = \frac{1}{2} C_s \rho A U^2. \quad (3.8)$$

The Reynolds numbers which occur in practical applications in connection with flat plate problems considerably exceed the range of 5×10^5 to 10^7. To obtain a drag formula valid for much higher Reynolds numbers, he used the logarithmic velocity-profile since the logarithmic formula may be extrapolated to arbitrarily large Reynolds numbers in the case of pipe flow. The drag coefficient C_s for this kind of velocity distribution was found to be

$$C_s = \frac{0.455}{(log R_l)^{2.58}} \quad (3.9).$$

The assumption of an identical velocity-profile between pipe flow and flat flow was checked by measurements on the boundary layer on a plate. The results showed that the velocity profile in the outer portion of a flat boundary layer deviates systematically upwards from the logarithmic law of a circular pipe. (Schlichting, 1979).

In the case of sea ice dynamic simulation, the air stress on the ice cover is commonly estimated from the product of a drag coefficient and the mean wind speed at 10-meter height, squared (Hibler, 1986). It is possible to calculate the air stress independently of the ice motion because the velocity of the air is so much larger than the velocity of the ice. The air stress $\vec{\tau}_a$ may be given as

$$\vec{\tau}_a = C_{10} \rho_a |\vec{V}_{10}| \vec{V}_{10} \quad (3.10)$$

With this formula, the air stress can be calculated with the empirical relation of surface wind and geostrophic wind, and the 10-meter wind drag coefficient, both of which are available from measurements (Albright, 1980; Banke et al., 1980).

The above formulation is convenient for a practical semi-empirical parameterization of the stress without specific knowledge of the characteristic scale heights, assumed eddy viscosities, or mean temperature distribution. In practice, the variational range of drag coefficient is much more than the range of velocity, therefore the determination of drag coefficient is more important than that of velocity.

To measure the wind drag coefficient, both the wind profile method and the more direct eddy correlation measurements can be used. Through the AIDJEX and other experiments a considerable body of information on the 10-meter drag coefficient, C_D (10m), has been obtained. Results of measurements show that the wind drag coefficients mainly depend on the air stability and surface roughness.

Leavitt (1980) shows coefficients as a function of stability based on wind profile measurement data (Figure 12). Low drag coefficients have been observed in conditions of highly stable stratification, generally associated with low wind speeds. In Banke et al. (1980), the drag coefficients show a similar relation with air stability, as obtained by eddy correlation measurements (Figure 13). They found, for near-neutral ($Z/L < 0.1$) relatively ice-ridge-free areas that

$$C_{DN} = (1.55 \pm 0.37) \times 10^{-3}. \tag{3.11}$$

The data indicated a decrease in C_D with increasing stability , approximately following

$$C_D = (C_{DN}^{-1/2} + 13Z/L)^{-2}. \tag{3.12}$$

Observations also indicated that stable stratification increases the turning angle. A

value of $C_{10} = 1.19 \times 10^{-3}$ was obtained in nearly neutral conditions for a smooth snow-covered ice surface in the Beaufort Sea AIDJEX experiment.

Their investigations also produced a relationship between drag coefficients and surface characteristics as shown in Figure 14. For a flat, snow-covered surface, a value of $C_{10} = 1.1 \times 10^{-3}$ was deduced from the regression relation, with correlation coefficient r=0.90.

While the drag coefficient is greatly reduced in stable conditions, this may not be particularly important in relating ice dynamics to measured surface (10 m) winds. Winds stronger than 6 m/s are usually associated with near-neutral stability, while in winds less than 6 m/s the wind stress is often so small that accurate representation of the drag coefficient is not necessary. A proof of this is the threshold wind speed of 5 m/sec for ice island motion found by Lu (1988).

In this simulation, the air drag force, $\vec{F}_a$, is assumed to act on an ice island surface in the direction of the wind. It is expressed with a quadratic dependence upon the wind velocity. This formulation, verified in numerous field observations(e.g. Brown, 1980; Banke et al., 1976), may be written:

$$\vec{F}_a = \rho_a C_a A |\vec{V}_a| \vec{V}_a \tag{3.13}$$

where $\rho_a = 1.3 kg/m^3$ is taken as the air density, $C_a = 0.0012$ is a skin drag coefficient for wind over smooth snow-covered ice at 10 meter height (Banke et al., 1980), A is ice island area, and V_a is the speed of the surface wind at 10-meter height. The very long wavelength undulations of the ice-island top surface are neglected in considering wind-shear force. An extensive review (McBean, 1986) of air-drag coefficients has shown this value to be a good approximation for smooth, snow covered ice, as is found on top of an ice island. The form drag term due to air flow over the ice

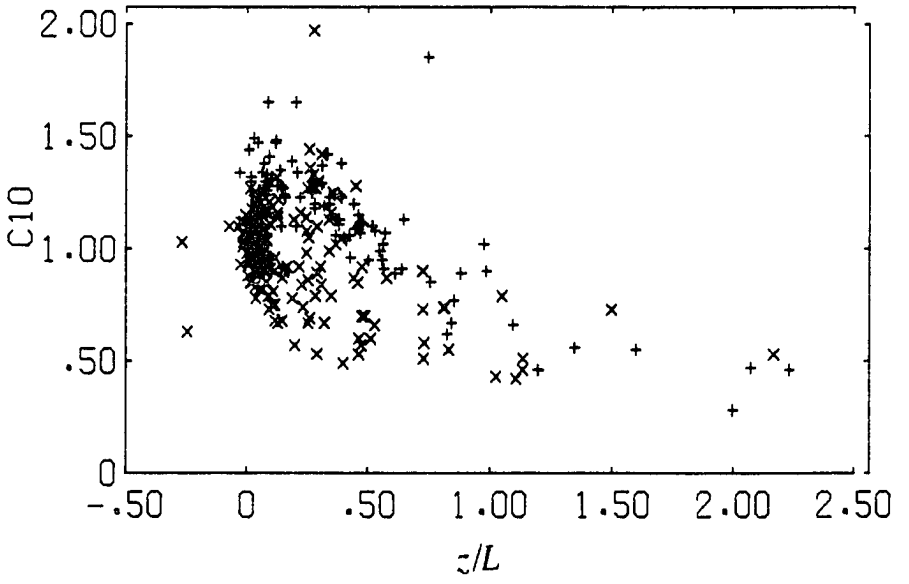

Figure 12: Relation of air drag coefficient C_{10} and air stability parameter Z/L (source:Leavitt, 1980).

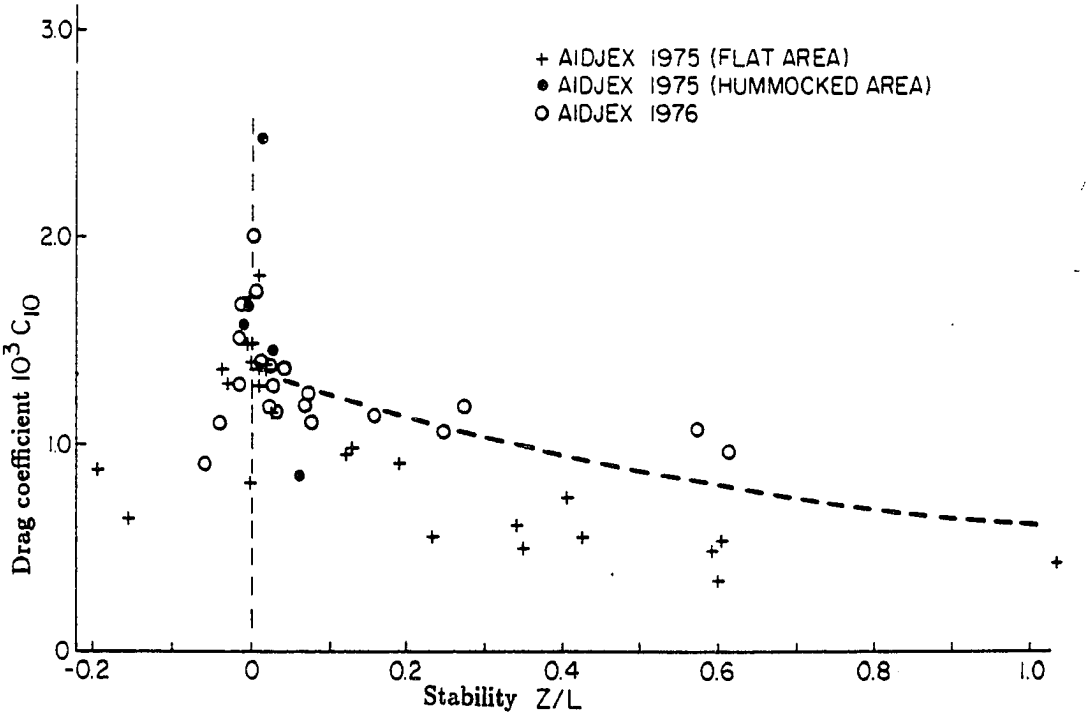

Figure 13: Relation of air drag coefficient C_{10} and air stability parameter Z/L (source:Banke et al., 1980).

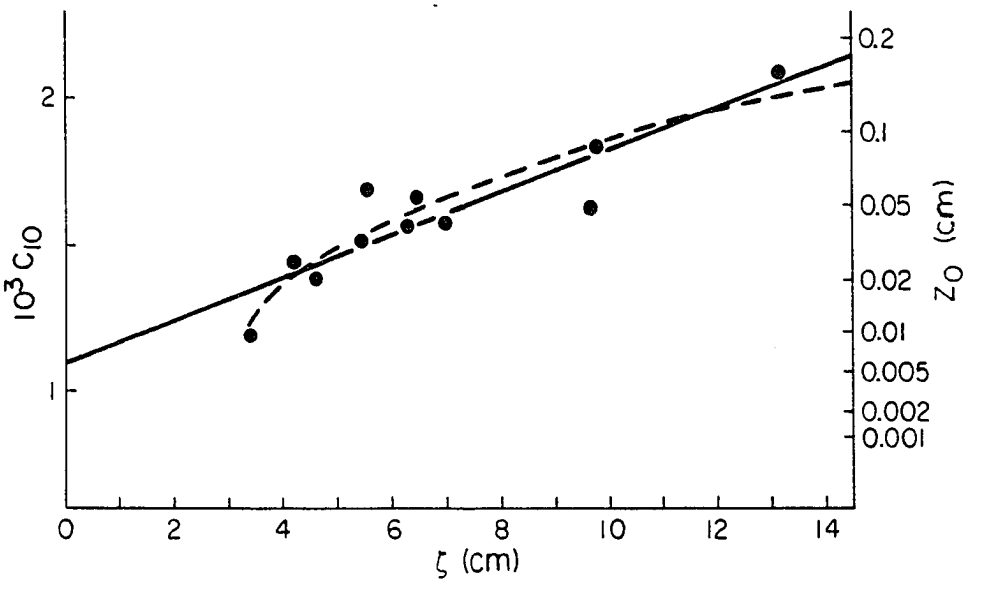

Figure 14: Relation of air drag coefficient C_{10} and ice surface roughness parameter ξ (source: Banke et al., 1980).

island edge is neglected because observations have shown that pack ice rubble and snowdrifts make this a relatively smooth, gradual transition. According to Albright's result (1980), a relation of $\vec{V}_a = 0.6\vec{V}_g e^{i26°}$ was used to transform geostrophic wind to surface wind, i.e. the surface wind speed is 0.6 times the surface geostrophic wind speed and the surface wind direction is turned an angle of $\eta = 26°$ to the left of the surface geostrophic wind in the Northern Hemisphere. From the analysis of observed data, a threshold wind speed of 5 m/s appears to be necessary to initiate ice island motion(Lu, 1988).

The air drag formula used in the simulation is different from Schlichting's drag formula (3.8) in the drag coefficient. The drag coefficient C_a in (3.13) is corresponding to the $(\frac{1}{2}C_s)$ in (3.8), and it's value is adopted from the field measurements, while Schlichting gave the C_f as a function of the Reynolds number. In the case of air turbulent flow over an ice island, the Reynolds number is approximately in the order of 10^{10} for a typical value of 10 m/sec wind speed, 10 km length of an ice island, and $\nu = 13 \times 10^{-6} m^2/sec$ at an air temperature of $0°C$. Thus, the drag coefficient C_s in (3.9) is

$$C_s = \frac{0.455}{(logR_l)^{2.58}} = 1.2 \times 10^{-3} \tag{3.14}$$

and the drag force ratio of formula (3.13) to (3.8) is

$$\frac{F_a}{D} = \frac{C_a \rho_a A V_a^2}{\frac{1}{2} C_s \rho_a A V_a^2} = \frac{2C_a}{C_s} = 2 \tag{3.15}$$

One reason that the value from Schlichting's formula is smaller than that from (3.13) can be explained by noting that Schlichting formula does not include the surface roughness effect on the turbulent flow drag force, and this effect is important for air drag force on the sea ice surface as shown in Figure 14.

3.3 Water Skin Friction

When ice moves on the ocean surface, driven by winds, the ice cover transmits a traction to the ocean on the ice undersurface. This force is the surface manifestation of a turbulent oceanic boundary layer (OBL) which provides the mechanism for momentum exchange between the ice and ocean. The OBL is affected by rotational (Coriolis) forces and therefore falls, together with the ABL, into the general category of planetary boundary layers. These two boundary layers are closely related in many respects. Approaches for estimating wind stresses in the ABL are effective for predicting water stresses in the OBL. But there are also some important differences from the viewpoint of sea ice dynamics, e.g. the water stress turning angle as introdued and explained by McPhee (1986).

Since normal geostrophic ocean currents are at most a few percent of the surface wind in magnitude, an approximation that the ocean state is at rest, for the upper ocean, is often used in the analysis of sea ice dynamics. Consider a free-drift steady-state ice cover under balance of three forces: wind driving force, Coriolis force and water drag force. The force balance is diagrammed in Figure 15a which represents average observed conditions during summer at the AIDJEX camps (McPhee, 1986). It shows that the OBL surface stress (which is the negative of the water stress on the ice cover undersurface shown in the Figure 15a) acts in an average direction about 25° to the left of the surface velocity. From this average of the observations, some structure of the OBL can be inferred. It helps to consider the velocity as viewed from the drifting ice, i.e. the velocity relative to the drifting ice. Near the surface the kinematic stress would be about the same as $\vec{\tau}_0$, and by analogy with other constant-stress , wall-bounded turbulent flows, one would expect a region of shear with relative velocity in the same direction as turbulent stress. As depth increases,

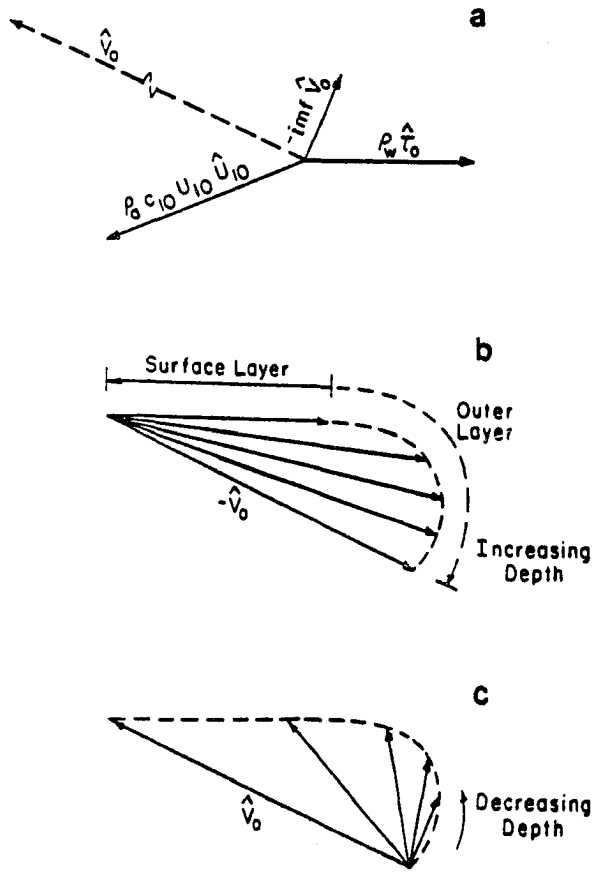

Figure 15: Schematic of ice force balance (a), plan view of OBL velocity as viewed from drifting ice (b), velocity as viewed in frame fixed to earth (c). (Sourse: McPhee, 1986).

the stress would diminish and veering of both the horizontal stress vector and the mean current would be noted. At some depth stress would vanish and the relative velocity reaches $-\vec{V}_0$, at this depth and greater depths (Figure 15b). That part of the profile close to the ice, where the relative velocity is unidirectional, is called the surface layer. This layer is usually only about 2 meters thick. The region farther from the interface, where the relative velocity veers noticeably, is called the outer, or Ekman layer. This layer thickness can be in the range of tens to a few hundred meters. The velocity profile relative to a fixed-to-earth reference frame is shown in Figure 15c (McPhee, 1986).

As in the case of the ABL, the water skin friction can also be estimated by the quadratic drag law. This drag law does appear to give adequate wind and water stress estimates for the ice drift, and has been used successfully to model ice drift (McPhee, 1979; Hibler, 1986). Therefore, for practical use, the important consideration should be the determination of the drag coefficient.

To provide a data-base for the determination of the drag coefficient, Langleben (1982) made eddy flux measurements of momentum in May, 1977 in the oceanic boundary layer under a first-year floe of fast sea ice in Barrow Strait, N.W.T. The measurement results yielded a value for the 1-m water drag coefficient of 1.32×10^{-3} with a standard deviation of 0.06×10^{-3}. Other measurements of water stress have been made principally under multi-year ice floes. Since such floes tend to present relatively large-scale roughness at the boundary with the ocean, the water drag coefficients are larger than in the case of first-year ice (Langleben, 1982).

In practice the water currents can be chosen independent of time, as a steady current. It can be estimated from geostrophic considerations by setting H equal to

the dynamic heights and computing currents by $\vec{V}_w = gf^{-1}\vec{k} \times \nabla H$, or one may directly adopt the observed height data if it is available.

In this simulation the water skin friction, $\vec{F}_{ws}$, was represented as a drag law with a quadratic dependence on the ice velocity relative to the water velocity as follows:

$$\vec{F}_{ws} = \rho_w C_w A |\vec{V}_w - \vec{V}_i| [\left(\vec{V}_w - \vec{V}_i\right) cos\theta + \vec{k} \times \left(\vec{V}_w - \vec{V}_i\right) sin\theta] \qquad (3.16)$$

where $\rho_w = 1032 kg/m^3$ is a representative sea water density. A quite flat bottom surface of ice islands has been revealed by radar sounding surveys with airborne impulse radar systems (Kovacs, 1977). Therefore a surface drag coefficient $C_w = 0.00132$ for water under smooth horizontal flat ice (Langleben, 1982) was chosen. The direction of $\vec{F}_{ws}$ is turned an angle of $\theta = 25°$ to the left of negative relative velocity $\left(\vec{V}_w - \vec{V}_i\right)$, to account for the Ekman spiral (McPhee, 1986), as an initial approximation.

The pattern of surface water movement in the Arctic Ocean is generally driven by average wind and ice motion, and forms a large clockwise gyre over the major part of the Arctic Basin. The greatest volume of water leaves the Arctic Ocean through the western part of the passage between Greenland and Svalbard (Smith, W.O. Jr., 1990).

The annually-averaged current speed of water entering the Arctic Ocean through the Bering Strait is 25 cm/sec. (Coachman and Aagaard, 1988), a not insignificant quantity, and the influence of those water currents on ice island motion in the Chukchi Sea is considered in the simulation. Time-invariant surface water current data for the Chukchi Sea (Johnson, 1987) were used to compute the water force. The data of Johnson (1987) show a velocity range from $0 - 30 cm/s$. The current is

one directed northwest toward Wrangel Island, and another toward the northeast along the Alaskan coastline from Point Hope to Point Barrow. Surface current data (Brower et al., 1977) near the Alaskan Beaufort Sea area were also used in some special simulation runs to compute total water stress. The currents along the Alaskan coast of the Beaufort Sea, given by the Climatic Atlas (Brower et al., 1977), are generally westward with a wide velocity range of $2cm/s$ to $30cm/s$. The tide amplitude in the Beaufort and Chukchi Seas is small with an average value of about 5 cm (Kowalik and Matthews, 1982), and the calculated maximum tidal current in this area is about 0.5 cm/sec in average, which is not significant. Tidal currents in the central basin of the Arctic Ocean are even smaller because of the great depth. These estimates are for the lunar semi-diurnal tide. Evidence from tide gauges around the basin summarized by Sverdrup (1926) implies that the lunar semi-diurnal (period 12.47 hr) and the solar semi-diurnal (12 hr) tides are the dominant tidal constituents in the Arctic Ocean. Considering the fact of ice cover during all seasons, and the limit of published data, the water current influence on ice island motion in the other areas of the Arctic Ocean was considered to be zero in this simulation.

3.4 Water Form Drag

An additional component of drag is due to the frontal and the trailing area of the ice island, which is called form drag. The general mathematical relation for water form drag is (e.g. Hoerner, 1965)

$$\vec{F}_{wf} = \frac{1}{2}\rho_w C_f A_f |< \vec{V}_w >_D - \vec{V}_i| \left(< \vec{V}_w >_D - \vec{V}_i \right) \tag{3.17}$$

where the C_f is a form drag coefficient. The quantity A_f is the cross-sectional area of the wetted portion of the ice island normal to the relative velocity $(< \vec{V}_w >_D - \vec{V}_i)$. $< \vec{V}_w >_D$ is the vertically-averaged water velocity over the frontal area A_f of an

$< \vec{V}_w >_D$ is the vertically-averaged water velocity over the frontal area A_f of an ice island, at a distance sufficiently far from the frontal surface so that the vertical component of water velocity due to the frontal surface is not present.

Several experiments have been made to determine the form drag coefficient, C_f, for different shapes and roughnesses of objects. Values of 0.45 for the roughened sphere and 0.35 for the roughened cube were obtained from water tank experiments by Russell et al. (1977). These values are lower than those obtained by others; the data sets used for the analysis of Russell et al. were selected mainly from the stage of the beginning of deceleration of the model motion, not from the steady-state motion as indicated by Shirasawa et al. (1984). Later, Shirasawa et al. re-examined Russell's data, and produced values of C_f from 0.63 to 0.91 for different shapes and roughnesses of objects, including 0.71 for a roughened cube (Shirasawa et al., 1984). Other values of C_f for sphere and cubes from wind-tunnel experiments (Hoerner, 1965), are 0.47 and 1.05 respectively. As to the values of C_f for an iceberg, the value of 1.2 was reported from towing experiments on three very small irregularly-shaped icebergs by Banke and Smith (1974).

In this simulation, C_f is taken as 0.71 in the dynamic calculations of ice island movement, from the results of Shirasawa et al. (1984) for the form drag of a cube. For calculating the water form drag, the submerged area portion A_f is set to be

$$A_f = (\frac{\rho_i}{\rho_w} H_i)\sqrt{A} \tag{3.18}$$

where H_i is ice island thickness. As an initial approximation, $< \vec{V}_w >_D$ was assumed equal to the average surface water current in the Chukchi Sea and Alaska Beaufort Sea areas. In other areas $< \vec{V}_w >_D$ was neglected as in the same manner as for surface water current in the above section.

The large section area of an ice island produces a large form drag. To compare the magnitudes of water skin friction and water form drag, one may calculate the ratio of these two forces, which yields

$$\frac{F_{wf}}{F_{ws}} = \frac{1}{2}(\frac{C_f}{C_w})(\frac{\rho_i}{\rho_w})(\frac{H_i}{\sqrt{A}}) \doteq 284(\frac{H_i}{\sqrt{A}}) \tag{3.19}$$

with numerical values of densities and drag coefficients as mentioned above (See Table 4). According to this result the form drag force will be greater than the water skin friction drag force on the bottom of the ice island when $H_i > \frac{\sqrt{A}}{284}$; most known ice islands fall in this range. The ratio of water form drag force and water skin friction drag force as a function of thickness H_i and the normalized horizontal dimension $\sqrt{A}$ of an ice island is shown in Figure 16.

3.5 Pack Ice Force

Force balance analysis for Hobson's Choice Ice Island, based on observed data, shows that the pack ice force may be significant and comparable to the Coriolis force (Lu, 1988). The pack ice force may be a function of the relative velocity between the ice island and the pack ice, of the pack ice concentration, and of the time within a movement sequence of the ice island (Sackinger, et al., 1988). In some nearshore areas, pack ice conditions will change seasonally, and it is expected that a relatively small pack ice force may be exerted on an ice island in summer. On the other hand, in the case in which the pack ice cover is compressed between the ice island and the shore, the pack ice force exerted on the ice island may restrain the movement of the ice island toward the shore. For Hobson's Choice Ice Island, an empirical relation between pack ice force and ice island velocity has been obtained (Lu, 1988) as below

$$F_p = 0.36 + 2.57V_i - 1.28V_i^2 \qquad 0 \leq V_i < 1.5cm/s \tag{3.20a}$$

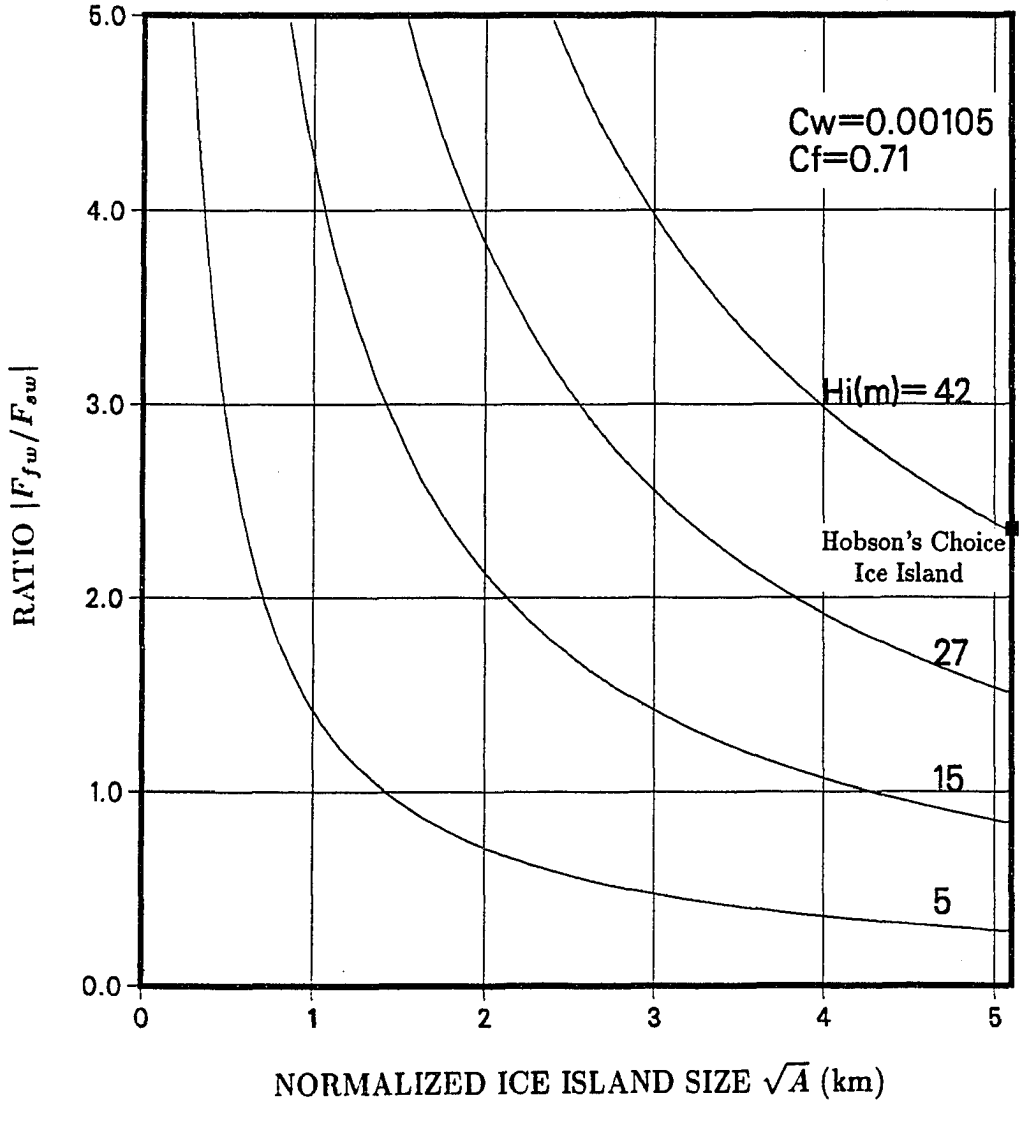

Figure 16: Ratio of ice island form drag to surface water drag, as a function of ice island normalized dimension $\sqrt{A}$.

and

$$F_p = 0.02 + 0.89V_i - 0.009V_i^2 \qquad 1.5cm/s \leq V_i \tag{3.20b}$$

with a direction angle α measured counterclockwise from the ice island velocity, of

$$\alpha = 108° + 26 \times ln(\frac{0.01V_a}{V_i}); \tag{3.21}$$

here F_p is the pack ice force in MN, V_a and V_i are in cm/s.

Because the pack ice force is a lateral force acting on the ice island's sides, its magnitude must be influenced by the ice island size. In the general case for various size of ice islands, there must be a dimensional dependence on the total pack ice force. This effect can also be shown by the fact that, for the events analyzed by Lu (1988), the pack ice force is comparable to Coriolis force, i.e.

$$F_p \doteq F_c = MfV_i = \rho_i H_i A f V_i = \beta A V_i \tag{3.22}$$

with

$$\beta = \rho_i H_i f$$

where f is the Coriolis parameter. Because F_p is an integrated value of pack ice pressure over the whole lateral contact area of the pack ice with an ice island, it can be written as

$$F_p = \int_0^L \int_0^{H(l)} \sigma dl dh = A_p \sigma_p \doteq \sqrt{A} H_p \sigma_p \tag{3.23}$$

where L is the contact length along the ice island edge; $H_p(l)$ is the contact thickness at length l; σ is the pack ice pressure distribution on the ice island, which varies with location (l, h) on the contact area; A_p is total contact area; σ_p is the average pack ice pressure, defined as

$$\sigma_p = \frac{1}{A_p} \int_0^L \int_0^{H(l)} \sigma dl dh; \tag{3.24}$$

$\sqrt{A}$ is the normalized length of the ice island; and H_p is the average thickness of the pack ice in contact with the ice island. The quantity σ_p is a function of the relative velocity of the pack ice and the ice island, and of the sea ice constitutive law. A maximum value for σ_p is the sea ice strength σ_u, i.e.

$$\sigma_p = Function(\vec{V}_p - \vec{V}_i, \sigma - \epsilon) \leq \sigma_u. \tag{3.25}$$

The mesoscale strength of sea ice, σ_u, is a function of strain rate, the temperature profile of the sea ice, and the size and density of naturally-occurring fractures in the sea ice near the ice island. For the general case in the simulation calculation, it was assumed that the average pack ice thickness H_p was constant in the pack ice zones, and that an invariant $\sigma - \epsilon$ relation held. The formula (3.23) was related to the empirical formula (3.20) for Hobson's Choice Ice Island with its original area $26 \times 10^6 m^2$, in the following way:

$$\begin{aligned} H_p\sigma_p &= \frac{F_p}{\sqrt{A}} \\ &= \frac{10^6}{\sqrt{26 \times 10^6}} \begin{cases} 0.360 + 257.000V_i - 12800.000V_i^2 & 0 \leq V_i < 0.015m/s, \\ 0.020 + 89.000V_i - 90.000V_i^2 & 0.015m/s \leq V_i \end{cases} \end{aligned} \tag{3.26}$$

or

$$(H_p\sigma_p) = 200 \times \begin{cases} 0.360 + 257.000V_i - 12800.000V_i^2 & 0 \leq V_i < 0.015m/s \\ 0.020 + 89.000V_i - 90.000V_i^2 & 0.015m/s \leq V_i, \end{cases} \tag{3.27}$$

H_p being in meters and σ_p in N/m.

For the general case, therefore, the pack ice force was calculated by the formula

$$F_p = 200\sqrt{A} \times \begin{cases} 0.360 + 257.000V_i - 12800.000V_i^2 & 0 \leq V_i < 0.015m/s, \\ 0.020 + 89.000V_i - 90.000V_i^2 & 0.015m/s \leq V_i \end{cases} \tag{3.28}$$

with pack ice force F_p in N, ice island area A in m^2, V_i in m/s. It was beyond the scope of this study to determine the parameters of pack ice pressure, and to consider the variation of pack ice thickness in space and time near the ice island.

3.6 Coriolis Force

Of the forces stated in the dynamic equation, only the Coriolis force, $\vec{F}_c$, has a precise formulation. The Coriolis force exerted on the ice island depends on the ice island velocity, the Coriolis parameter, and the mass of ice island, which can be written as

$$\vec{F}_c = -Mf\vec{k} \times \vec{V}_i \tag{3.29}.$$

In this simulation the Coriolis parameter was taken as a variable due to the large latitude scale motion of the ice island as $f = 2\Omega \sin\phi$. Ω is the angular speed of rotation of the earth as $\Omega = 7.292 \times 10^{-5}/s$, and ϕ is the latitude of the ice island position. The vector $\vec{k}$ is the vertical unit vector, positive upwards. The Coriolis force is larger than that for the same area of sea ice, due to the huge mass per unit area of an ice island, but the magnitude of the Coriolis acceleration

$$a_c = \frac{F_c}{M} = -fV_i \tag{3.30}$$

may be small for low values of ice island speed.

3.7 Sea Surface Tilt Force

Sea surface tilt force may be expressed as

$$\vec{F}_t = -mg\nabla H. \tag{3.31}$$

In this equation m is the mass of the ice island, g is the acceleration due to gravity, ∇ is the two-dimensional gradient operator, $\nabla = \vec{i}\frac{\partial}{\partial x} + \vec{j}\frac{\partial}{\partial y}$, and H is the dynamic

height of the sea surface. H can, in principle, include the variation of the sea surface height due to atmospheric pressure changes as well as to geostrophic current balance.

To evaluate the sea surface tilt force, Lu (1988) examined its magnitude by dynamic height calculations with sea level air pressure charts. For the typical case of Hobson's Choice Ice Island, he found that the sea surface tilt force was very small ($\leq 0.01MN$) in many movement episodes. The largest value he found was 0.7 MN, still very small compared to other forces in the same particular circumstances when the pack ice forces were 11.9 MN and 11.7 MN. In his maximum estimate, the sea surface tilt force was only about 5% of the pack ice force. Considering this, the sea surface tilt force was neglected in dynamic calculations of ice island movement for this simulation.

The values of parameters used in the dynamic simulation of ice island motion are listed in Table 2.

Table 2: Numerical parameters used in standard simulation.

$\rho_a = 1.3kg/m^3$	$\rho_w = 1032kg/m^3$
$C_a = 0.0012$	$C_w = 0.00132$
$\eta = 26°$ (wind turning angle)	$\theta = 25°$ (water drag turning angle)
$\rho_i = 872kg/m^3$	$C_f = 0.71$
$\Omega = 7.292 \times 10^{-5}$ rad/s	

CHAPTER 4

MONTE CARLO MODEL OF RANDOM WIND GENERATION

Since wind-driven motion was considered in this study as the primary cause of ice island movement, only the wind was considered as a random driving force in the simulations of the dynamic equation. In the Monte Carlo simulation of such ice island movement, one must generate the random wind according to its statistical distribution. For convenience, a Cartesian coordinate system was chosen with the North Pole as the origin, the X axis along the Greenwich meridian, and the Y axis along $90°E$. The geostrophic wind vector was considered in the form of two components u and v, along the X and Y axes respectively.

4.1 Two Independent Random Processes of Wind Components

For the correlation of the two components of wind, u and v, Thorndike (1982) obtained a zero covariance of u and v at two surface points. This implies zero correlation and one can therefore consider the wind random process as two independent random processes u(t) and v(t). From the time correlation function (Thorndike, 1982) for geostrophic wind components (u and v) at zero space lag, the correlation coefficient is less than 0.2 when the time lag is greater than 4 days (Figure 17). The correlation coefficient is even smaller for non-zero space lag and greater than 4 days time lag. As an approximation, the time dependency of wind components were considered within 4 days and a time-step of 2 days. Both of the distribution functions of the random processes u(t) and v(t) can be written as $F_3(x_1, x_2, x_3; t_1, t_2, t_3)$ where $t_2 = (t_1 + 2)$ days and $t_3 = (t_1 + 4)$ days. We assume an approximately Gaussian

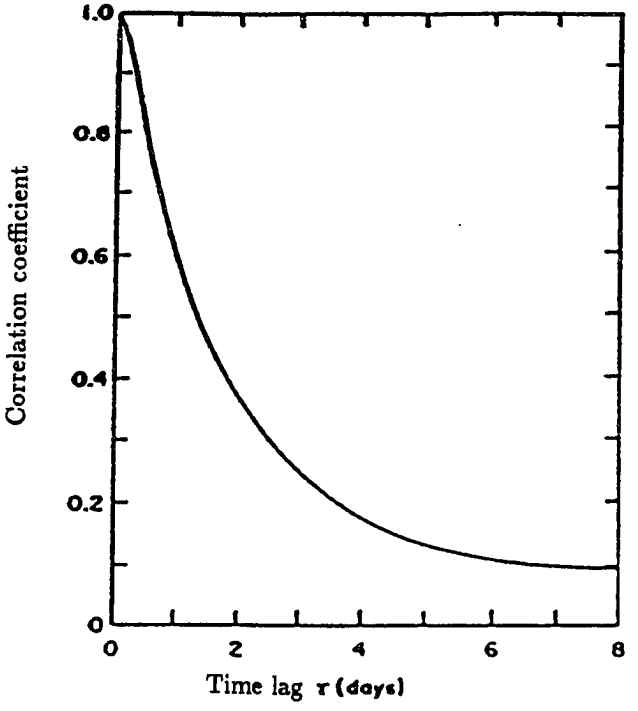

Figure 17: Observed time correlation function for geostrophic wind at zero lag. The variances are var(u) = var(v) = 44 $m^2 s^{-2}$ (source: Thorndike, 1982).

random process with a density function

$$f_3(x_1, x_2, x_3; t_1, t_2, t_3) = \frac{1}{\sqrt{(2\pi)^3 |C|}} exp[-\frac{1}{2}\left(\vec{X} - \vec{\mu}\right)' C^{-1}\left(\vec{X} - \vec{\mu}\right)] \qquad (4.1)$$

where the variable vector is

$$\vec{X} = \begin{pmatrix} x_1 \\ x_2 \\ x_3 \end{pmatrix}. \qquad (4.2)$$

the mean vector is

$$\vec{\mu} = \begin{pmatrix} \mu_x(t_1) \\ \mu_x(t_2) \\ \mu_x(t_3) \end{pmatrix}. \qquad (4.3)$$

and the autocovariance matrix

$$C = (c_x(t_i, t_j)) \qquad i, j = 1, 2, 3. \qquad (4.4)$$

is symmetric. $|C| = det.C$. This Gaussian process is completely determined by $\vec{\mu}$ and C.

4.2 Determination of Mean Vector $\vec{\mu}$ and Autocovariance Matrix C

The determination of the mean vector μ and the autocovariance matrix C may be obtained as follows. The mean vector of the geostrophic wind was obtained for each month from the mean surface pressure field charts by

$$\vec{V}_g = c\vec{k} \times \vec{\nabla} P \qquad (4.5)$$

where V_g is geostrophic speed, $c = (\rho_a f)^{-1}$, and P is sea level pressure. The monthly-averaged pressure maps of the Arctic Ocean (see Figures 18 to 29) (Colony, 1987) represented a refinement as compared to the previous use of quarterly maps (Li et al., 1988).

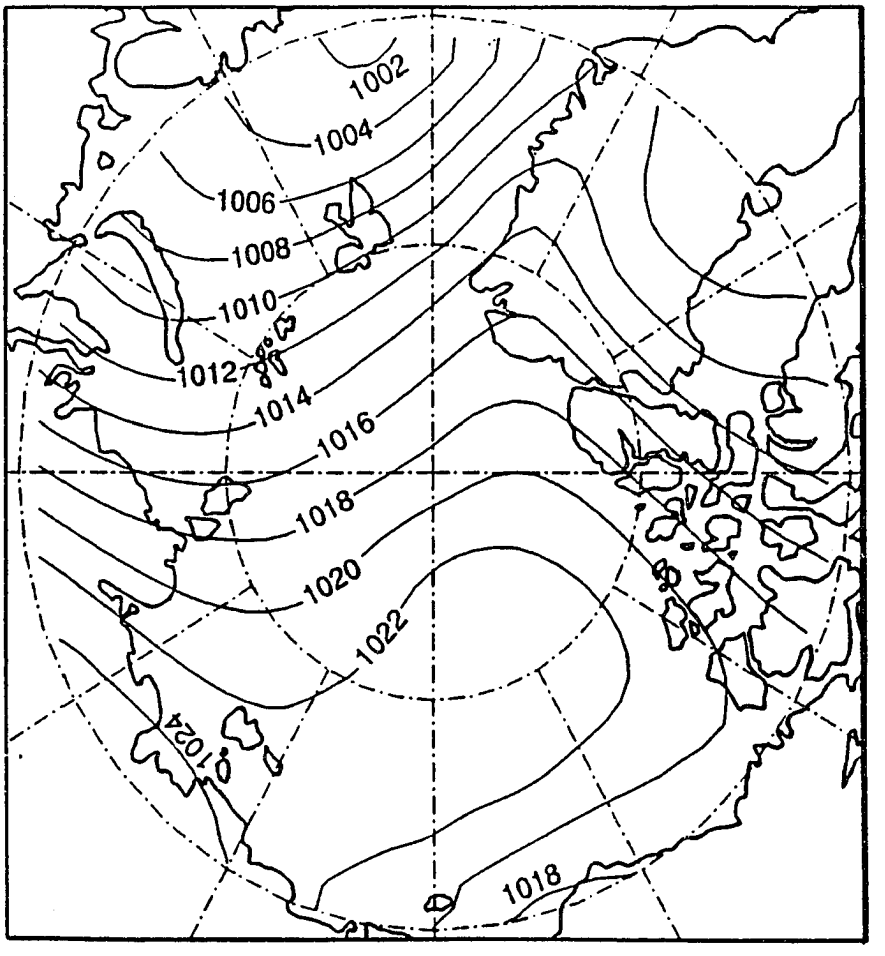

Figure 18: Monthly averaged pressure map over the Arctic Ocean for January (in millibars) (after Colony, 1987).

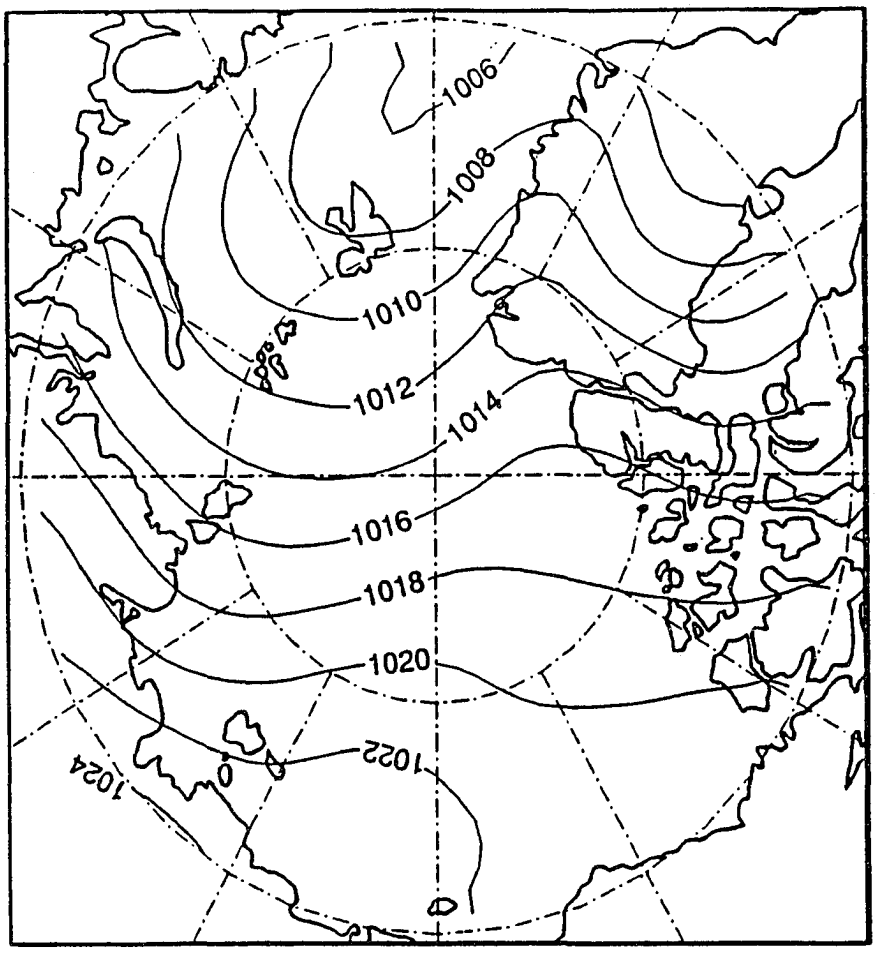

Figure 19: Monthly averaged pressure map over the Arctic Ocean for February (in millibars) (after Colony, 1987).

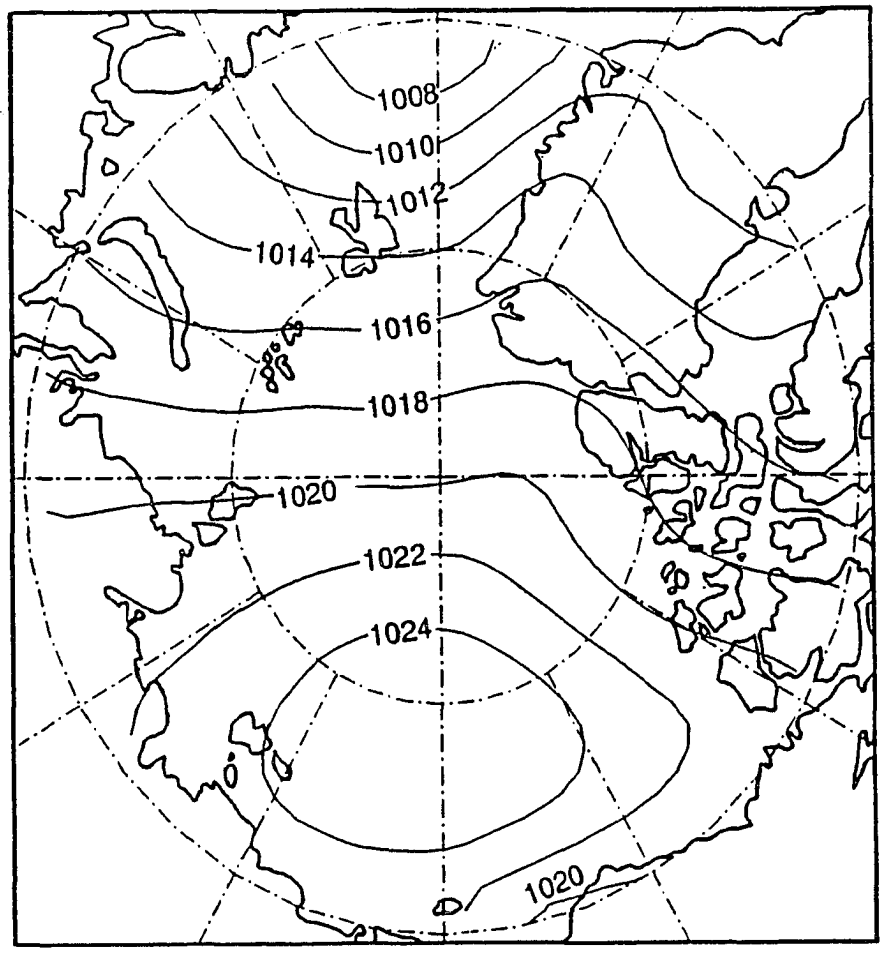

Figure 20: Monthly averaged pressure map over the Arctic Ocean for March (in millibars) (after Colony, 1987).

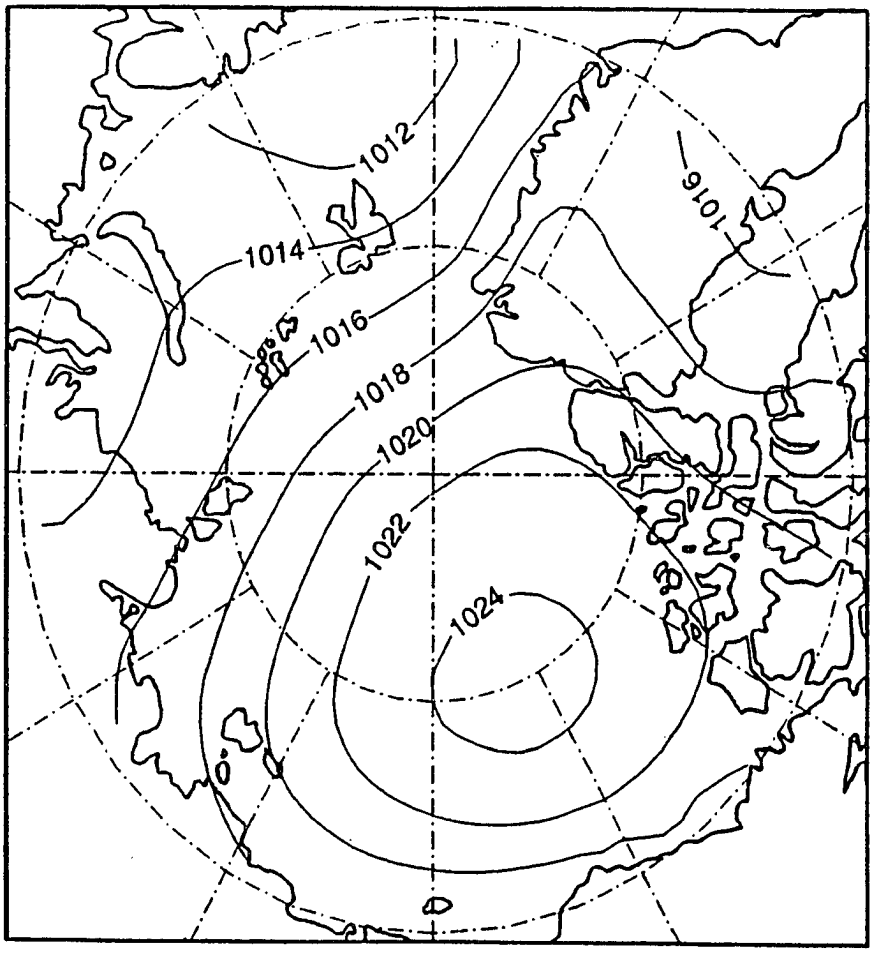

Figure 21: Monthly averaged pressure map over the Arctic Ocean for April (in millibars) (after Colony, 1987).

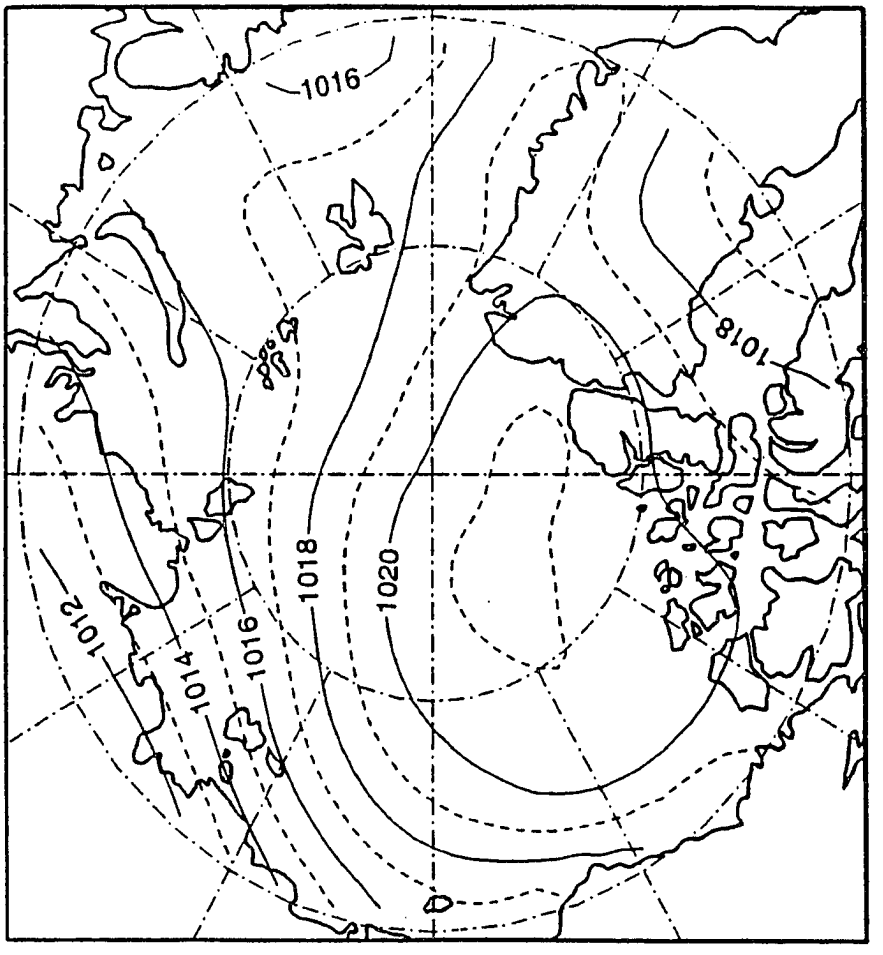

Figure 22: Monthly averaged pressure map over the Arctic Ocean for May (in millibars) (after Colony, 1987).

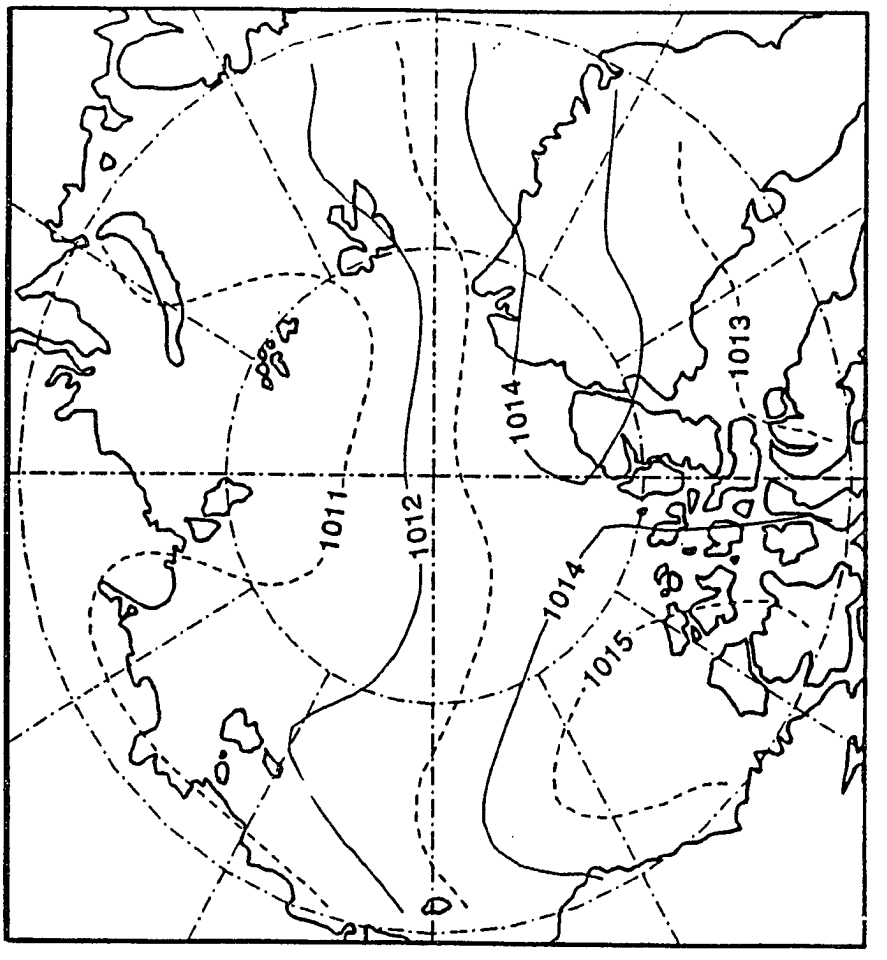

Figure 23: Monthly averaged pressure map over the Arctic Ocean for June (in millibars) (after Colony, 1987).

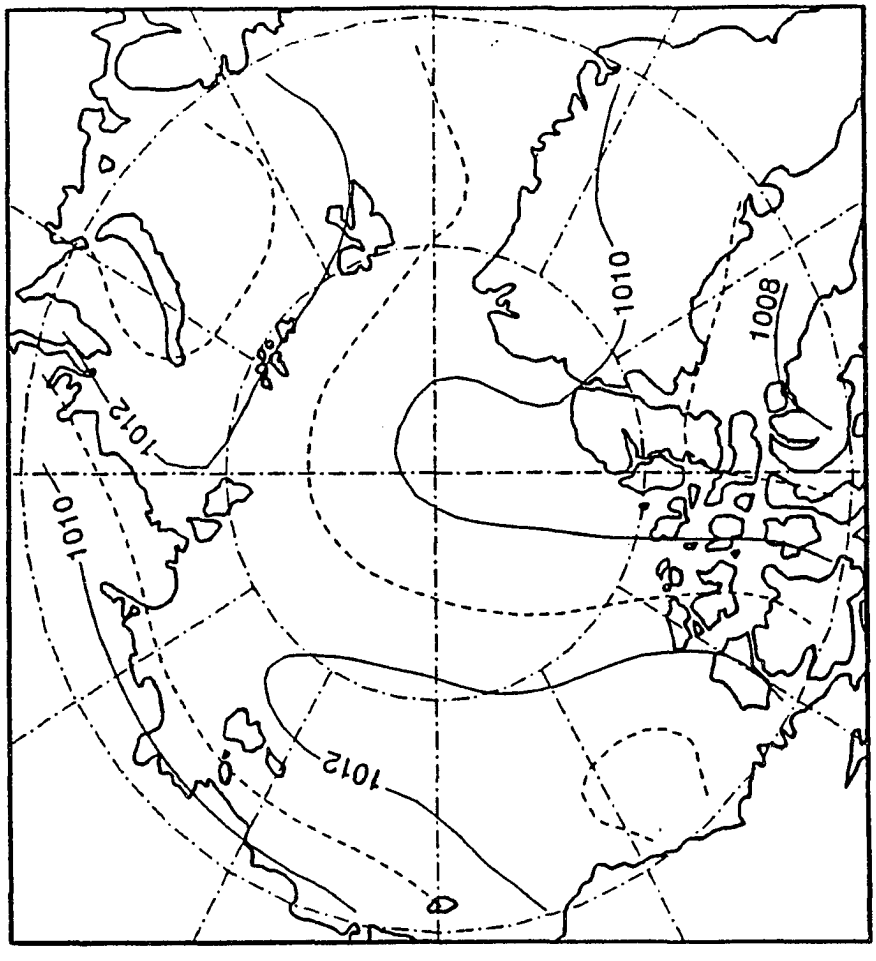

Figure 24: **Monthly averaged pressure map over the Arctic Ocean for July (in millibars) (after Colony, 1987).**

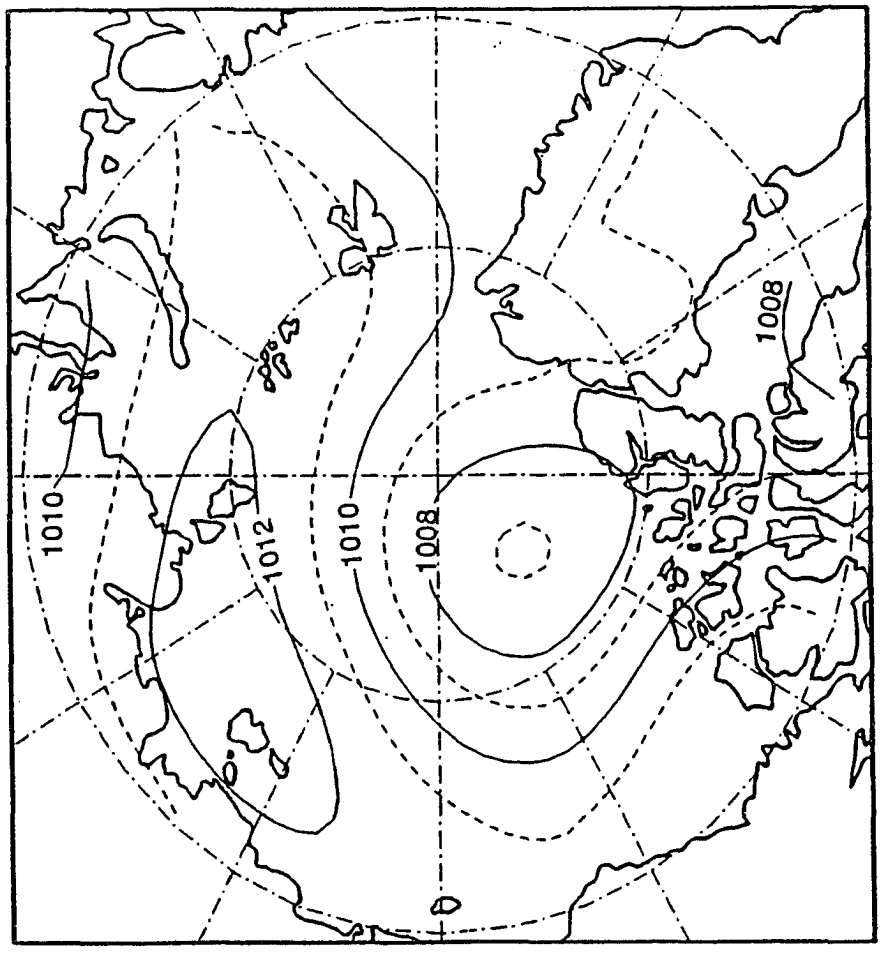

Figure 25: Monthly averaged pressure map over the Arctic Ocean for August (in millibars) (after Colony, 1987).

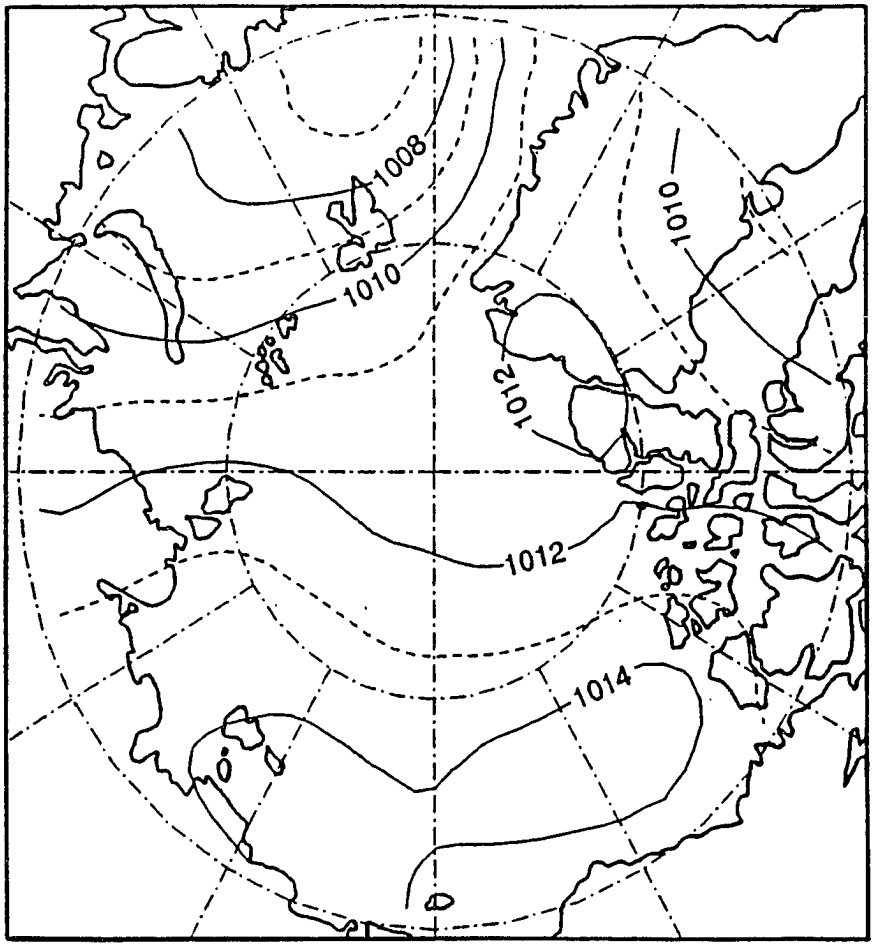

Figure 26: **Monthly averaged pressure map over the Arctic Ocean for September (in millibars) (after Colony, 1987).**

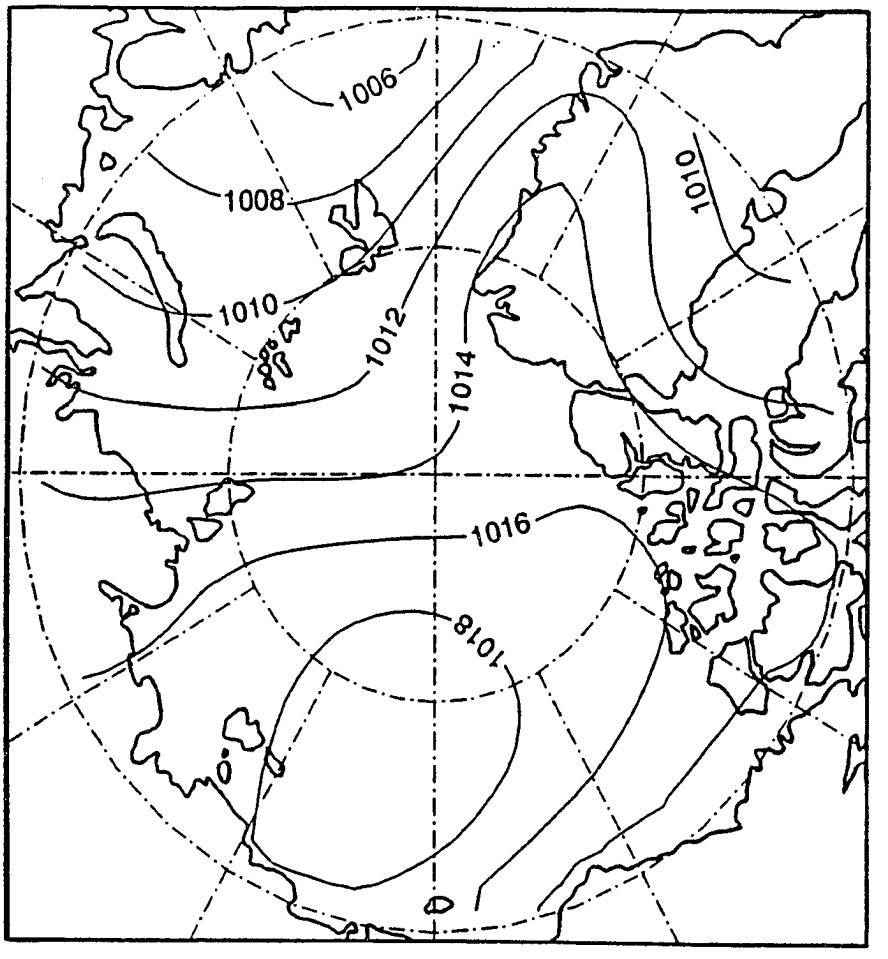

Figure 27: **Monthly averaged pressure map over the Arctic Ocean for October (in millibars) (after Colony, 1987).**

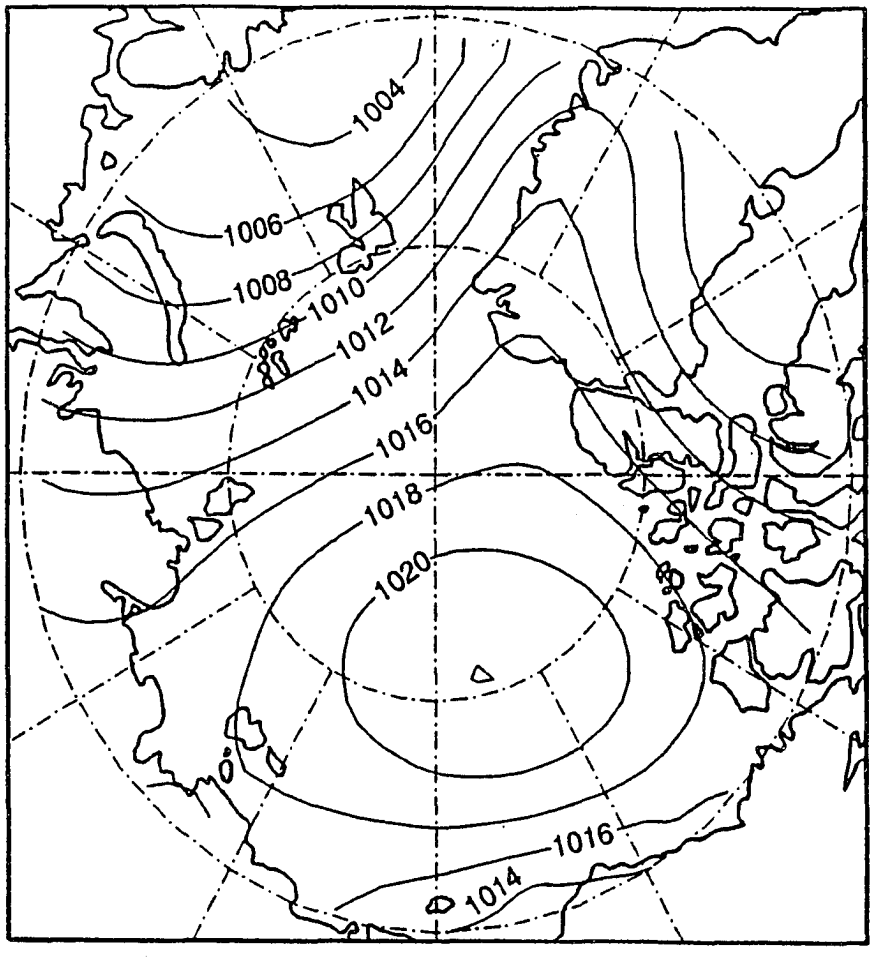

Figure 28: Monthly averaged pressure map over the Arctic Ocean for November (in millibars) (after Colony, 1987).

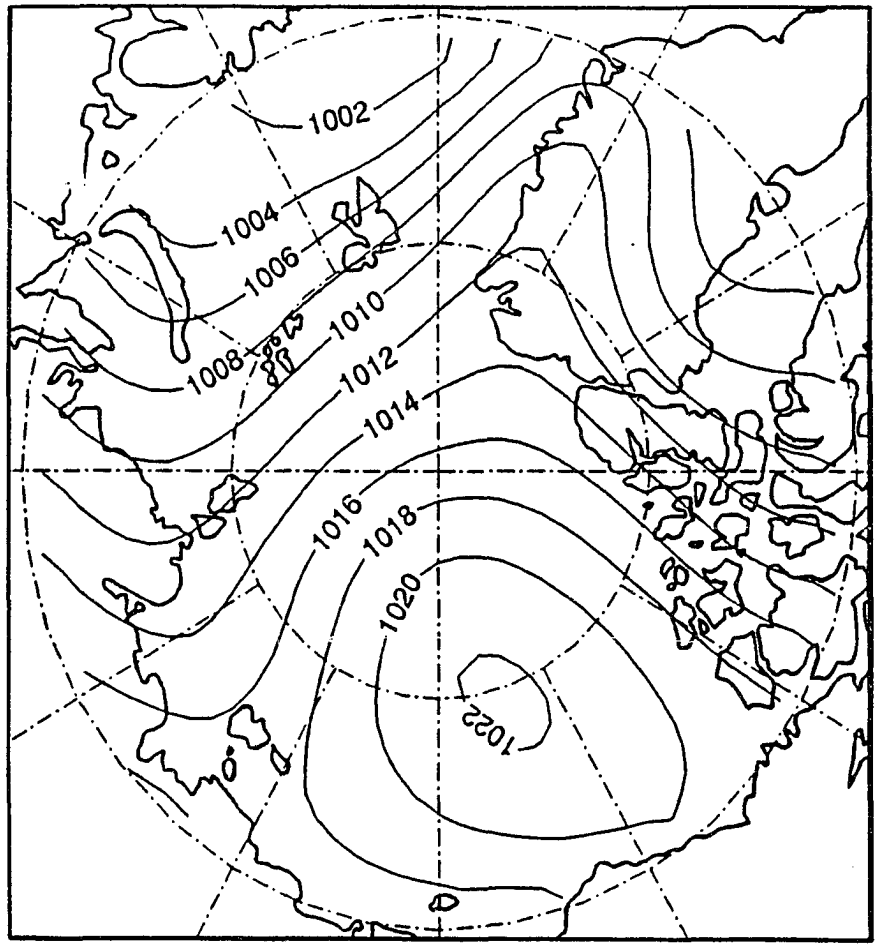

Figure 29: Monthly averaged pressure map over the Arctic Ocean for December (in millibars) (after Colony, 1987).

In general, the annually-averaged surface geostrophic wind field over the Arctic Ocean (Figure 30) (Colony, 1987) is an anticyclonic system. When considered over short periods of time (months), however, it is more variable. The maps from October to May show that the average sea level air circulation is often dominated by a large high pressure center over the west portion of the Arctic Ocean, i.e., anticyclones are common over the frozen winter ocean. The highest mean pressure gradient period, on the average, appears in December. After May, the mean pressure field undergoes rapid change, high pressure gradients are weaker and the prevailing air streams are directed from the Chukchi Sea to the Greenland-Spitsbergen area. In summer (August), there is commonly a relatively weak mean low pressure centered near the North Pole, and the prevailing circulation is cyclonic. In September, there is an average prevailing weak air stream from the Siberian continent over the polar region to the Canada-Greenland area.

From an analysis of observed data, a threshold wind speed of about $5m/s$ appears to be necessary to initiate ice island motion (Lu, 1988). A $5.00m/s$ threshold wind speed therefore was used in the simulation.

Thorndike (1982) presented a variance of $44m^2s^{-2}$ for u and v, and a formula for calculating the autocovariances of wind components, which can be written as

$$C_i(t,t+\tau) = c^2\Big[\Big(\frac{\Delta x_i^2}{r^3} - \frac{1}{r}\Big)\frac{\partial R(r,\tau)}{\partial r} - \frac{\Delta x_i^2}{r^2}\frac{\partial^2 R(r,\tau)}{\partial r^2}\Big] \quad i = 1,2. \qquad (4.6)$$

where $C_i = C_u$ and $\Delta x_i = \Delta x$ for $i = 1$, $C_i = C_v$ and $\Delta x_i = \Delta y$ for $i = 2$. The term r is space lag in kilometers, the quantity τ is time lag in days, and $R(r,\tau)$ is the autocovariance function of pressure shown in Figure 31 (Thorndike, 1982). For a time lag of zero, two and four days, $R(r,\tau)$ can be approximately expressed as

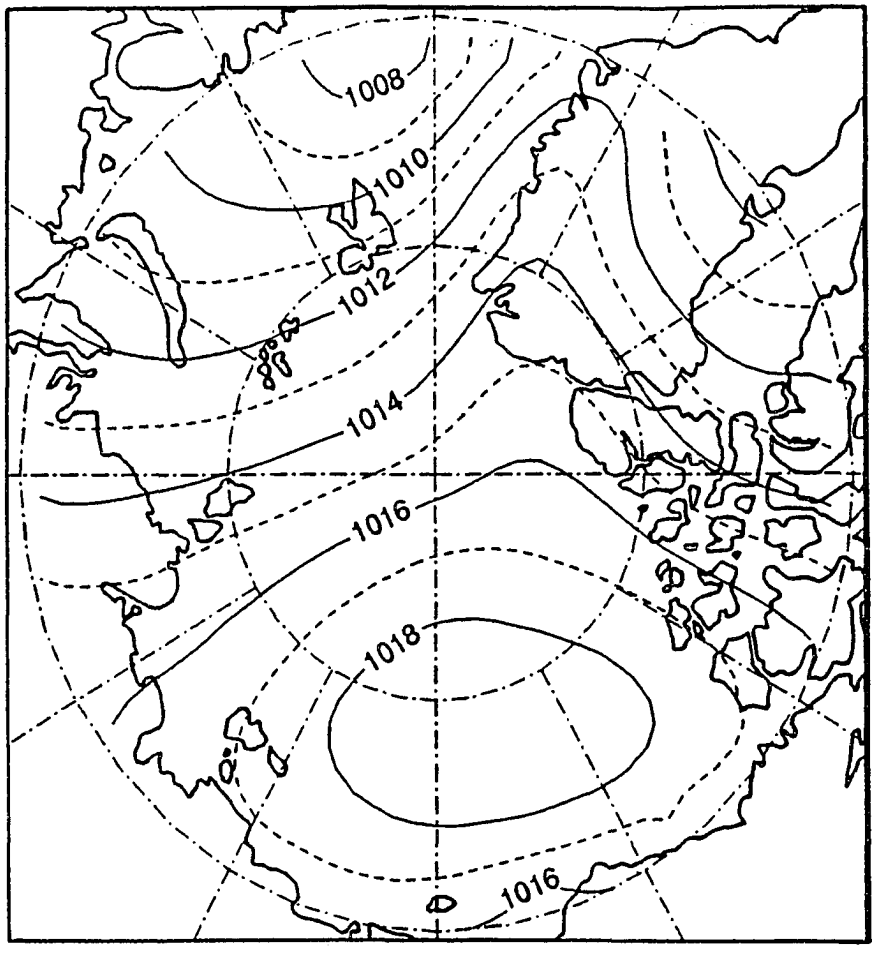

Figure 30: Annually averaged pressure map over the Arctic Ocean (in millibars) (after Colony, 1987).

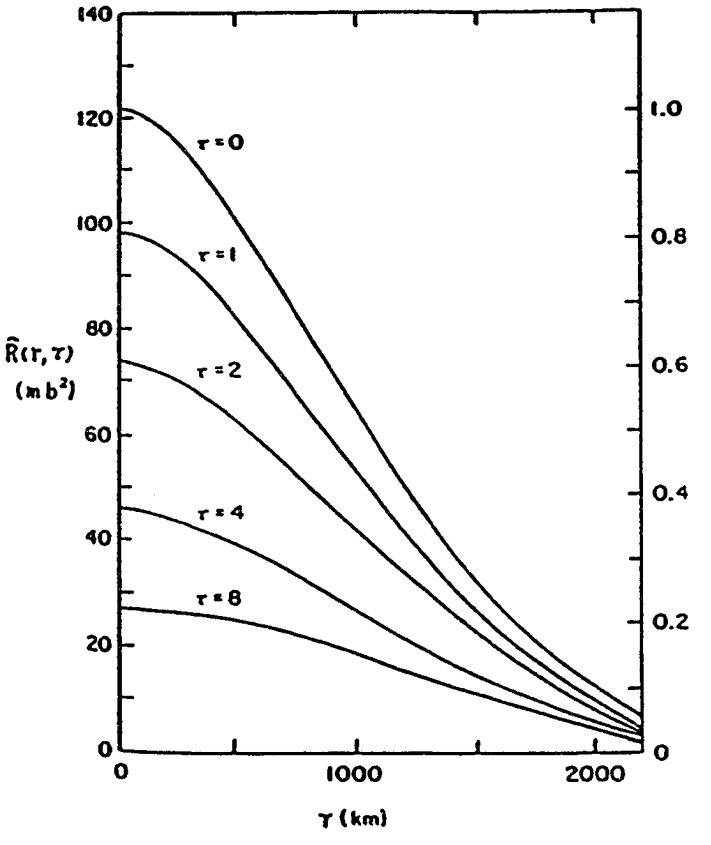

Figure 31: Observed autocovariance function for pressure at space lag r(km) and time lag τ (days) (from Thorndike, 1982).

$$R(r,\tau) = \sigma(\tau)^2 exp[-r^2/1300^2] \tag{4.7}$$

where

$$\sigma(\tau)^2 = \begin{cases} 122 & \text{if } \tau = 0, \\ 74 & \text{if } \tau = 2 \text{ days}, \\ 46 & \text{if } \tau = 4 \text{ days}. \end{cases} \tag{4.8}$$

Then from $R(r,\tau)$, one may obtain

$$C_i(t,t+\tau) = 0.36\left[1 - 2\left(\frac{\Delta x_i}{1300}\right)^2\right] exp\left[-(r/1300)^2\right]\sigma(\tau)^2 \quad i = 1,2. \tag{4.9}$$

Thus the elements of the autocovariance matrix of the geostrophic wind C are:

$$\begin{aligned} C_x(t_j,t_j) &= 44 && j = 1,2,3. \\ C_x(t_1,t_2) &= C_x(t_2,t_3) = C_i(t,t+2) && i = 1,2. \\ C_x(t_1,t_3) &= C_i(t,t+4) && i = 1,2. \end{aligned} \tag{4.10}$$

4.3 Transformation From Uniform Random Numbers to a Gaussian-distributed Random Vector

To produce a Gaussian-distributed random vector of geostrophic wind $\vec{X} = [x(t_1), x(t_2), x(t_3)]$, which has a mean vector $\vec{\mu}$ and autocovariance matrix C, from uniform random numbers generated directly by the computer, procedures described by Shreider (1962) were used. For independent random numbers λ_i $(i = 1,2,\ldots,n)$ uniformly distributed over the interval $(0,1)$, the mean is $\frac{1}{2}$ and the standard deviation is $\frac{1}{2\sqrt{3}}$. From the Central Limit Theorem, one can obtain a Gaussian-distributed random number ξ, by the relationship

$$\xi = \lambda_1 + \lambda_2 + \cdots + \lambda_{12} - 6 \tag{4.11}$$

which has zero mean and variance of 1.

To produce a Gaussian-distributed random vector $\vec{\eta} = (\eta_1, \eta_2, \eta_3)$ whose mean vector $\vec{\mu} = 0$ with three independent Gaussian-distributed random numbers ξ_i $(i = 1, 2, 3)$ whose mean $E(\xi_i) = 0$ and variance $D(\xi_i) = 1$, a linear transformation was chosen as

$$\begin{aligned} \eta_1 &= a_{11}\xi_1 \\ \eta_2 &= a_{21}\xi_1 + a_{22}\xi_2 \\ \eta_3 &= a_{31}\xi_1 + a_{32}\xi_2 + a_{33}\xi_3 \end{aligned} \tag{4.12}$$

where a_{ij} $(i, j = 1, 2, 3)$ are to be found from the conditions

$$E[(\eta_k - 0)(\eta_l - 0)] = E(\eta_k \eta_l) = C_{kl} \quad k = 1, 2, 3 \tag{4.13}$$

and

$$E[(\xi_k - 0)(\xi_l - 0)] = E(\xi_k \xi_l) = \delta_{kl} \quad l = 1, 2, 3, \tag{4.14}$$

where C_{kl} are elements of the autocovariance matrix of vector $\vec{\eta}$. Therefore we have

$$E(\eta_1^2) = a_{11}E(\xi_1^2) = a_{11}^2 = c_{11}, \tag{4.15}$$

and

$$a_{11} = \sqrt{c_{11}}. \tag{4.16}$$

Similarly, we have

$$a_{21} = \frac{c_{21}}{a_{11}} \tag{4.17}$$

$$a_{22} = \sqrt{c_{22} - a_{21}^2} \tag{4.18}$$

$$a_{31} = \frac{c_{31}}{a_{11}} \tag{4.19}$$

$$a_{32} = \frac{c_{32} - a_{21}a_{31}}{a_{22}} \tag{4.20}$$

$$a_{33} = \sqrt{c_{33} - a_{31}^2 - a_{32}^2} \tag{4.21}$$

Then one obtains a Gaussian-distributed random vector $\vec{X}$ with mean vector $\vec{\mu}$ by the relation

$$\vec{X} = \vec{\eta} + \vec{\mu}. \tag{4.22}$$

CHAPTER 5

SIMULATION DOMAIN AND MESH

5.1 Simulation Domain

The domain used in the ice island movement simulation includes most of the Arctic Ocean and some marginal seas, except the shallow water areas, and is surrounded by simulated land boundaries and four open water boundaries(Figure 32). Ice islands will ground on the sea floor when they move towards the shore in shallow water coastal zones, and the water depth at which they will ground depends on the ice island thickness. On the basis of recent ice island thickness observations(Jeffries et al., 1988), a 36-meter water depth contour was considered to be appropriate as the land boundary, with some simplification on the broad continental shelf off Siberia. In the simulation, once the ice island reaches the boundary it stops moving towards the coast and can only move in a direction along or away from the coast depending on the wind direction. The open water boundaries are considered to be the main connections of the Arctic Ocean with other oceans, allowing ice islands to move out of the Arctic Ocean. The first one is simply represented as a straight line from the northeast end of Greenland to Severnaya Zemlya. The second one is at the shallow and narrow Bering Strait. The third one is at the mouth of Nares Strait. The final open water boundary is at the Amundsen Gulf, between Banks Island and the North American mainland. Once an ice island moves beyond one of the open water boundaries, it is considered to have escaped permanently from the Arctic Ocean. There are also other connections from the Arctic Ocean through the Canadian Arctic Archipelago channels. However, these passages are usually covered by fast ice, and

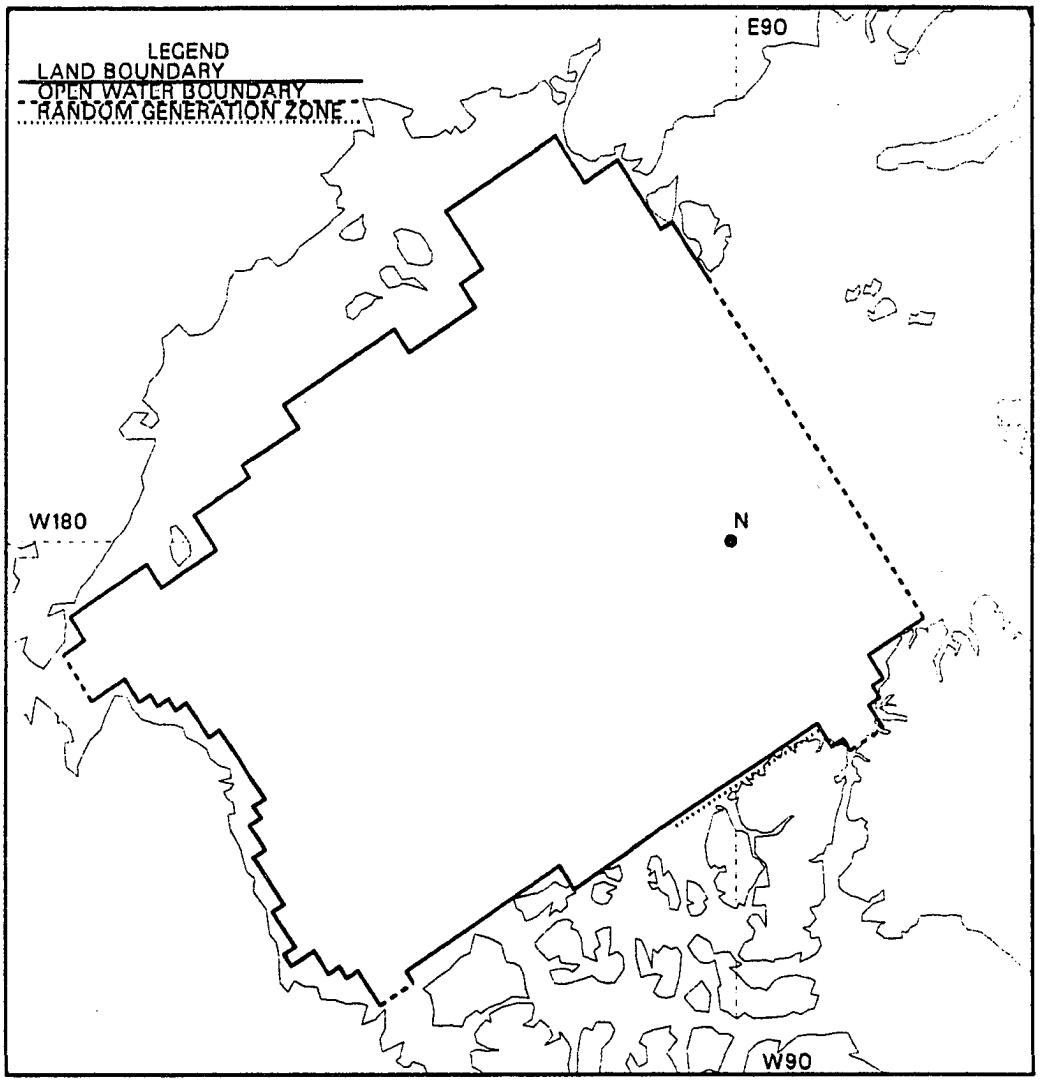

Figure 32: Ice island movement simulation boundaries.

ice islands penetrate them only infrequently; thus, these connections are considered as land boundaries in the simulation.

5.2 Simulation Mesh

The simulation is performed on a 56×51 element grid with a resolution of 50 km for recording movement events of ice islands(Figure 33), and with a 10×9 element grid with a resolution of 300 km for the monthly-averaged wind field, and for the water current field(Figure 34).

5.3 Probability Calculation of Ice Island Trajectories

The simulation area is divided into grid blocks, each with a dimension of $50 \times 50 km$ for recording the passage of an ice island. The event of one ice island passing into an individual block(i,j) during every 2 days is recorded as 1 and added to the accumulated sum $S_{i,j}$ for this block. After a long running time, normalized in n years, one obtains an approximation of the probability of ice islands passing through a block during n years as

$$P_{i,j} = \frac{S_{i,j}}{\sum_{i,j=1}^{i=56,j=51} S_{i,j}}.$$

The return period (years) for block(i,j) is

$$R_{i,j} = \frac{n}{S_{i,j}}.$$

5.4 Simulation Program Flow Chart

For completeness the computer program flow chart for the simulation of random ice island trajectories is shown in Figure 35.

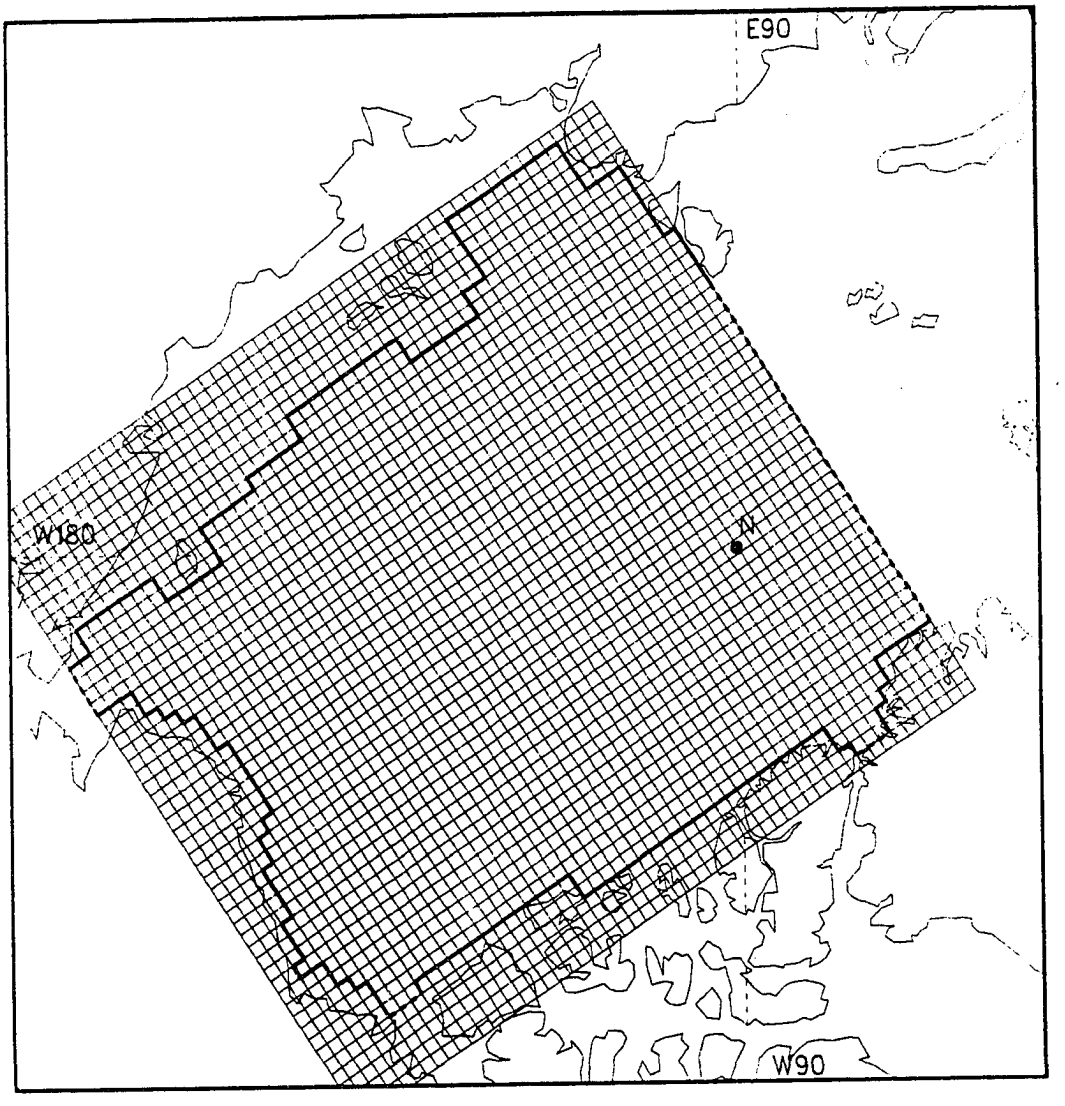

Figure 33: Simulation mesh for trajectory calculation, 56 x 51 elements with 50 km spacing.

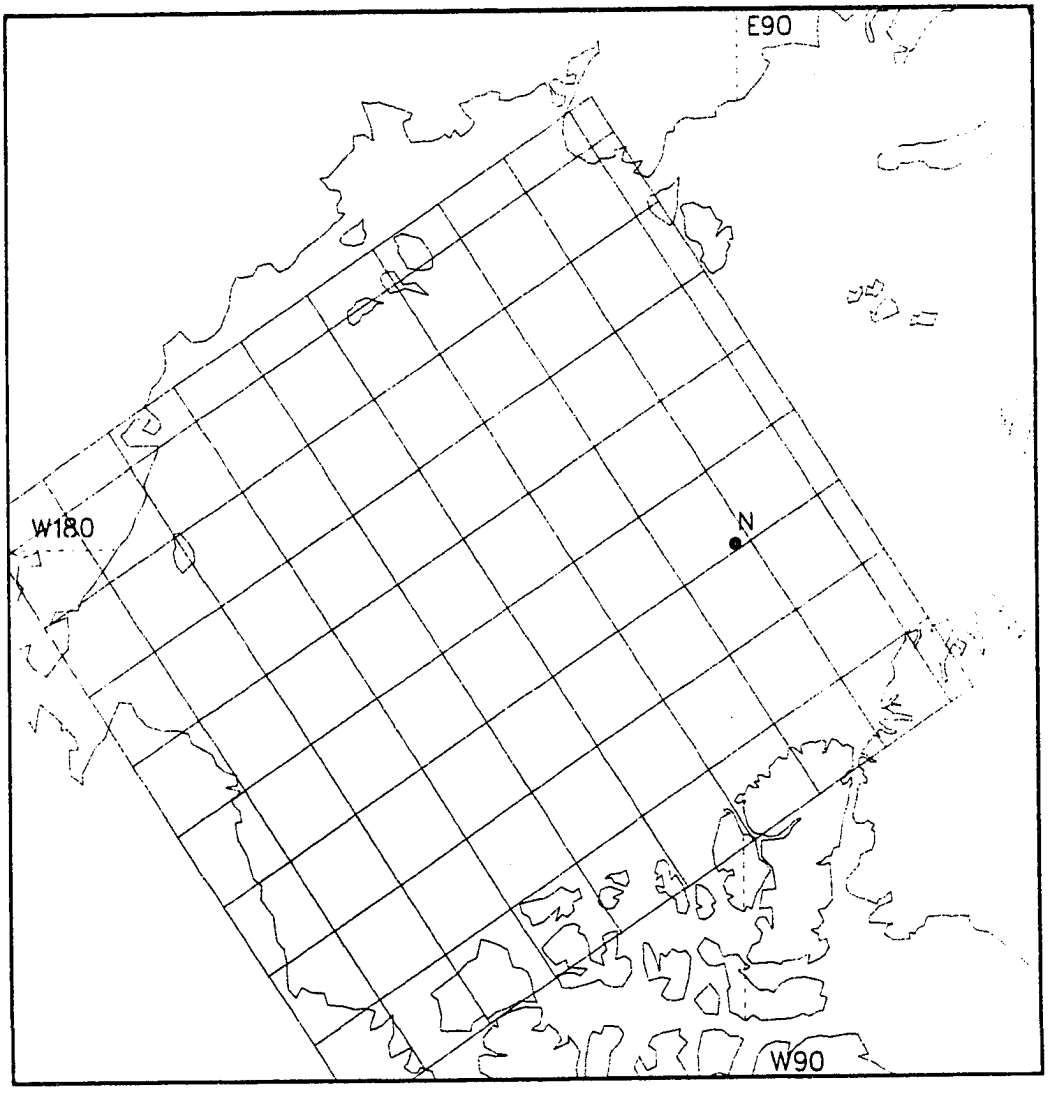

Figure 34: Simulation mesh for wind calculation, 10 x 9 elements with 300 km spacing.

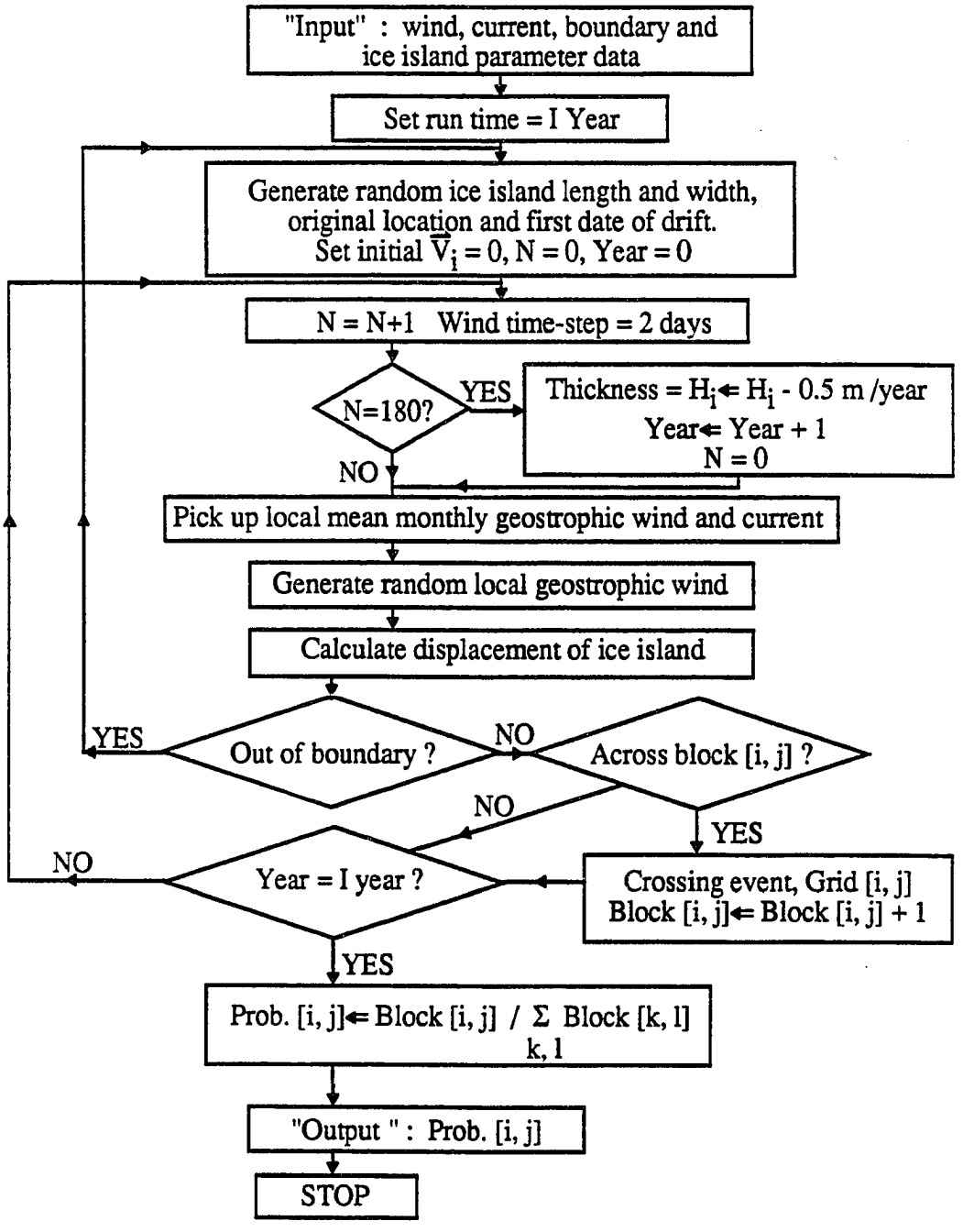

Figure 35: Computer simulation program flow chart.

CHAPTER 6

SIMULATION RESULTS AND COMPARISONS

Several results were recorded in the simulation, including random trajectories, lifetimes of ice islands, total numbers of live ice islands in the Arctic Ocean, frequencies of ice island ejection through each open water boundary, and probability recurrences (in years) of ice island trajectories. All of these results are explained and compared with observed data, to the extent that the data are available. Certain sensitivity tests are also described.

6.1 Trajectory Patterns

In the simulation, each random ice island trajectory can be tracked, and the first 21 trajectories were recorded in this simulation. A total of 776 ice island trajectories were, however, used, over a generation interval of 1000 years. In order to be more explicit, these figures are plotted in different data point intervals, as shown in Figure 36 to 56.

From these random trajectories, two basic patterns of ice island trajectories can be seen. The first pattern is a short trajectory near the northern side of Axel Heiberg and Ellesmere Islands, directed to an ejecting route at north Greenland (Figure 41) and Nares Strait (Figure 55, 56). Few ice island trajectories are in this pattern with only about 14% frequency, calculated from these results. The ice island WH-5, which is known to have entered Robeson Channel, Nares Strait shortly after generation, is the closest known example of this brief lifetime (Nutt, 1966). The second pattern is the clockwise circulation or gyre pattern, in a large scale, covering the Beaufort Sea,

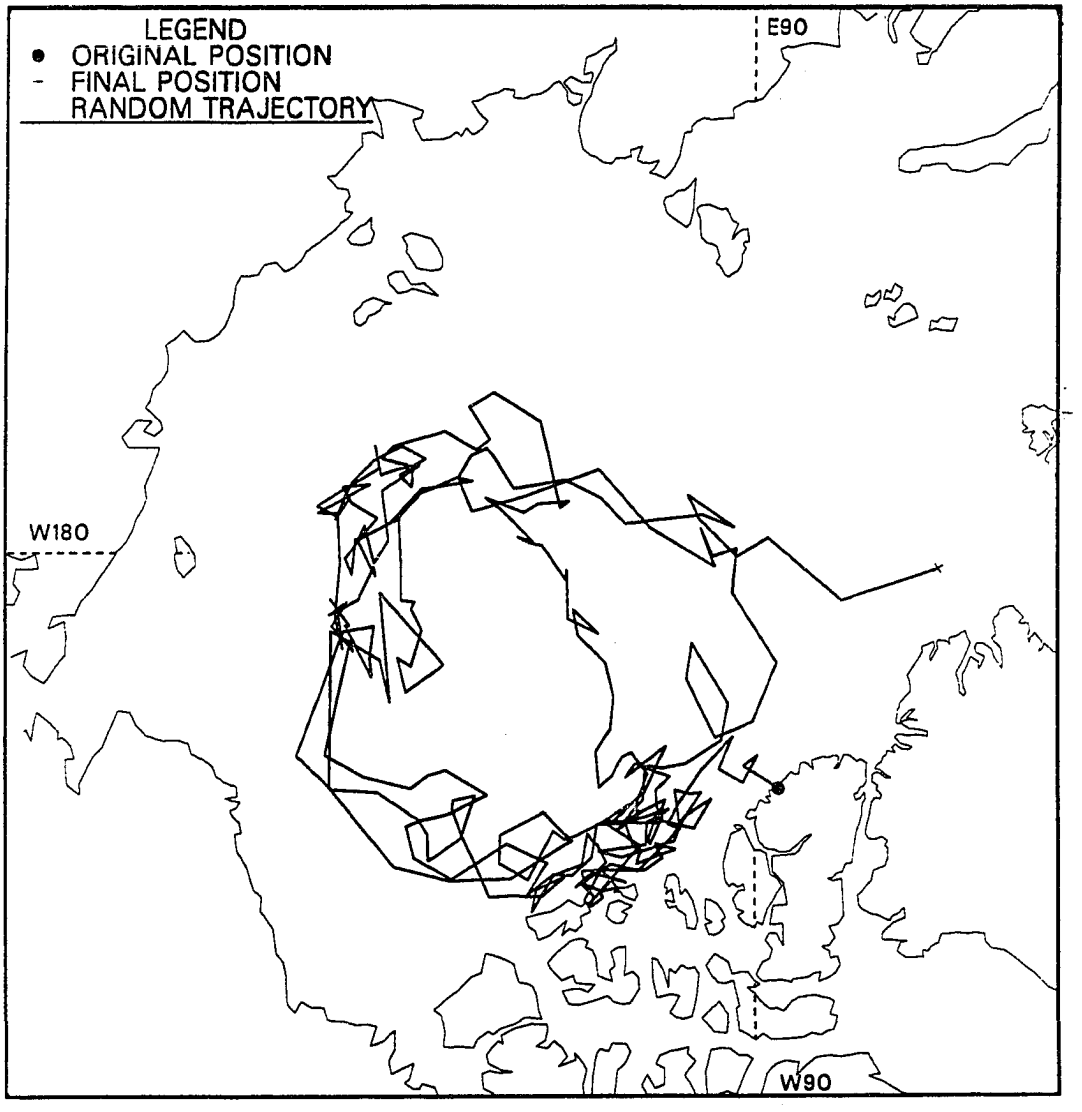

Figure 36: Random ice island trajectory 1.

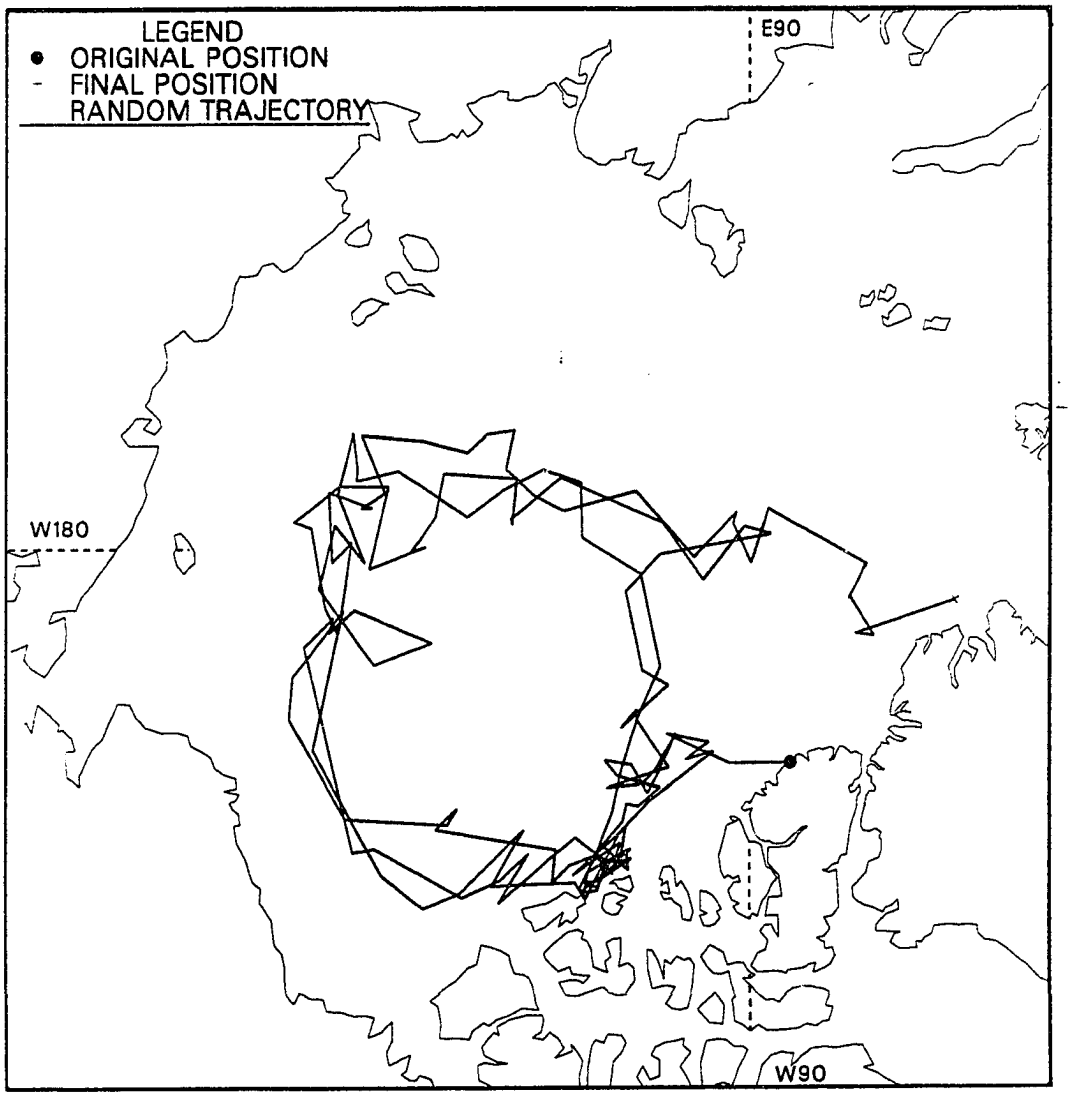

Figure 37: Random ice island trajectory 2.

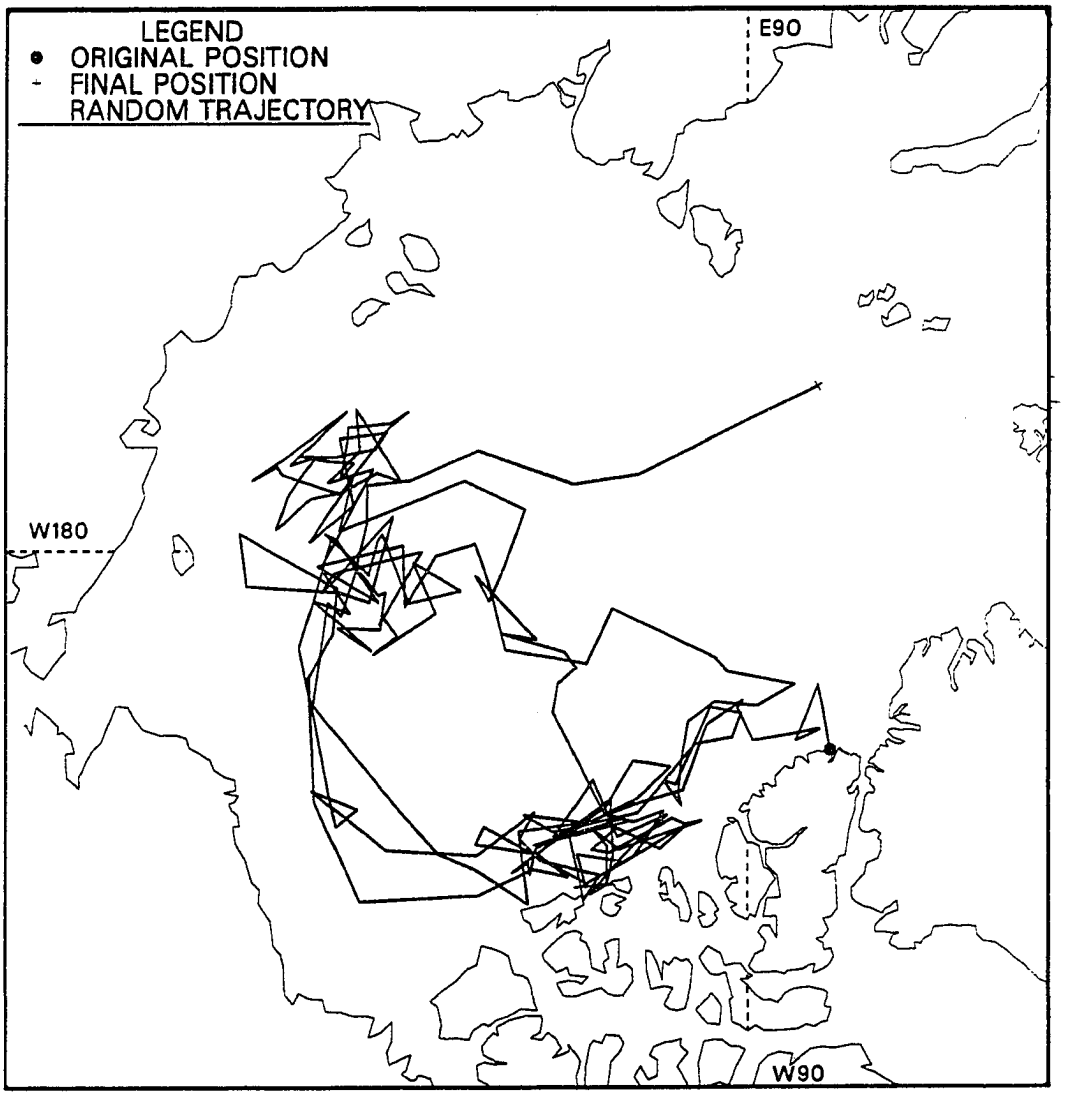

Figure 38: Random ice island trajectory 3.

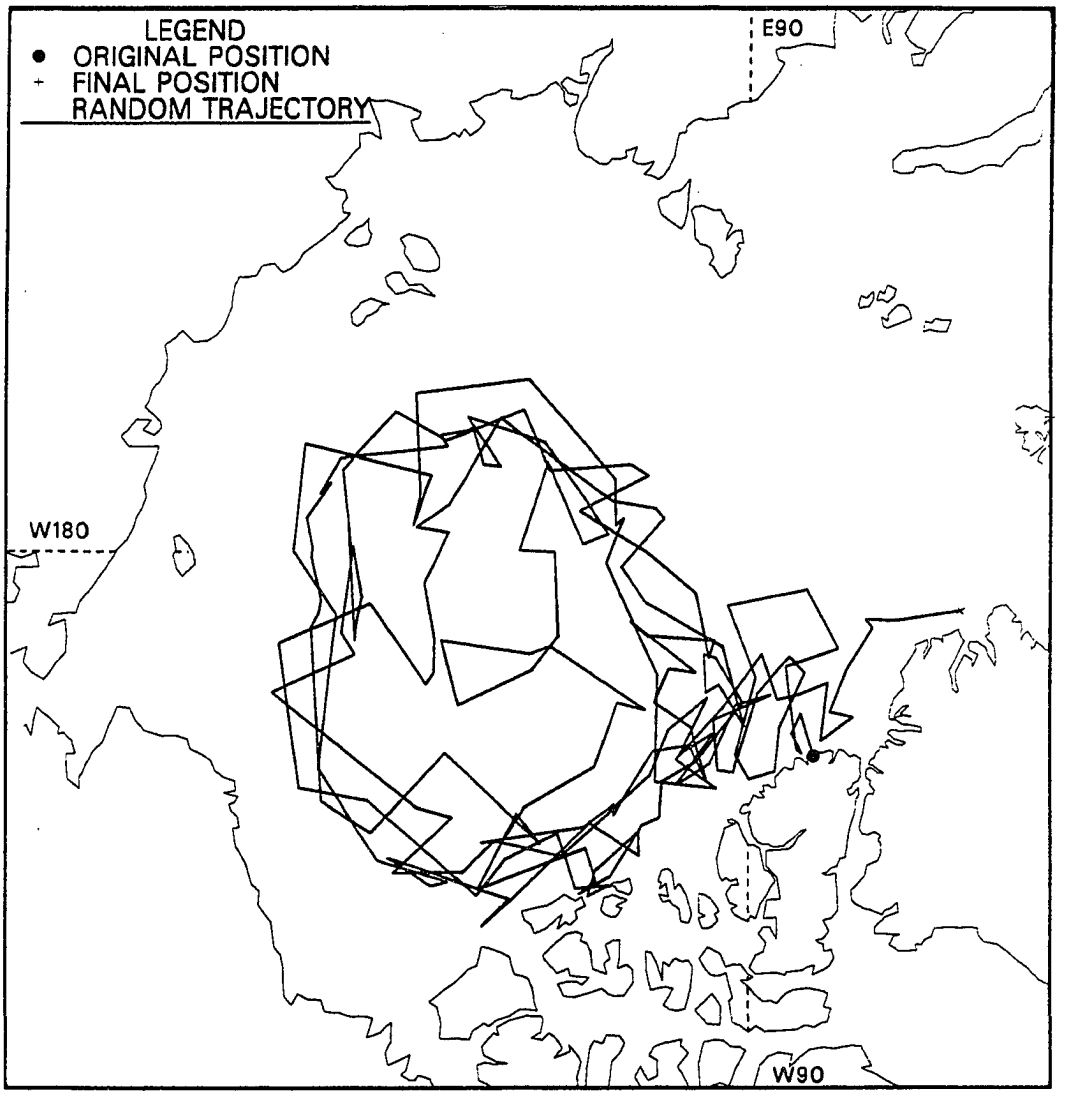

Figure 39: Random ice island trajectory 4.

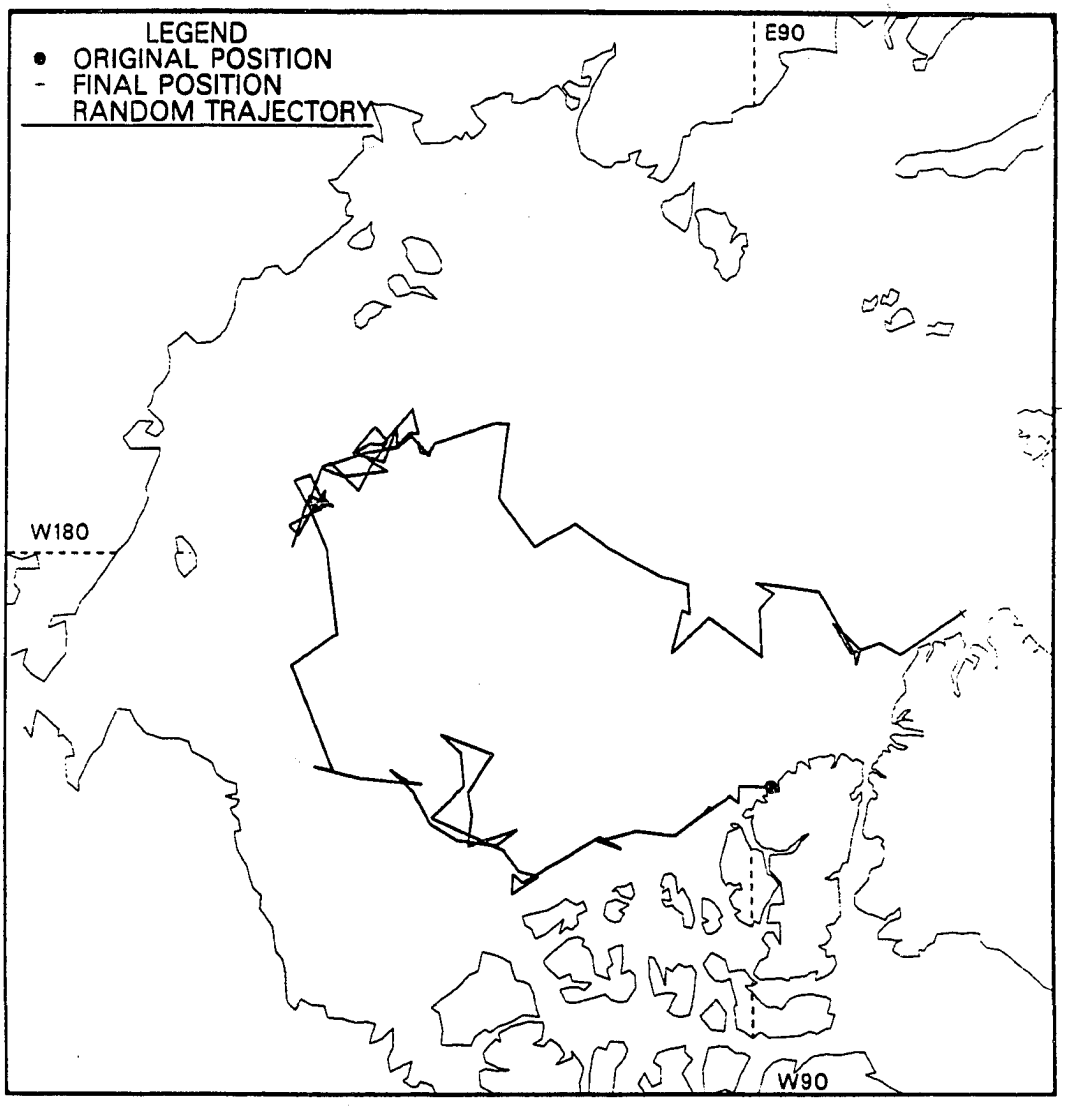

Figure 40: Random ice island trajectory 5.

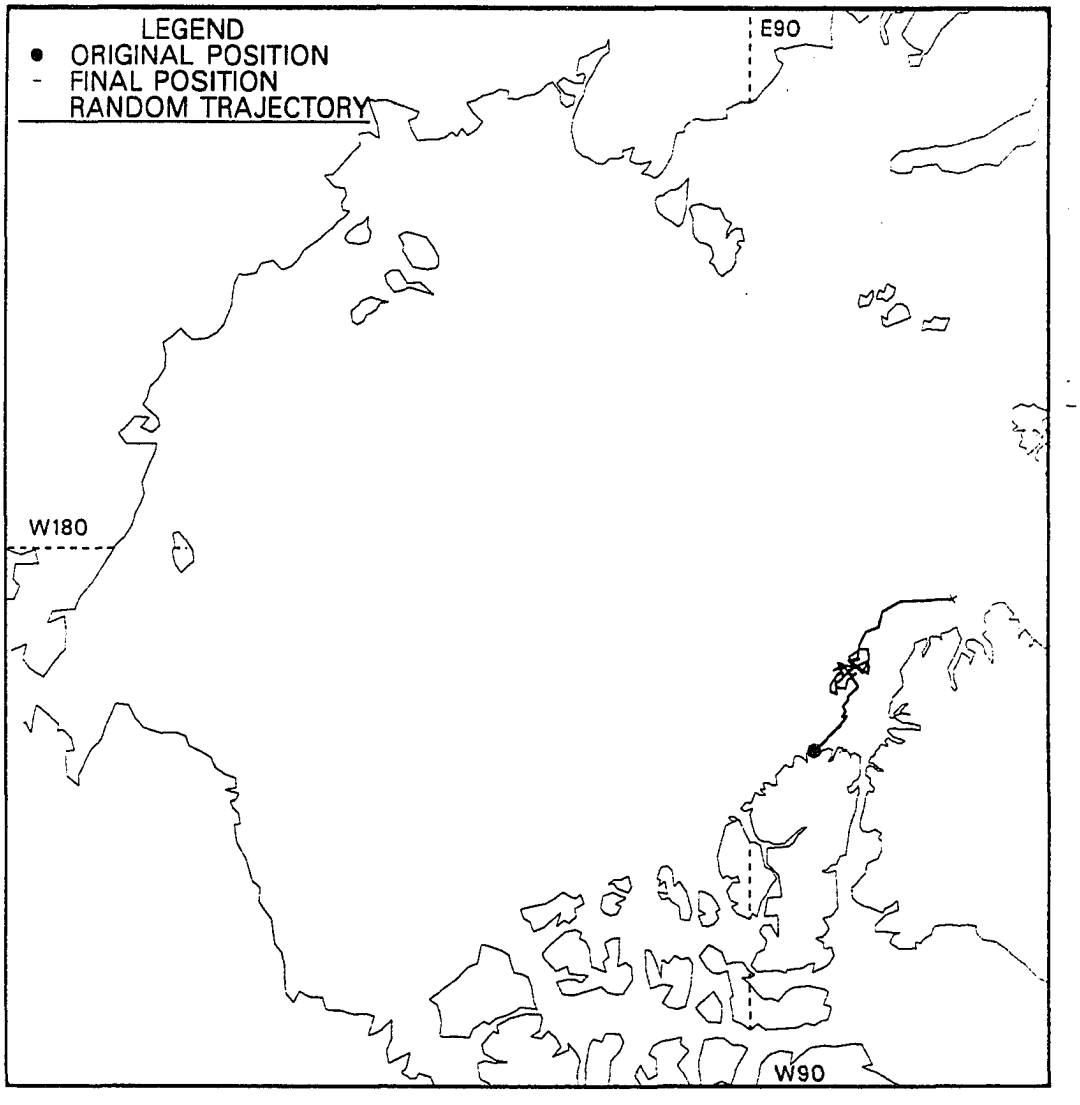

Figure 41: Random ice island trajectory 6.

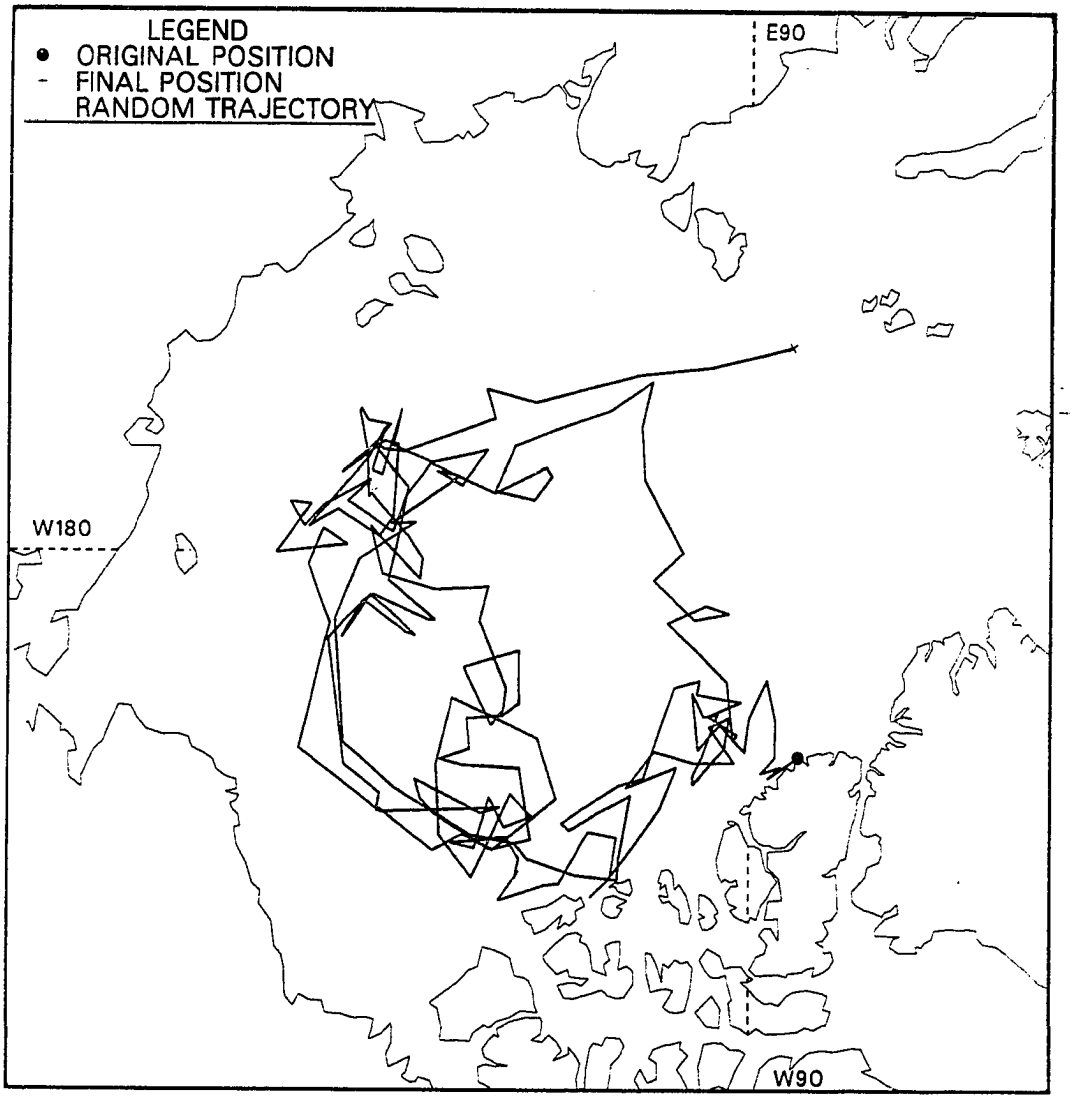

Figure 42: Random ice island trajectory 7.

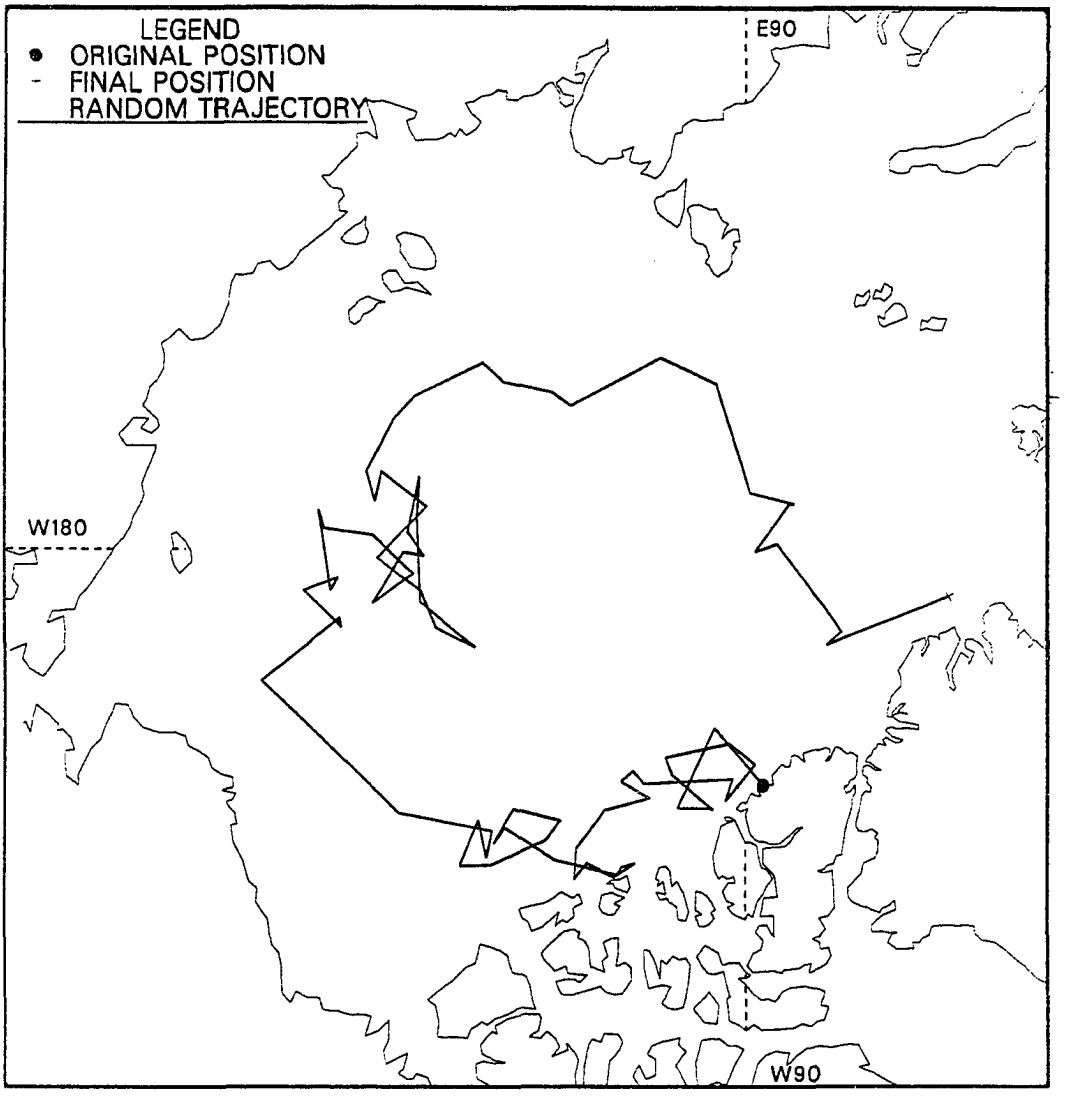

Figure 43: Random ice island trajectory 8.

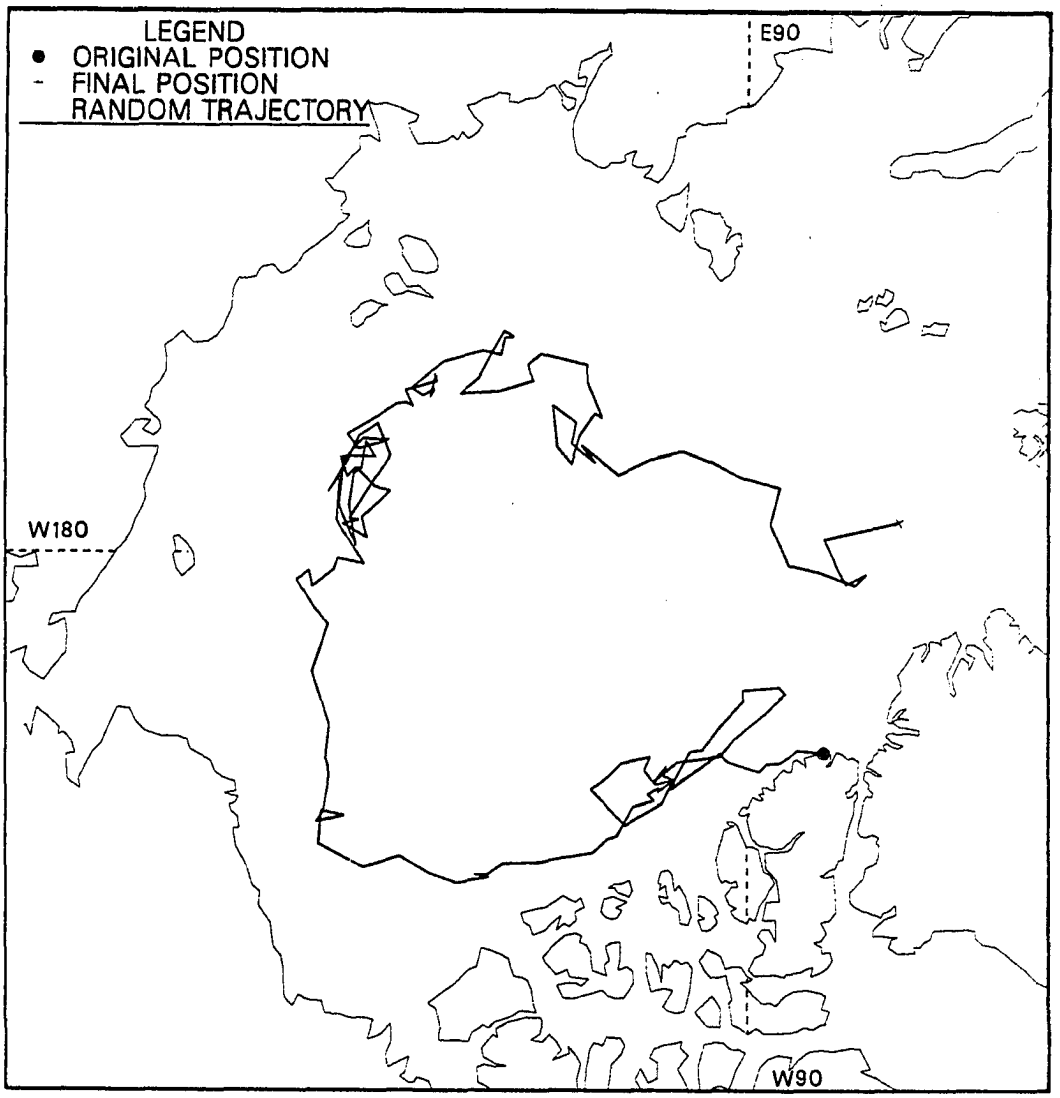

Figure 44: Random ice island trajectory 9.

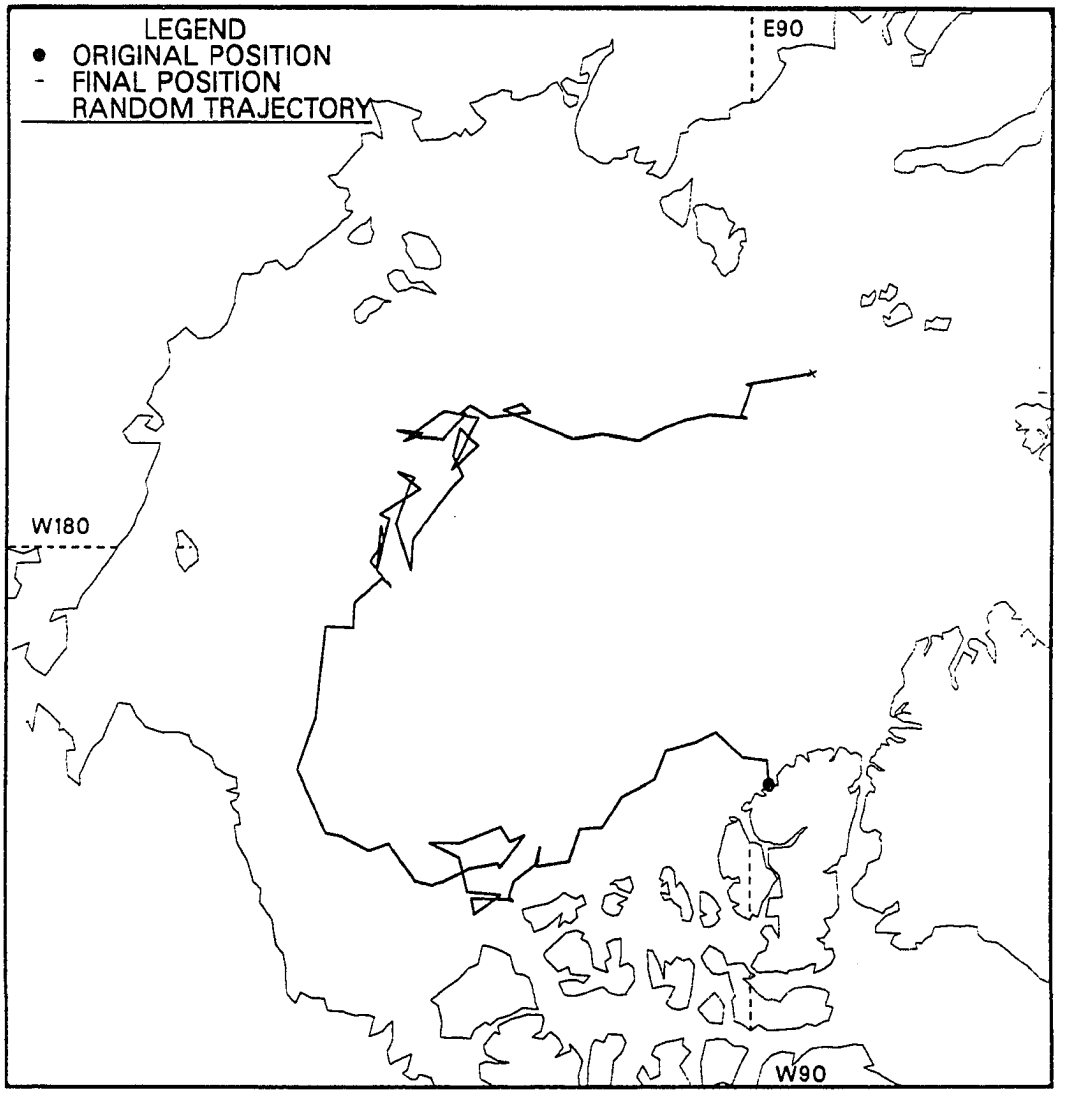

Figure 45: Random ice island trajectory 10.

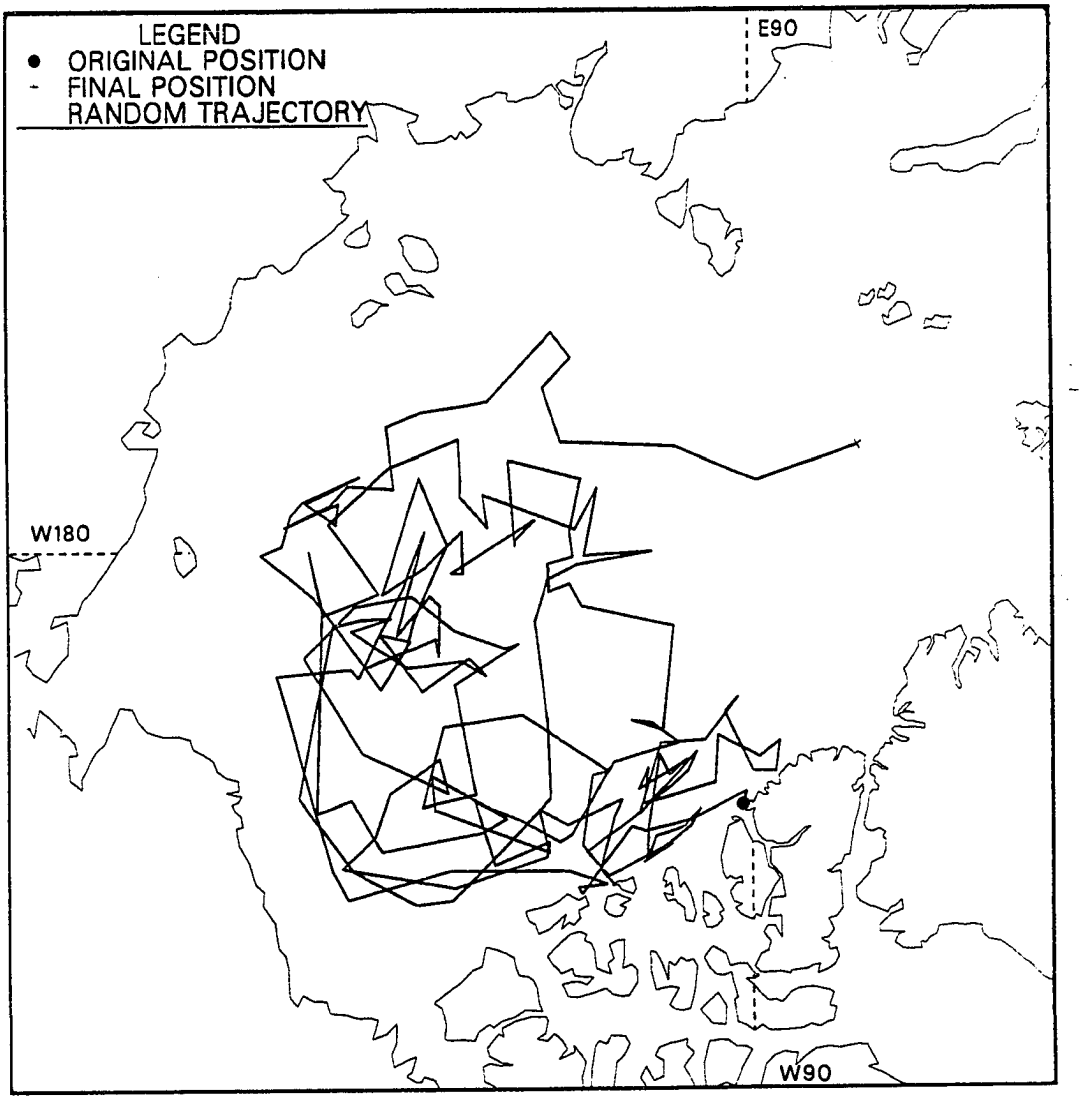

Figure 46: Random ice island trajectory 11.

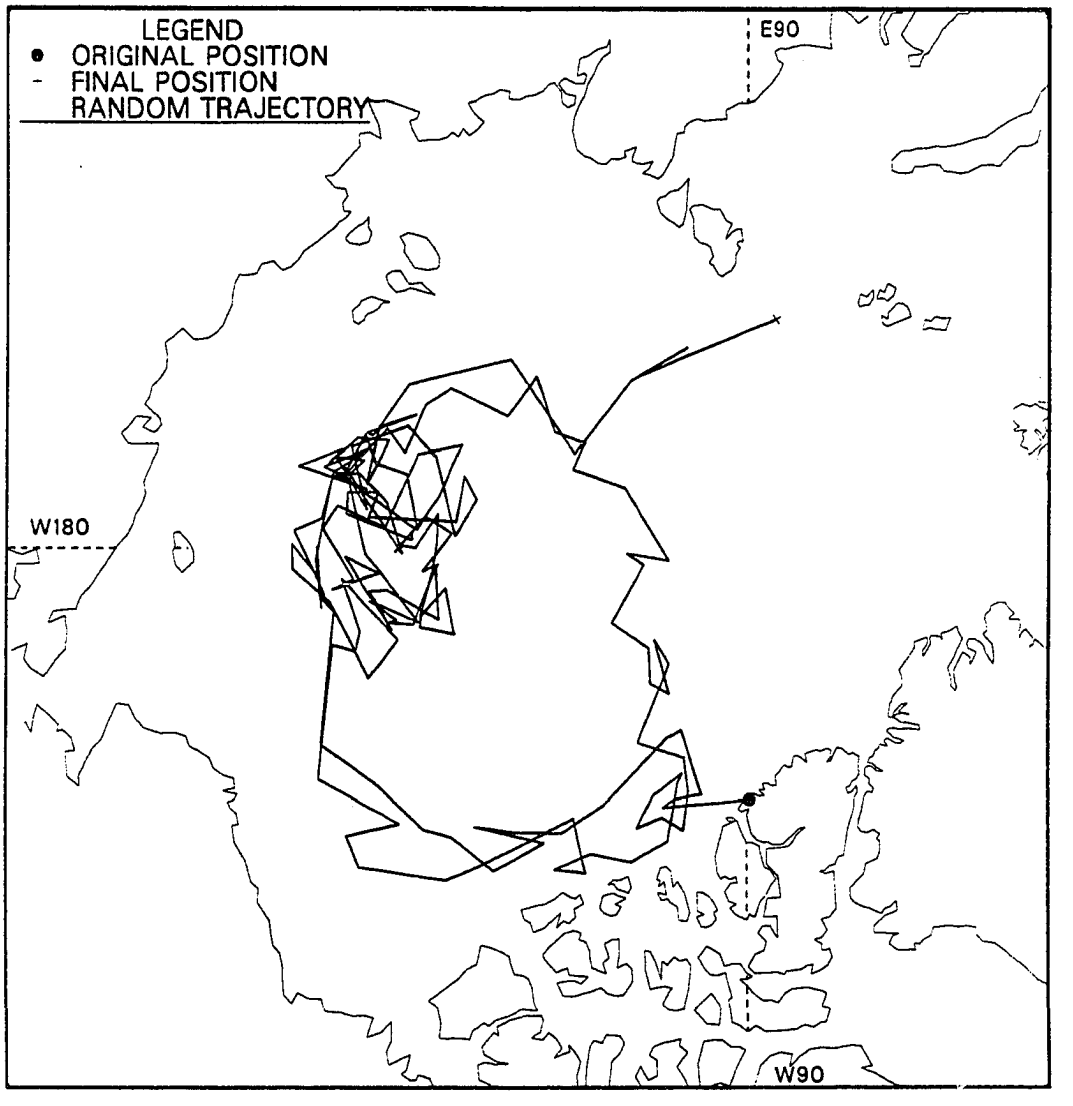

Figure 47: Random ice island trajectory 12.

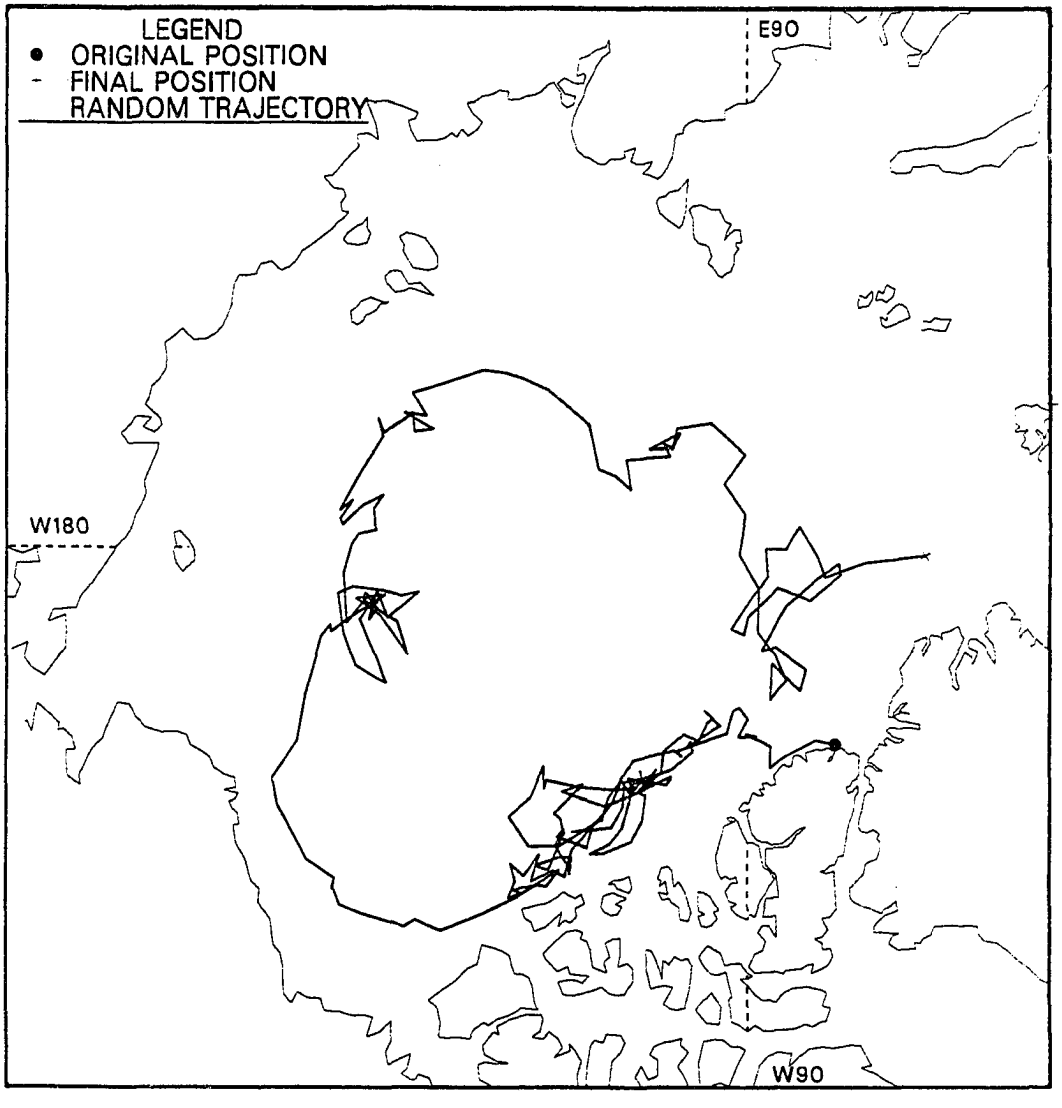

Figure 48: Random ice island trajectory 13.

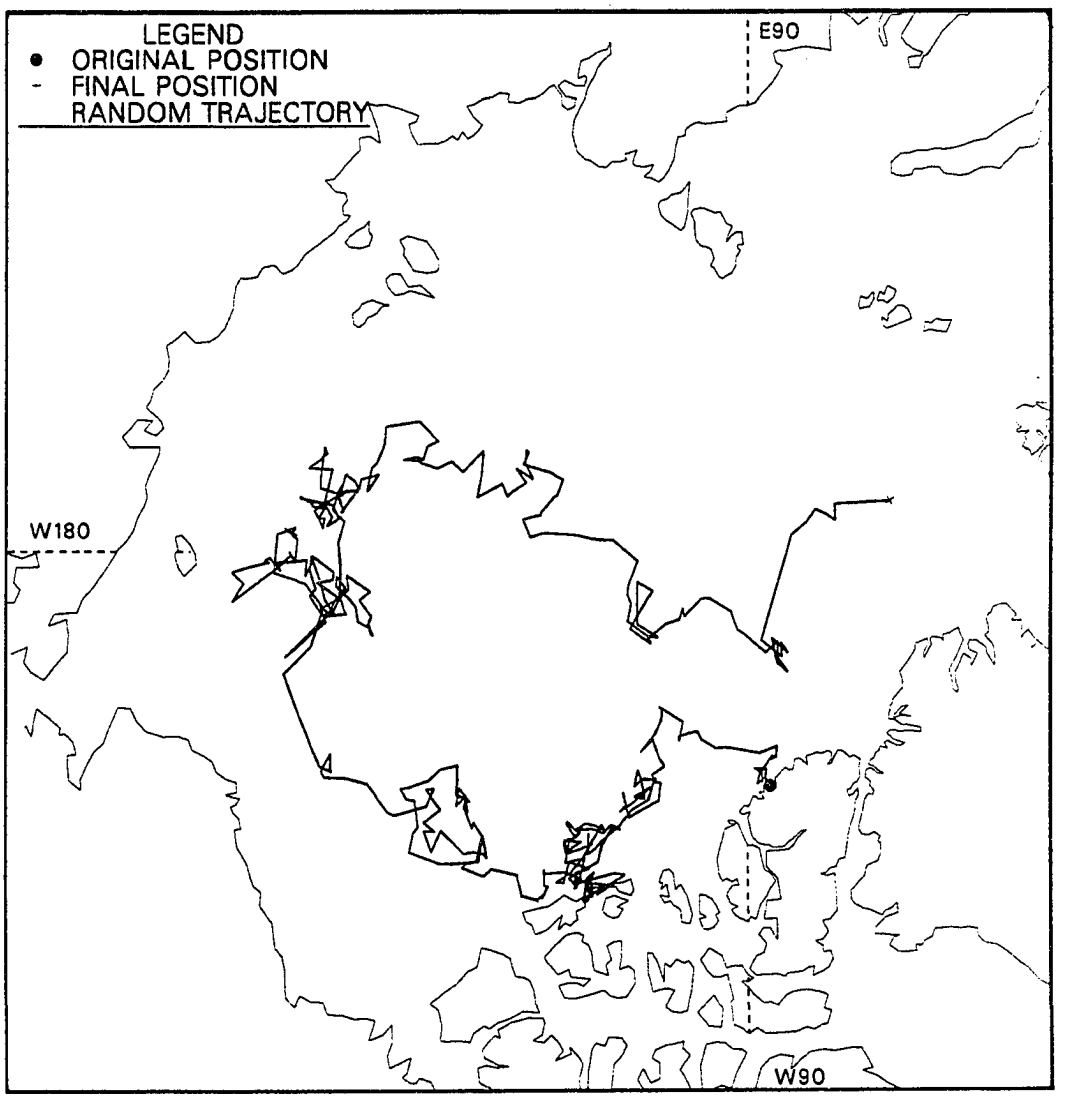

Figure 49: Random ice island trajectory 14.

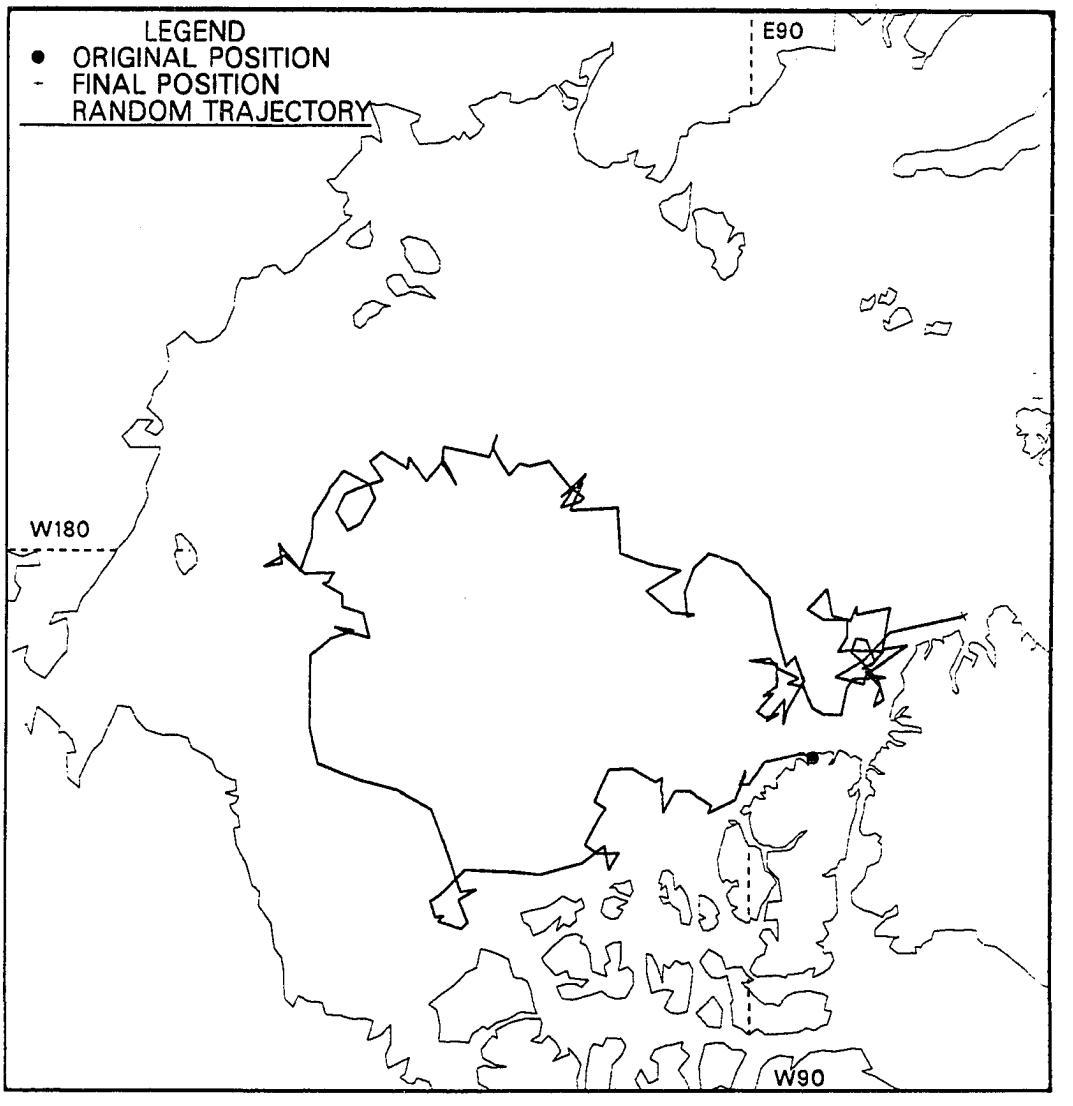

Figure 50: Random ice island trajectory 15.

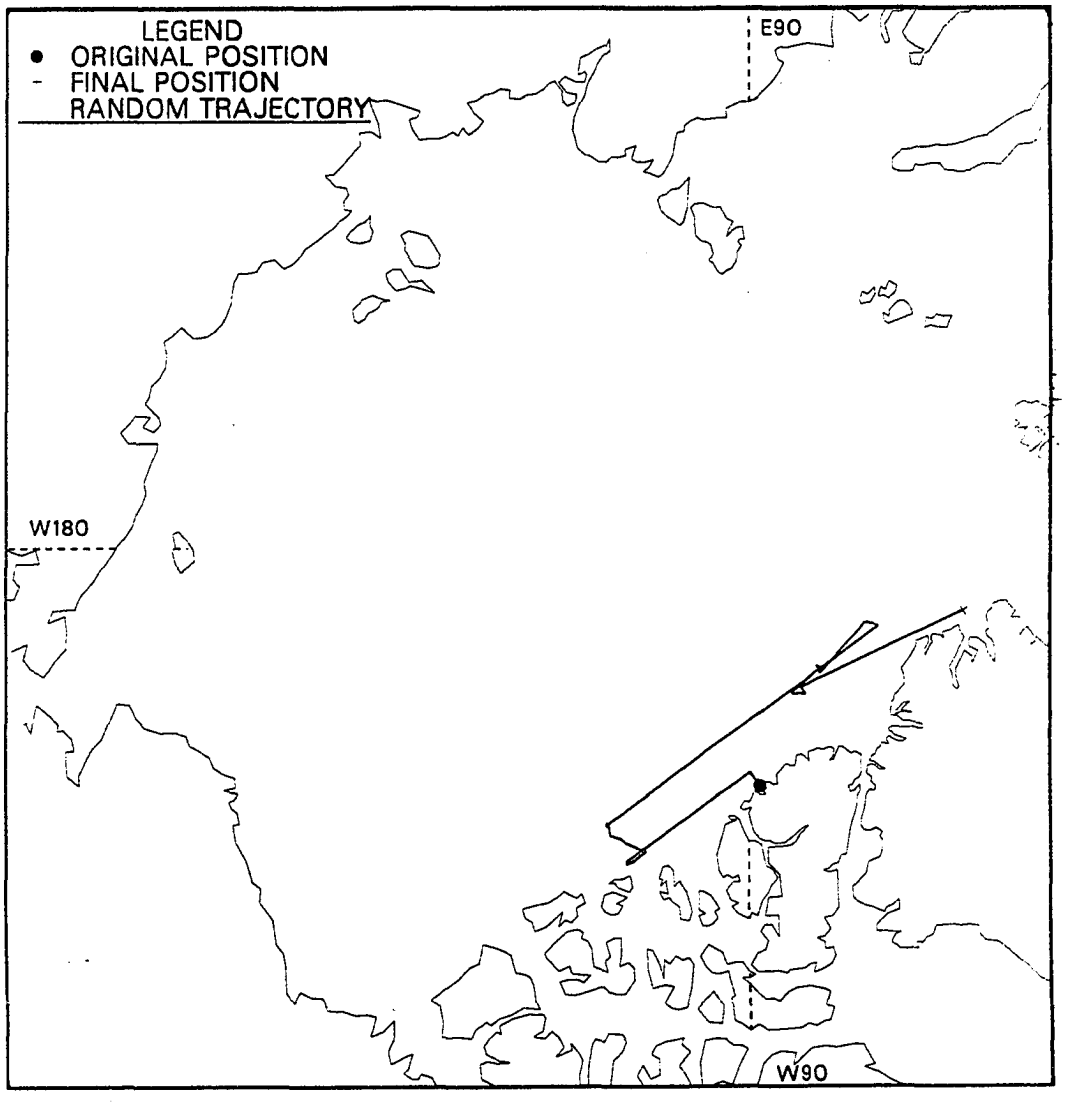

Figure 51: Random ice island trajectory 16.

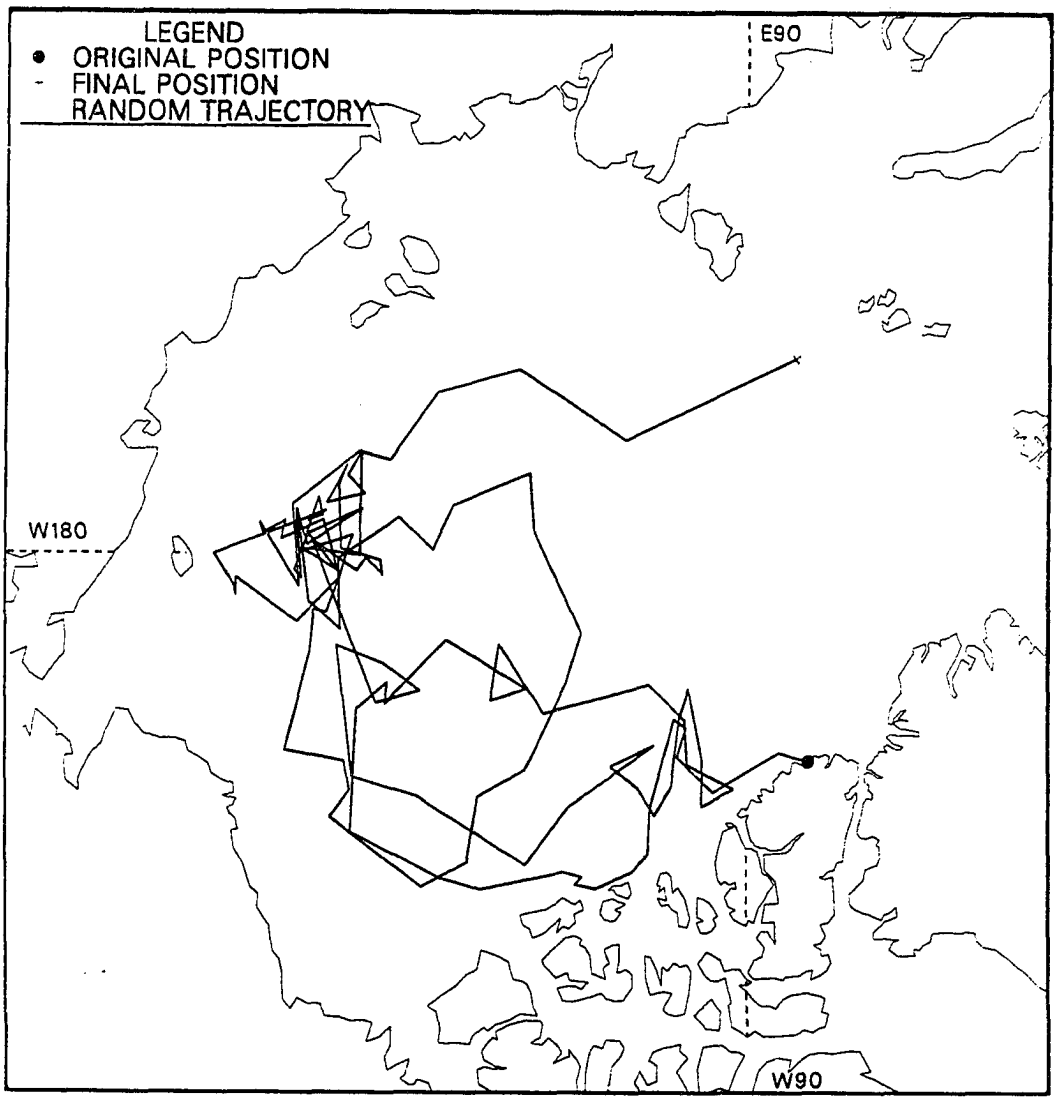

Figure 52: Random ice island trajectory 17.

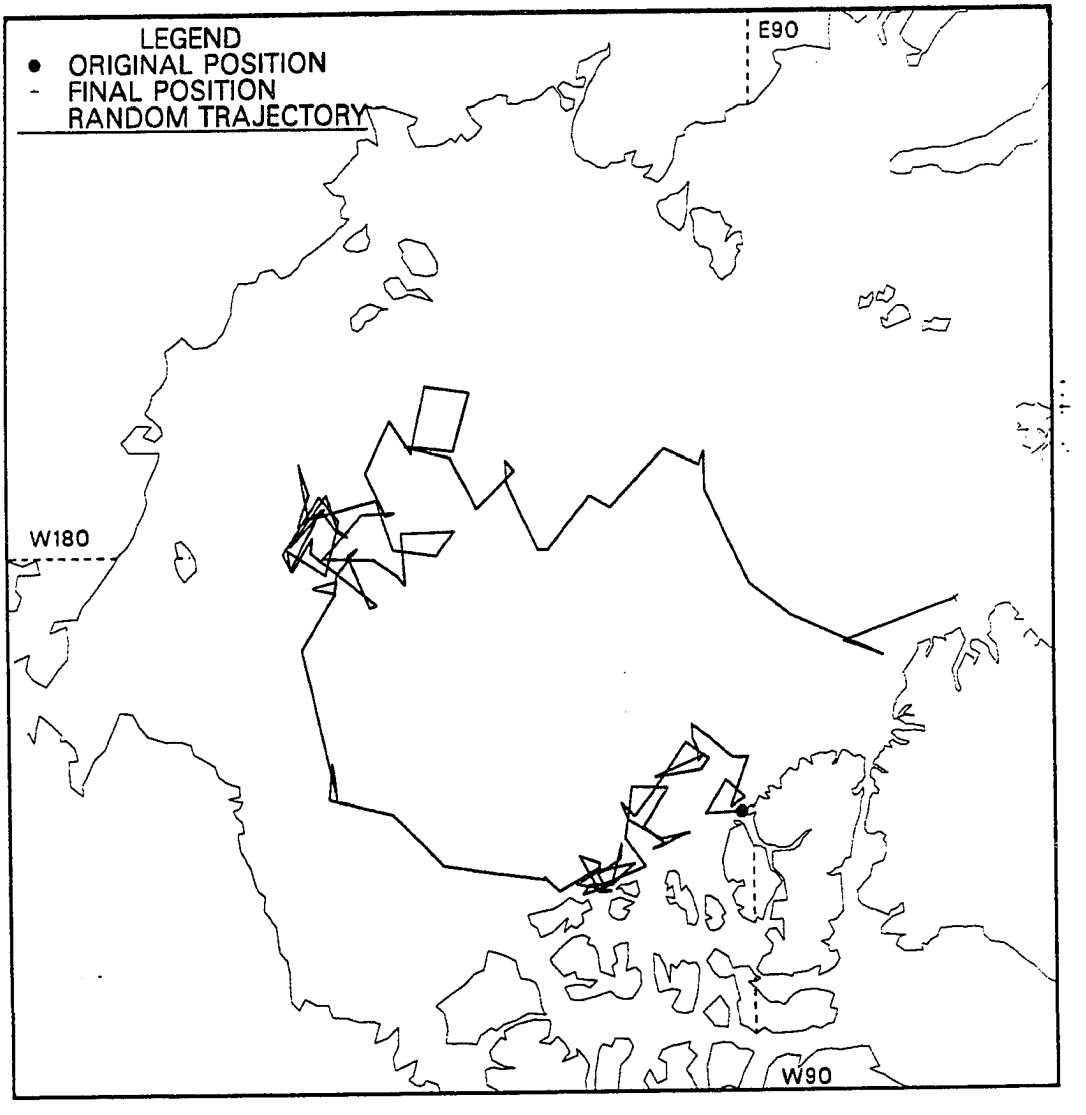

Figure 53: Random ice island trajectory 18.

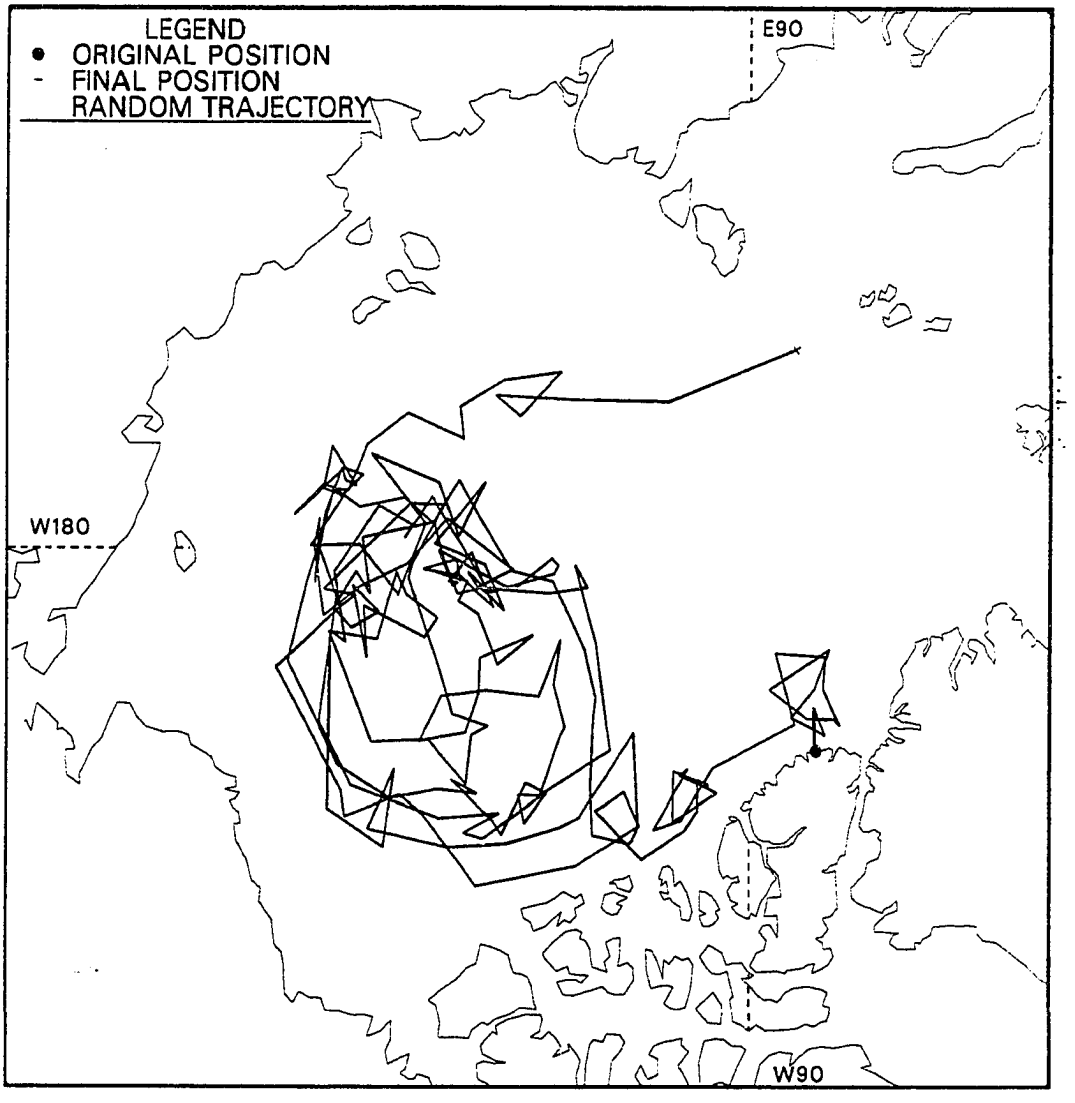

Figure 54: Random ice island trajectory 19.

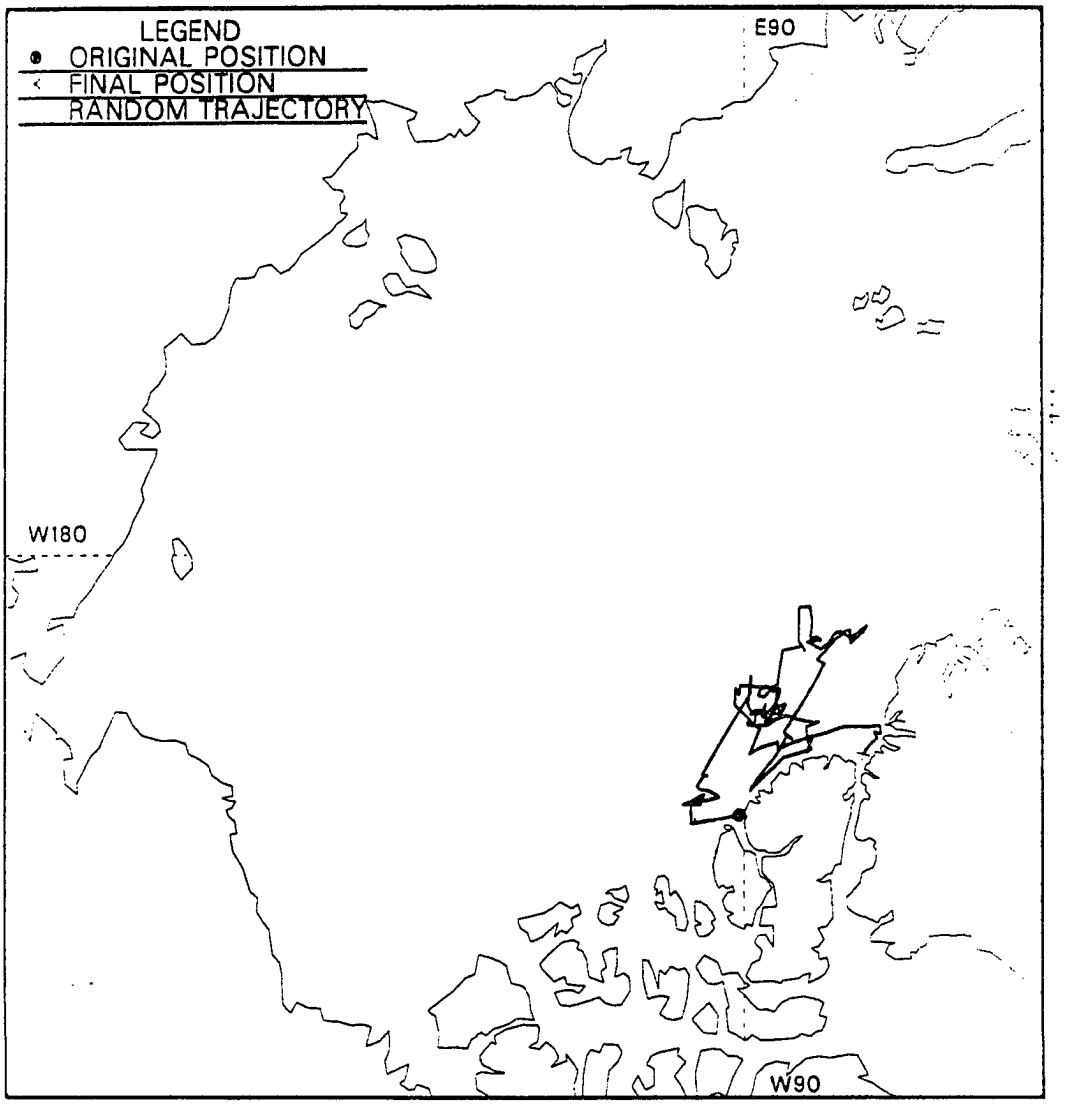

Figure 55: Random ice island trajectory 20.

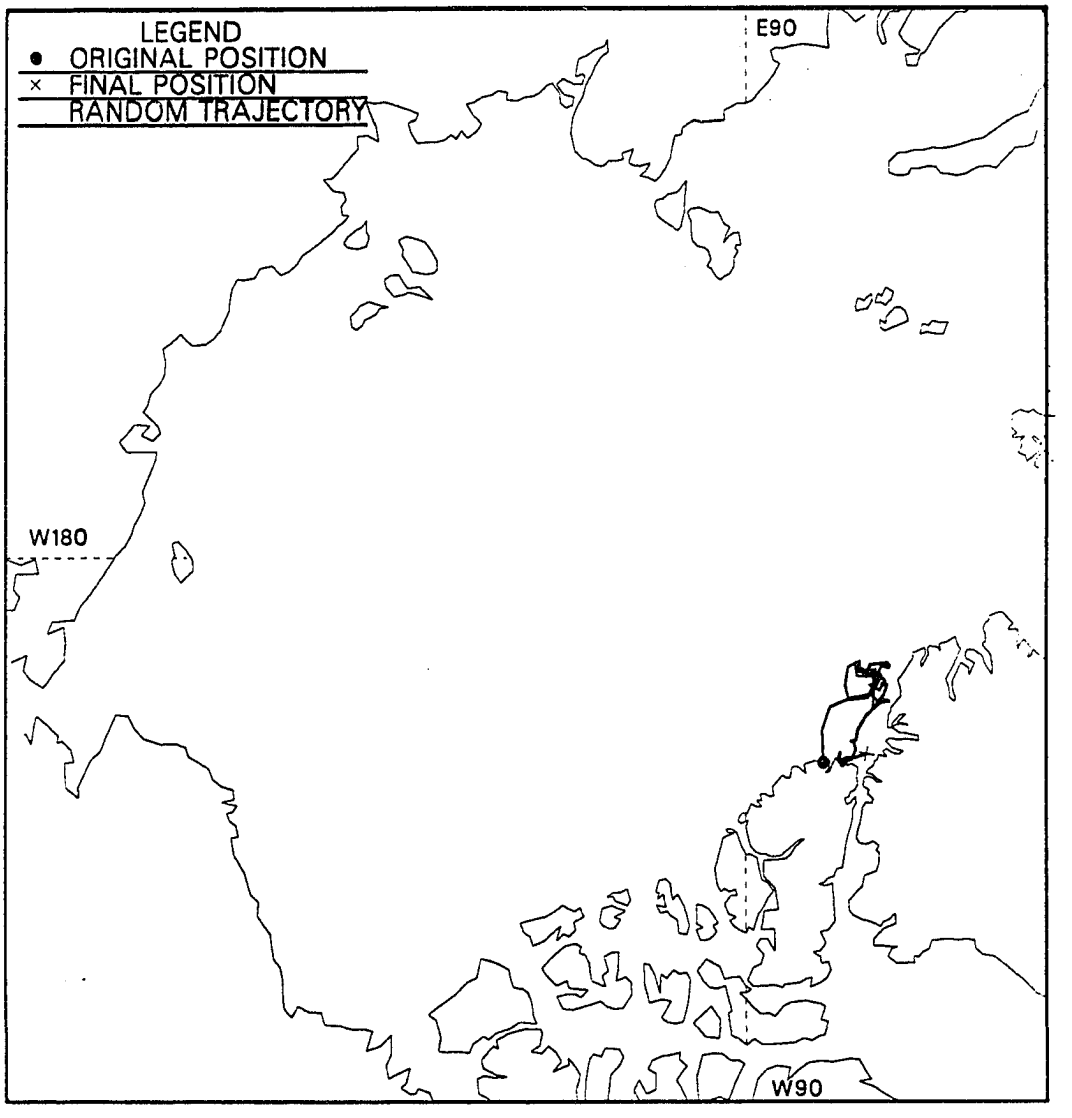

Figure 56: Random ice island trajectory 21.

as shown in Figure 36 to 54 (except for Figure 41). Most ice island trajectories are in this pattern, with a frequency of 86% according to these simulated results. After generation, ice islands move down towards the southwest, along Ellesmere and Axel Heiberg Islands, with more intensive loops in the area near the Canadian Beaufort Sea coast. Then they turn right and move northwest to the Chukchi Sea, and often move into another intensive loop area nearby. Further, in their path, they move clockwise in the large scale gyre. Some ice islands simply complete one circulation before being ejected out of the Arctic Ocean while others may complete two, three or even four circulations in the Arctic Ocean with frequencies of 47%, 6%, 29% and 18% respectively. The most frequent behavior is 47% for one circuit. To examine this second pattern, the ice island T-3 drift track in the Arctic Ocean is shown in Figure 57. The ice island T-3 completed 3 circuits of the Beaufort Gyre from 1950 to 1979 before it drifted out of the Arctic Ocean (Sackinger et al., 1985). There is a common character in both trajectory patterns, in that the large scale trajectory consists of many small loops, either clockwise or anti-clockwise as shown in Figure 58, which is the random trajectory 8 in Figure 43 plotted with more detailed data points. This behavior can be compared with the tracking of Hobson's Choice Ice Island, as shown in Figure 59.

6.2 Distributions of Lifetime and Number of Active Ice Islands

In the case of real ice island drift, the probability of ice island trajectories is related to the ice island lifetime and number of active ice islands in the Arctic Ocean. These two factors were automatically produced from this simulation. By recording these two values in the simulation, the distributions of lifetime and number of active ice islands were obtained as shown in Figure 60 and 61.

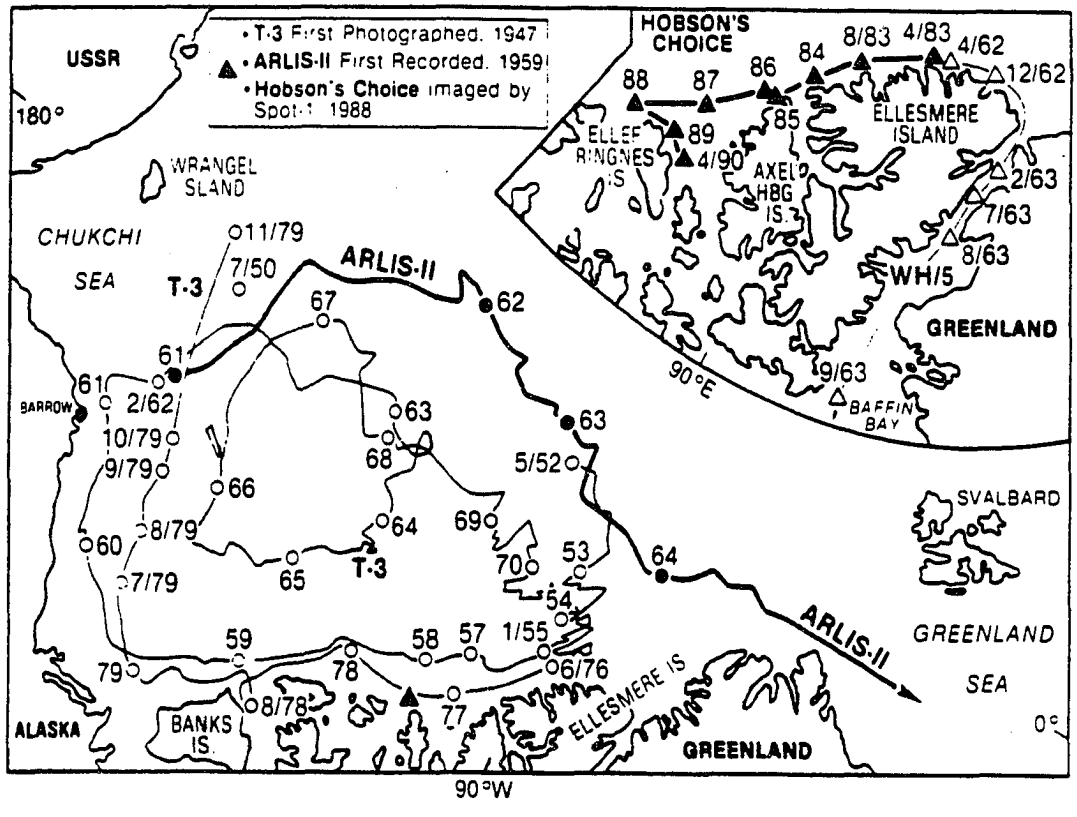

Figure 57: Drift records of Arlis II and T-3 ice islands. ○66 – Location in the year of 1966. ▲88 – Location in the year of 1988. △12/62 – Location in December, 1962. (source: Sackinger et al., 1990).

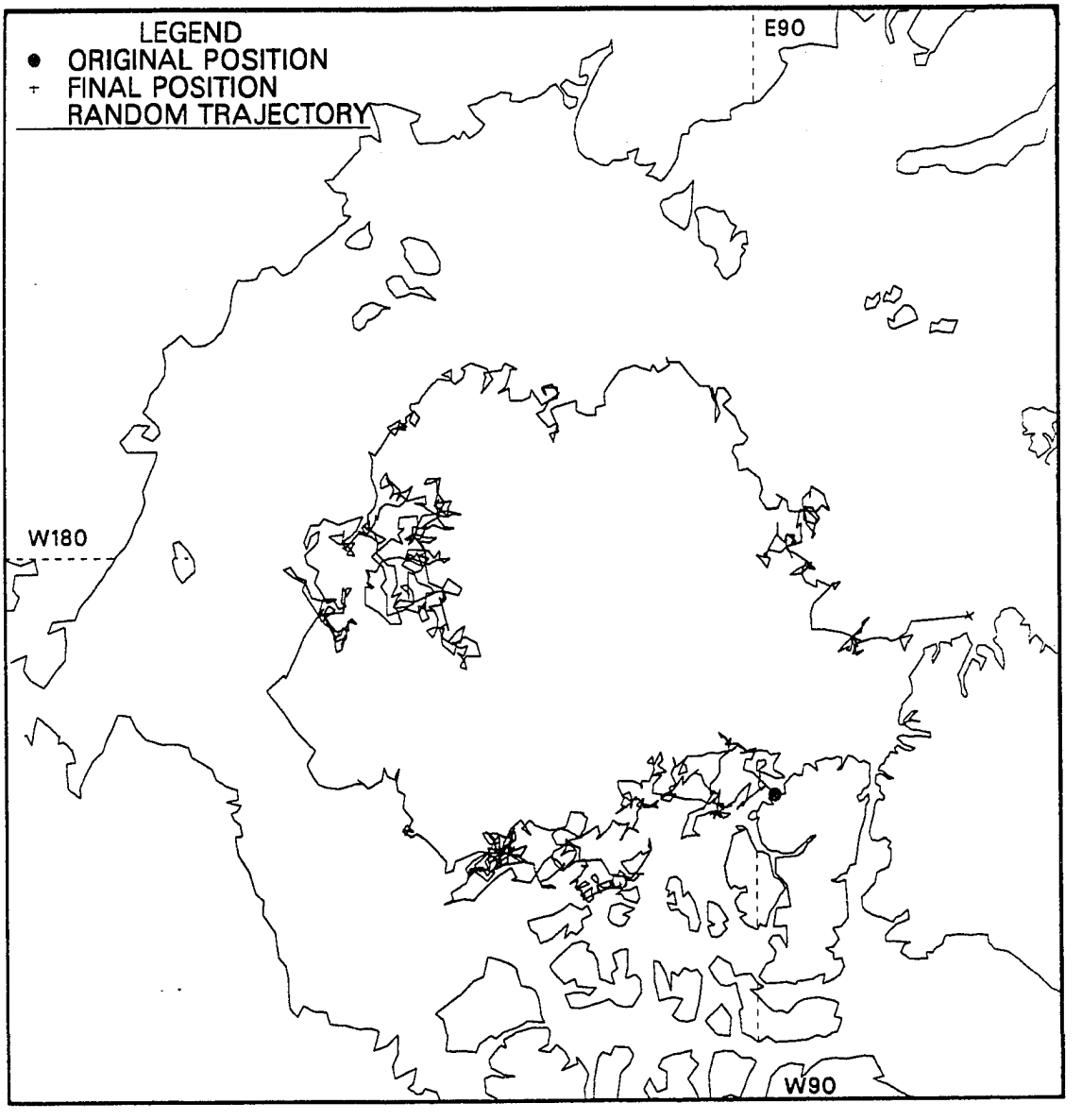

Figure 58: Random ice island trajectory in fine detailed scale showing many small loops.

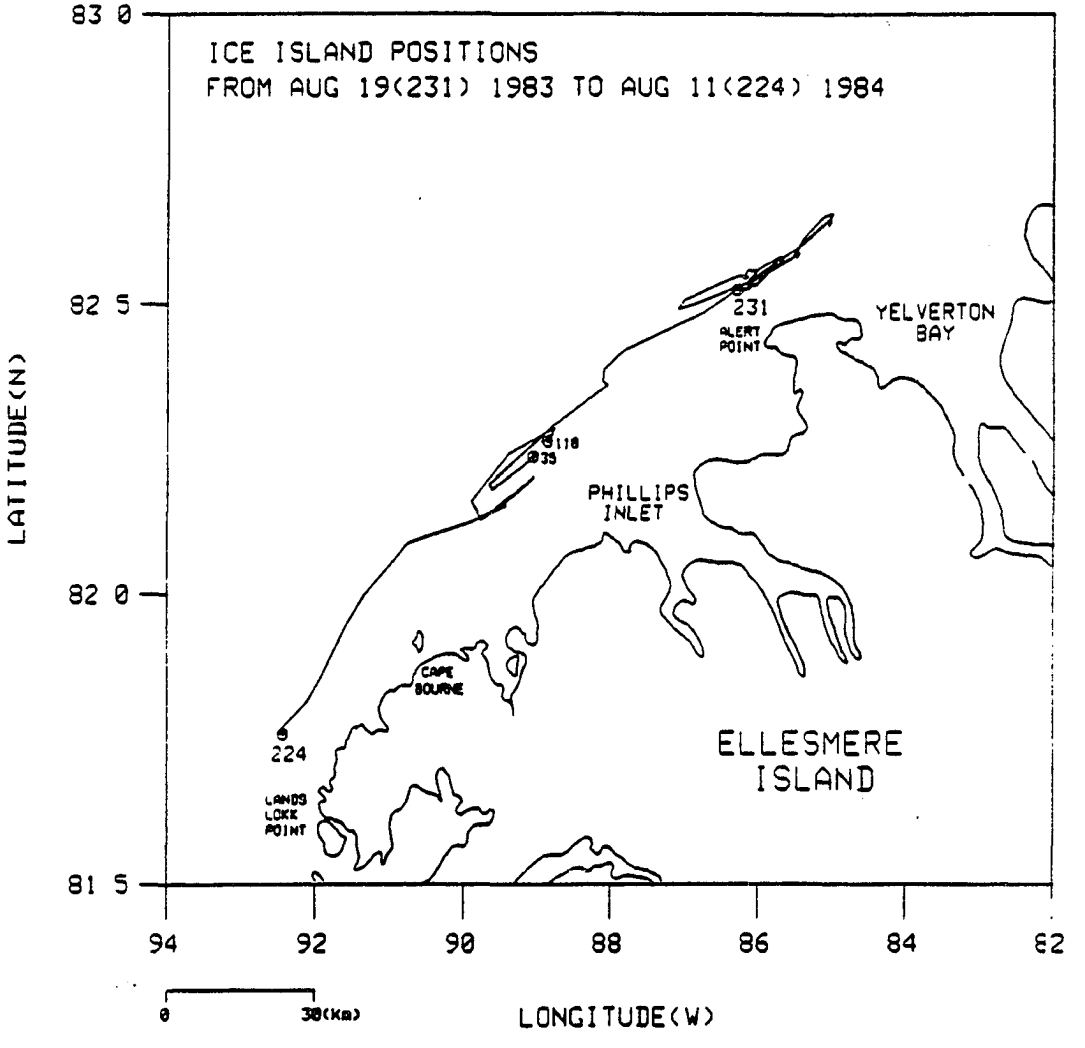

Figure 59: Hobson's Choice Ice Island track showing many small loops (source: Yan, 1986).

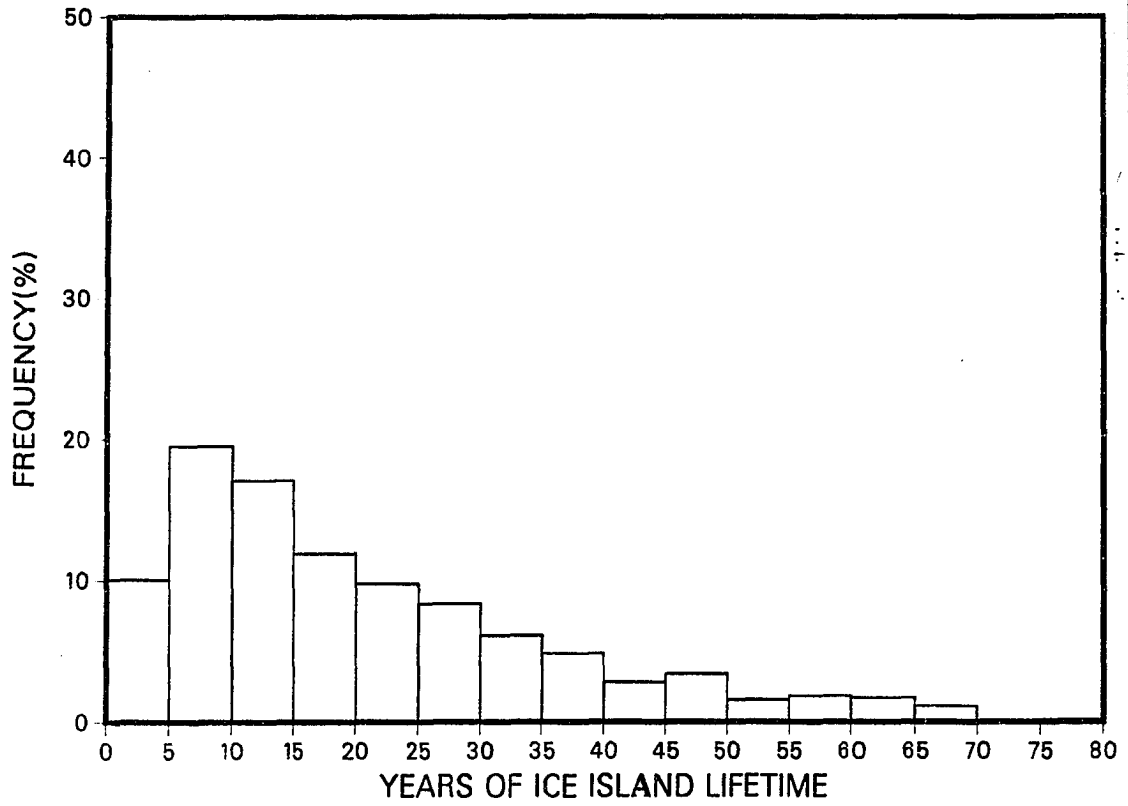

Figure 60: Frequency of ice island lifetime in the Arctic Ocean (4-year interval of generation).

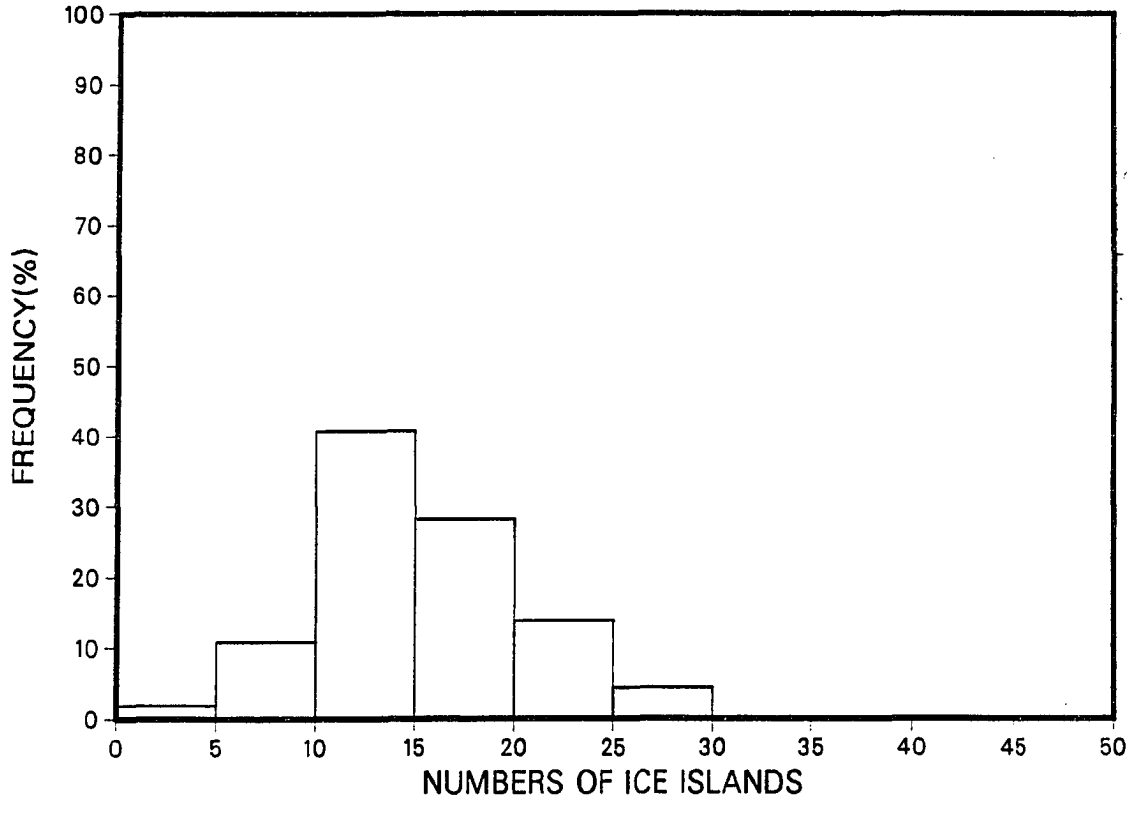

Figure 61: Frequency of ice island numbers in the Arctic Ocean (4-year interval of generation).

In Figure 60 a distribution of ice island lifetimes in the Arctic Ocean is given, with cumulative frequencies of approximately 40% between 5 to 15 years and 85% less than 35 years. The approximate 14% frequency for less than 6 years is consistent with the frequency of the short trajectory pattern. This means that ice islands moving in the second trajectory pattern (circulation covering the Beaufort Gyre) will drift at least 6 years to complete one circuit in the Arctic Ocean. This is consistent with the estimation of one Beaufort Gyre circuit time of 5 to 10 years for ice island T-3 (Jeffries et al., 1988).

In Figure 61, the distribution of the number of live ice islands in the Arctic Ocean is shown. This is approximately a Gaussian distribution with mean value of 18, and less than 30 ice islands existing in the Arctic Ocean at any one time. This is only for ice islands with length greater than or equal to 1 kilometer; the real number of ice islands, including fragments, may well be greater than this. More detailed examination has shown that these distributions are not affected appreciably by the time intervals of ice island generation, which have been tried at 3, 4 and 5 year intervals.

6.3 Probabilities of Ice Island Trajectories

The results of probabilities of simulated ice island trajectories are plotted in the form of differential return period (years) contours over the Arctic Ocean (Figure 62). The contours represent the recurrence interval (years) of ice islands in each square area of $50 \times 50km$. The results show that there are two zones of highest recurrence. One is near the Canadian Beaufort Sea, which is likely due to ice islands originating at Ellesmere Island which are then driven southwestward by northeasterly winds along the Canadian coast. Another high recurrence zone is near the Chukchi Sea, which is

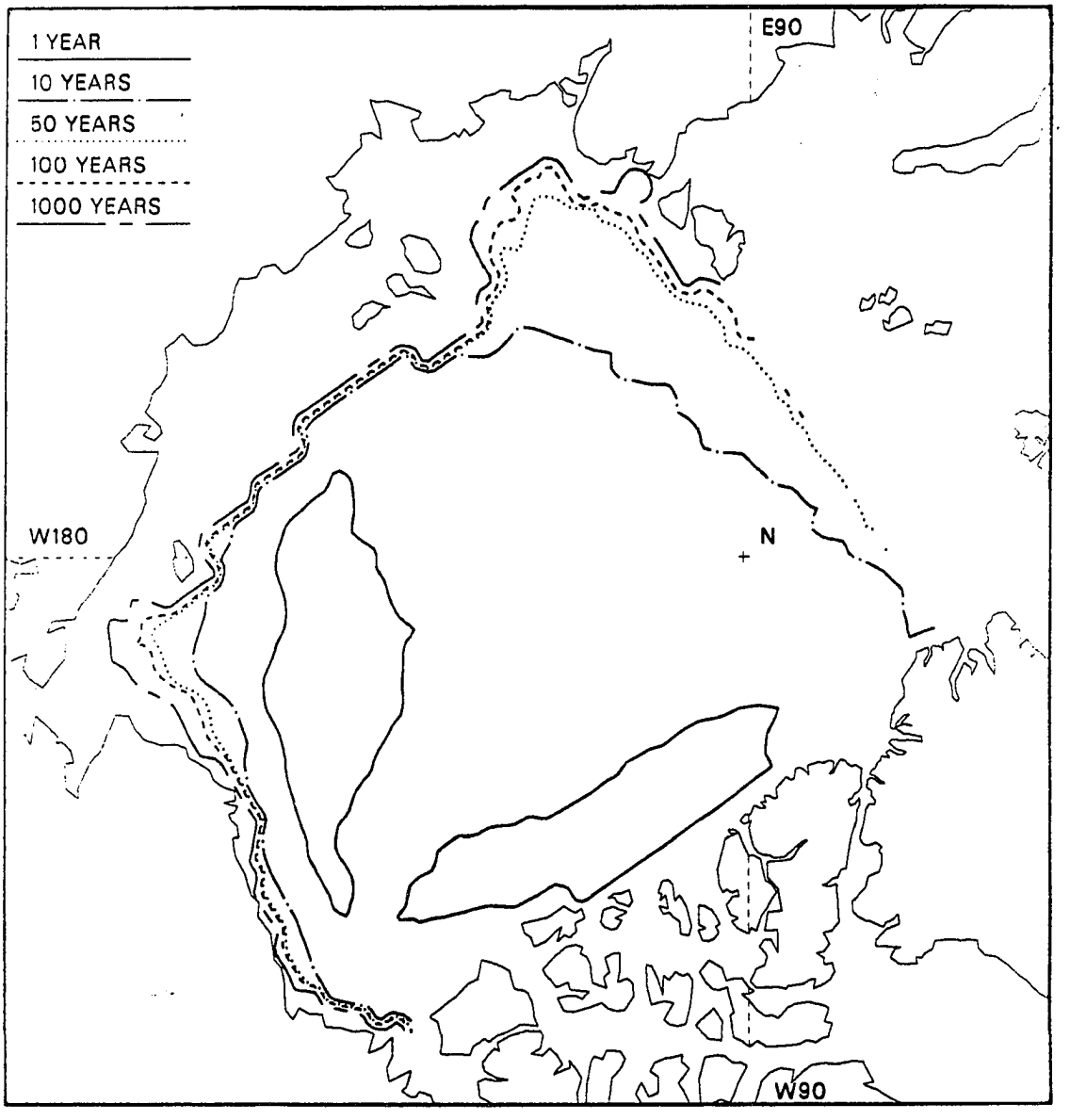

Figure 62: Return period contours (years) of simulated ice islands in the Arctic Ocean.

likely due to ice islands being driven through the Alaskan Beaufort Sea by easterly winds to the boundaries of the Chukchi Sea, where they are temporarily confined to some extent by the boundaries and by the currents from the Bering Strait, and then are pushed back to the Arctic Ocean under the influence of ocean currents and winter geostrophic wind. There is a broad area of 1 to 10 year recurrence interval in the central ocean, and the gradient of probability is high along the Alaskan Beaufort Sea coast and in the Chukchi Sea. The contours are deflected toward the Arctic Ocean at the Chukchi Sea due to the influences of Bering Strait water inflow. There is a high probability zone near the north end of Greenland, which implies that most of the ice islands escape out of the Arctic Ocean through the Fram Strait between Greenland and Svalbard.

To quantify the frequencies of ice islands ejected out of the ocean at each open water boundary, a record was made of the numbers of ice islands ejected through each boundary and the number of ice islands melted down in the Arctic Ocean, as shown in Table 3.

Table 3: Frequencies of ejection of ice islands.

Ejection Route	Number of Ice Islands Ejected	Frequency
Between Greenland and Svalbard	582	75.0%
Nares Strait	151	19.5%
Amundsen Gulf	42	5.4%
Bering Strait	0	0.0%
Melted down in ocean	1	0.1%

From Table 3 the most frequent situation is ejection at the boundary between Greenland and Svalbard, which is consistent with observations. Less frequent ejection at the Nares Strait and Amundsen Gulf are noted with zero chance for ice islands to escape out of the ocean by the Bering Strait. The number of ice islands melted down in the ocean is not significant, and has a frequency of 0.1%.

6.4 Effects of Wind Field and Water Current

Because wind force is the only random driving force on the ice islands considered in this simulation, pressure maps averaged over a short time period (monthly) were used to calculate the wind field. The maps in Figure 19 - 30 show an extremely variable surface geostrophic wind field, from an anticyclonic pattern in winter to a cyclonic pattern in summer. The annually-averaged surface geostrophic wind field over the Arctic Ocean is an anticyclonic system as shown in Figure 31. To compare the effects of these two types of different time-averaged wind fields, the simulation program was run with the annually averaged wind field as input wind for each month. The probability of ice island trajectory occurrence obtained is shown in Figure 63 in the form of contours representing different recurrence intervals (years) of ice islands in a square area of $50 \times 50 km$. Comparing this result with that shown in Figure 62, we can see that the regions of 1-year return interval are along the Canadian and Alaskan Beaufort Sea coastline, rather than covering the entire Beaufort Gyre. The influence of the Chukchi Sea current in reducing the frequency of ice islands on the Chukchi Shelf was offset by the wind patterns assumed in the calculation which produced Figure 63. The results in Figure 62 are believed to be closest to reality.

To examine the sensitivity to the water current effect near the Chukchi Sea and Alaska Beaufort Sea, the simulation program was also run, neglecting the water

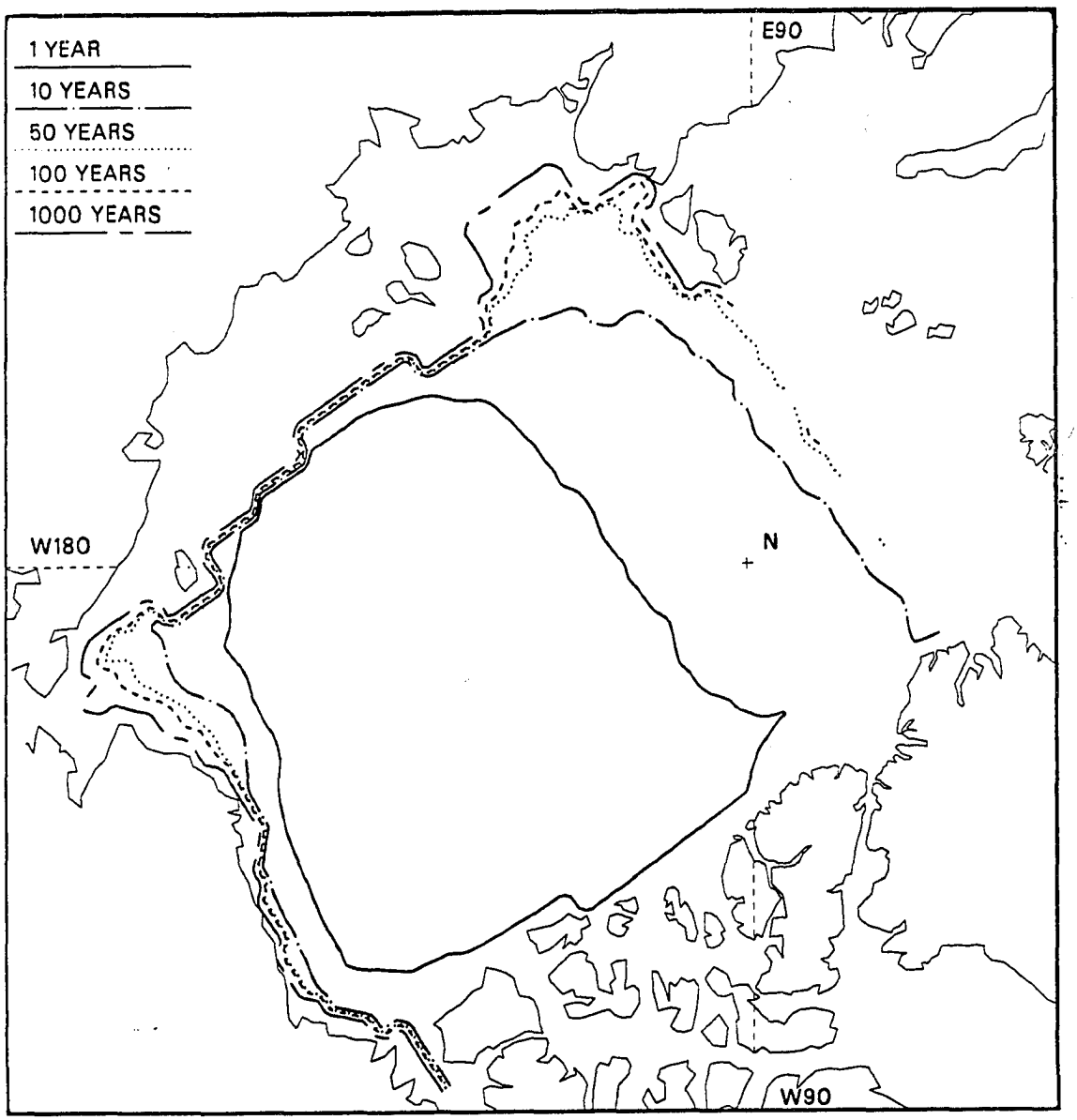

Figure 63: Return period contours (years) of simulated ice islands in the Arctic Ocean for the case where the annually-averaged pressure field was used throughout the year for wind generation. This is less exact than Figure 62.

current in these areas. The simulation results are shown in Figure 64. By comparison of this result with that shown in Figure 62, we can see that the dominant effect of the Chukchi Sea currents is to increase the return period from 1-10 years to 10-100 years in the northern Chukchi Sea.

The main Arctic Ocean surface currents are driven by wind stress transmitted by ice cover in the large-scale. Mean current speeds are slow in the central ocean, about 0.02 m/s, but increase as water exits the ocean toward the Fram Strait. There are two main currents through the Fram Strait. The West Spitsbergen Current is a northward-flowing extension of the Norwegian-Atlantic current. It flows through Fram Strait off the west coast of Spitsbergen into the Arctic Ocean. The East Greenland Current, which lies west of the East Greenland Polar Front, is the main current out of the Arctic Ocean (Smith, W.O. Jr., 1990). Many buoy drifts out of the Arctic Ocean along the east Greenland were recorded (Thorndike, Colony and Muñoz, 1980 to 1985). Some of these drift directions could be related to the surface geostrophic wind directions. Some drifts, however, were perpendicular or even opposite to the geostrophic wind directions. This means there are other forces than wind force driving the buoy motion in some circumstances. One of these forces may be the drag force of the East Greenland Current. It is important to study the real dynamic mechanisms of ice island motion in this area, and it should be done after more data become available in the future.

6.5 Ice Island Size Effect

In this simulation, the ice island motion was driven by wind acting on the ice island surface. The air drag force was calculated as proportional to the ice island surface area, and the water form drag was proportional to the ice island frontal

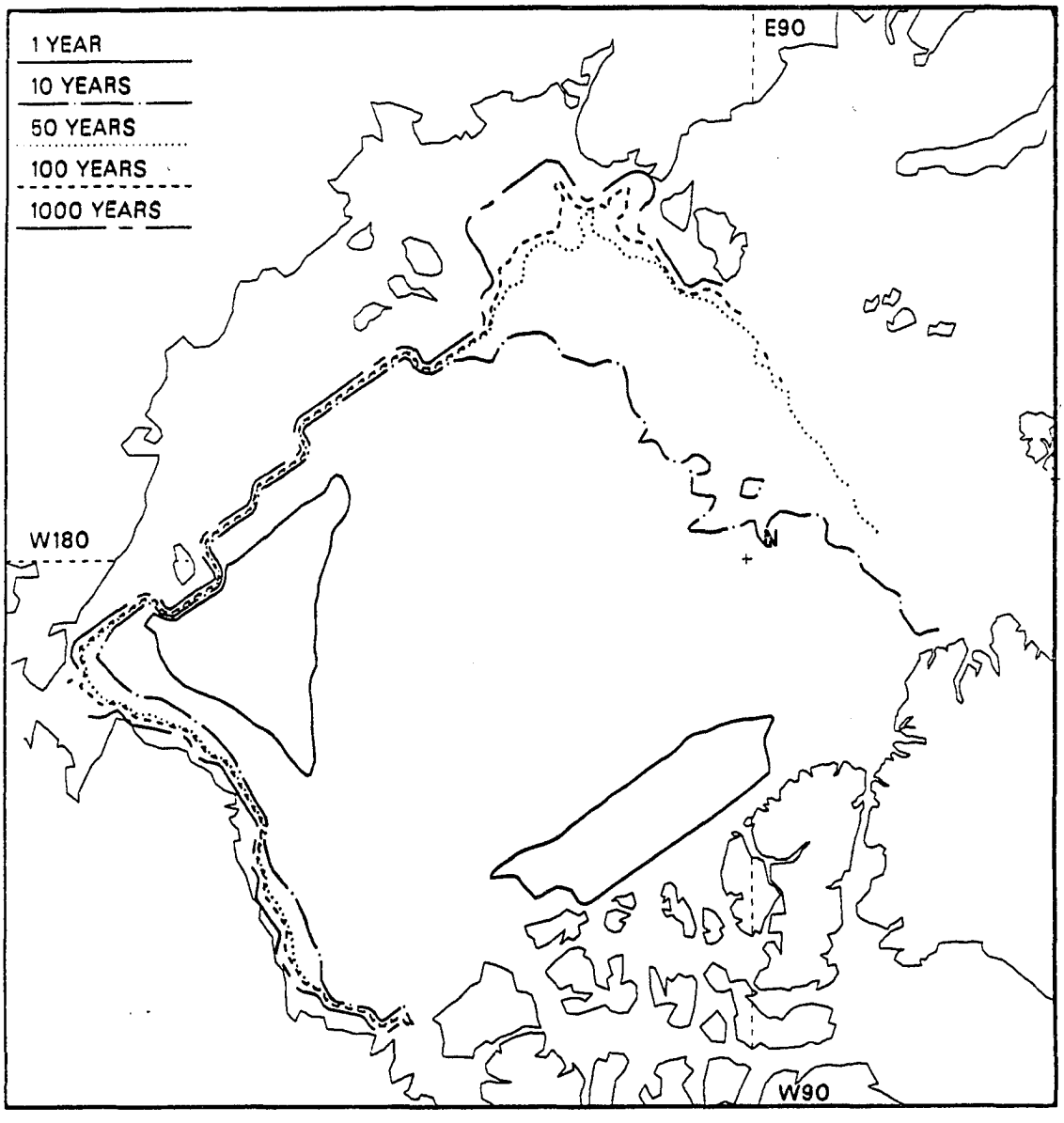

Figure 64: Return period contours (years) of simulated ice islands in the Arctic Ocean for the case where the Chukchi and Beaufort Sea water currents were set to zero. This is less exact than Figure 62.

wetted area. So for ice islands with the same thickness, the ratio of air drag force to water form drag force increases as the ice island size increases. In the same environmental conditions, consequently, the larger size ice island would move faster and have stronger right-turning tendency due to the Coriolis force, relative to small size ice islands.

To examine this effect, the simulation program was run for different size ice islands. Figures 65, 66 and 67 represent three simulated trajectories of ice islands which have surface areas of 700 km^2, 300 km^2 and 1 km^2 respectively. These ice islands had the same thickness of 42.5 meters and were generated at the same location with the same initial random winds. Because of the location dependency, the randomly-generated winds might be different for different ice islands after they moved into different areas at the same times. Comparing these trajectories, one can see that the ice island of 700 km^2 experienced two and a half clockwise circulations in large scale around the Beaufort Sea. The ice island with 300 km^2 area had a strong tendency to circulate clockwise in the Beaufort Sea but failed to complete one circuit. The small ice island with 1 km^2 area drifted smoothly parallel to the coast lines of the Alaskan Beaufort Sea and Canadian Beaufort Sea, and showed an obvious trend to follow the Beaufort Gyre. Moreover, it drifted very slowly compared to the 300 km^2 ice island and 700 km^2 ice island, which was the fastest one during the Beaufort Sea drift. This speed difference is related to the different surface areas on which the air drag force is acting. The larger area ice island will move faster under the same environmental conditions. As a result, the faster ice island of 700 km^2 was subjected to a larger Coriolis force and completed large scale circulations in the Beaufort Sea. The relatively slow-moving ice islands of 300 km^2 and 1 km^2 area were subjected to a relatively smaller Coriolis force which could not force them

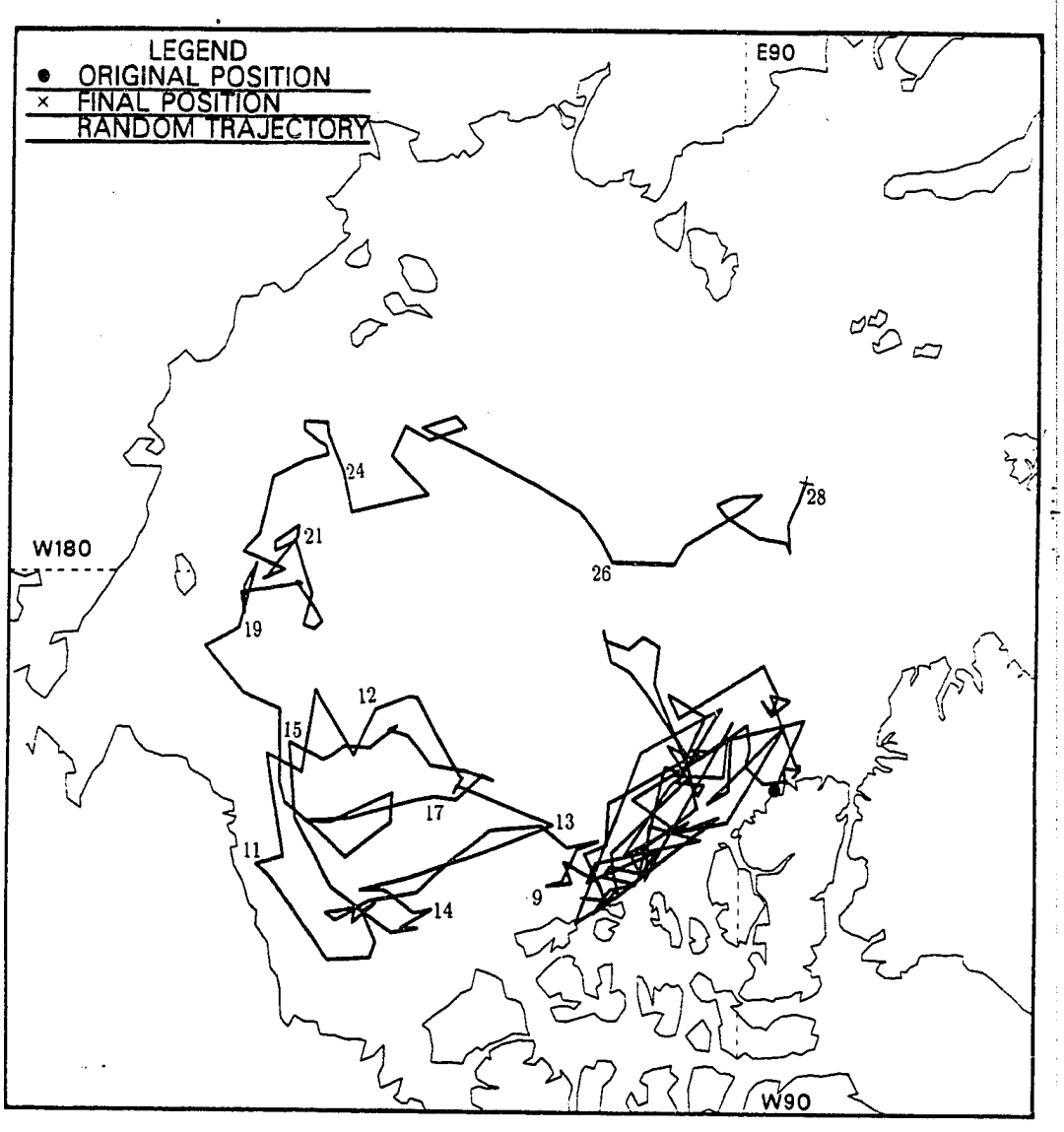

Figure 65: Simulated trajectory of ice island with surface area of 700 km^2. Numbers are years of drift time.

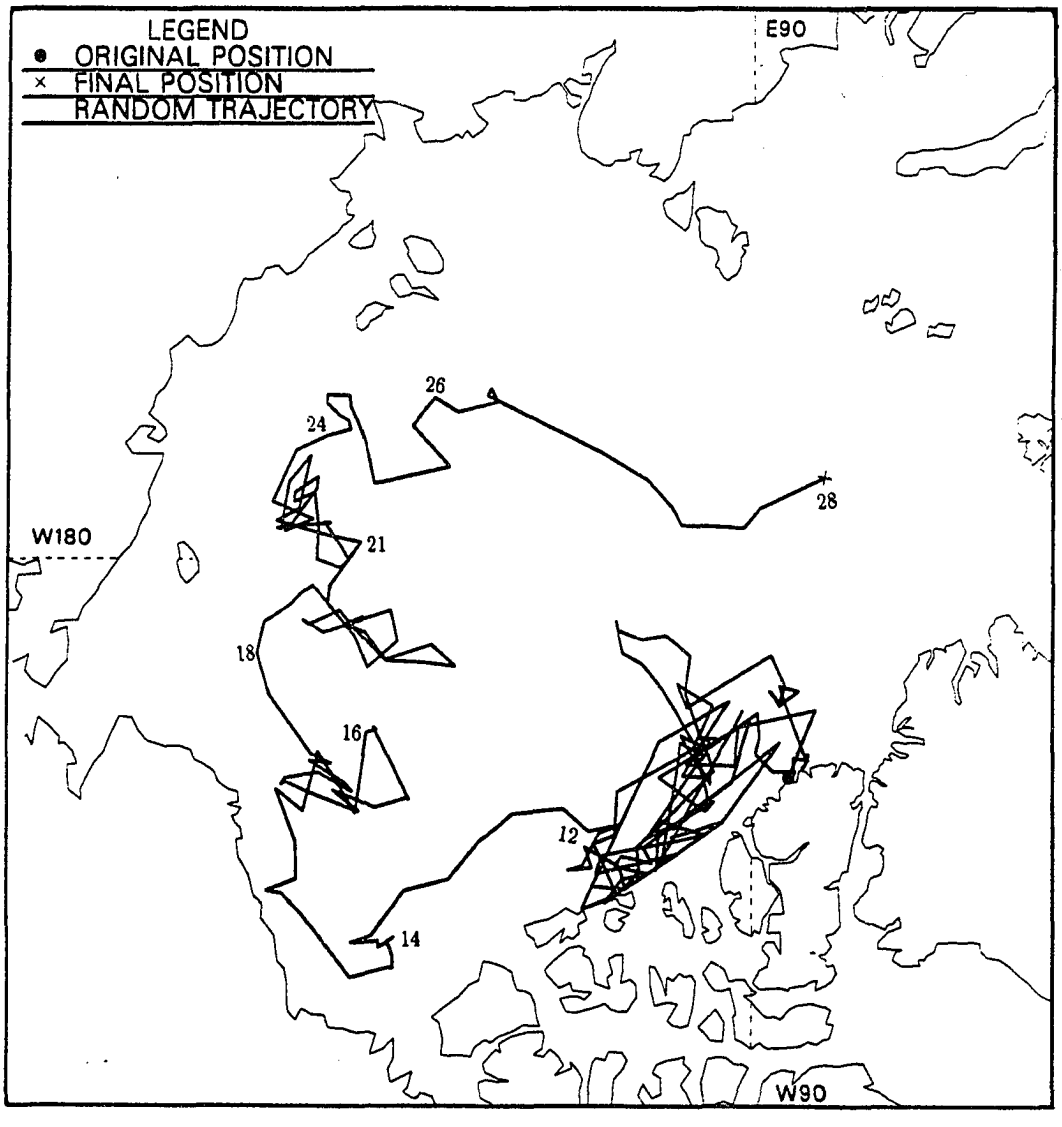

Figure 66: Simulated trajectory of ice island with surface area of 300 km^2. Numbers are years of drift time.

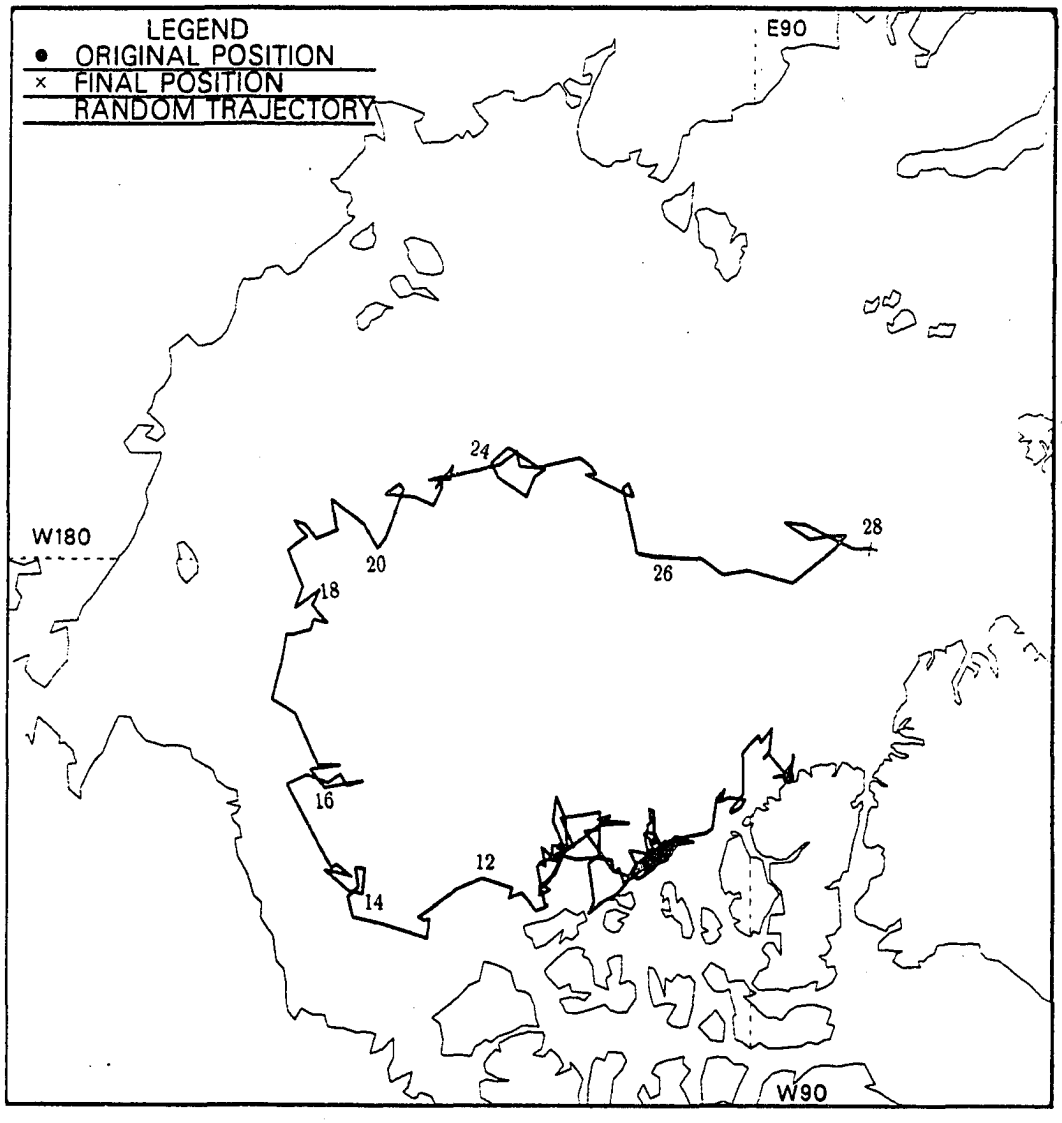

Figure 67: Simulated trajectory of ice island with surface area of 1 km^2. Numbers are years of drift time.

large scale circulation. Generally, the ice island size has an effect on its drift speed and large-scale circulation.

6.6 Thinning Rate Test

During the drift in the Arctic Ocean, ice islands experience thinning due to ablation and the ice island thickness may decrease at variable rate at different latitudes. The thinning rate used in the standard simulation is 0.82 meter per year. To examine whether the thinning rate has an effect on the probability of ice island trajectories, the simulation program was also run with thinning rates of 1 meter and 0.5 meter per year respectively. The results are shown in Figures 68 and 69. Comparing these figures together with Figure 62, one can see that the return period contours have the same patterns and no obvious differences exist. These show that the thinning rate of an ice island has only a very minor effect on the recurrence probability of ice islands in the Arctic Ocean.

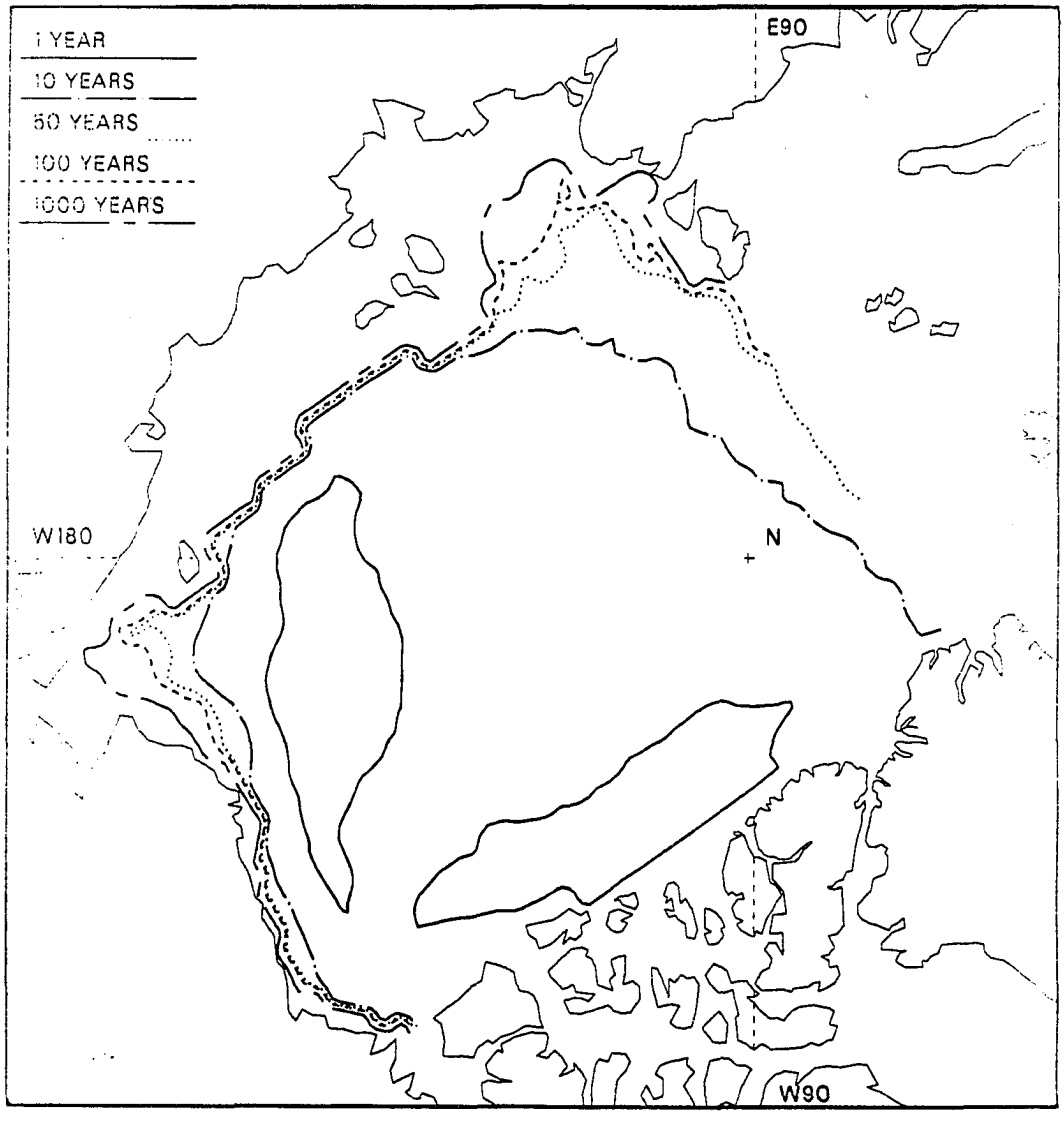

Figure 68: Return period contours (years) of simulated ice islands in the Arctic Ocean for the case of 1 meter per year thinning rate of ice island thickness.

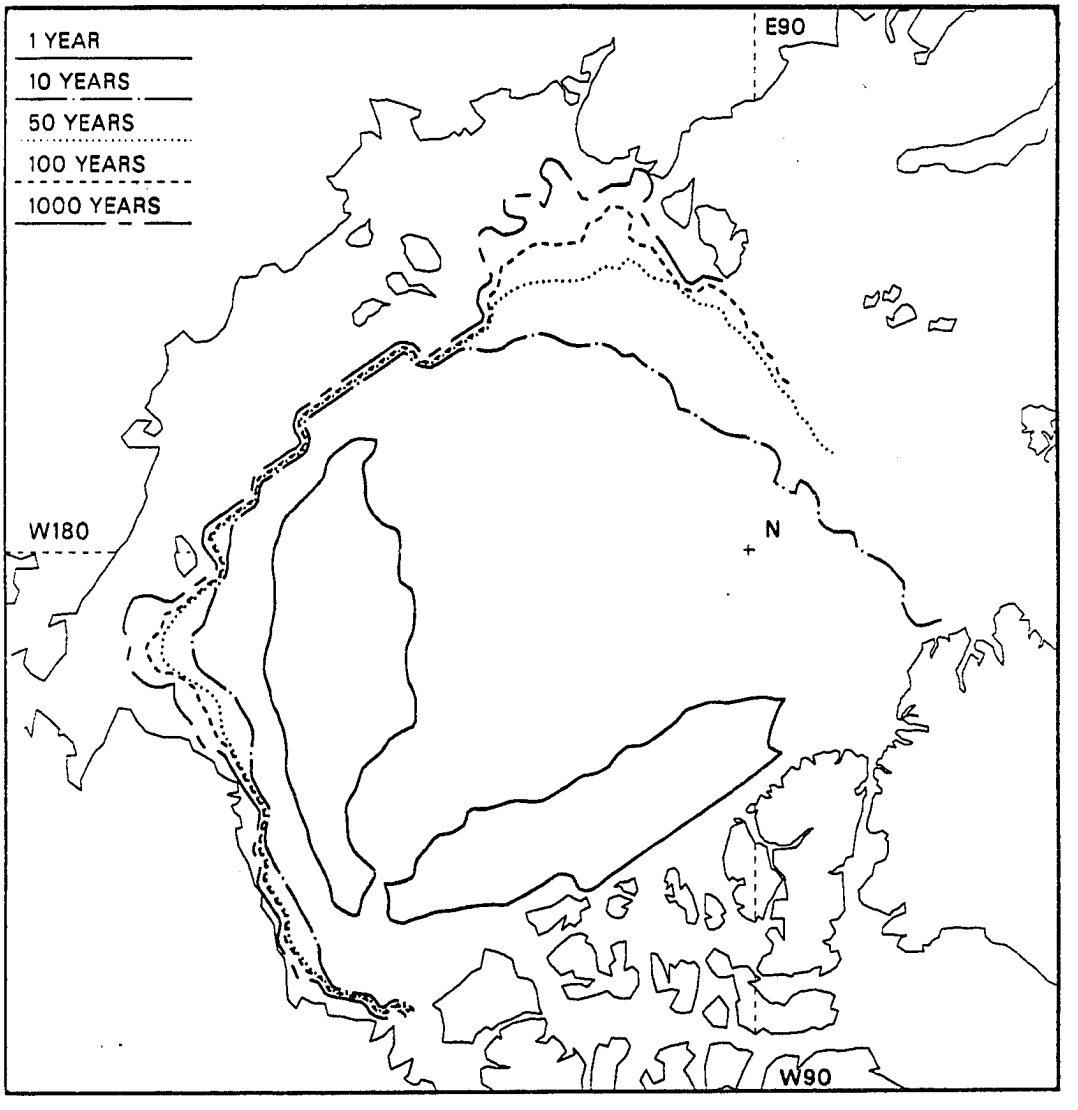

Figure 69: Return period contours (years) of simulated ice islands in the Arctic Ocean for the case of 0.5 meter per year thinning rate of ice island thickness.

CHAPTER 7

CONCLUSIONS

A random ice island motion model has been established which is capable of simulating random ice island movement and the probability of ice island occurrence over the Arctic Ocean. The model is unique in that it uses a dynamic equation and the Monte Carlo method to overcome the difficulty of lack of extensive field data on ice island trajectories, and makes use of statistical data of wind fields, ice island generation, and movement laws as inputs, which are available at the present time.

One important factor affecting the probability of ice island occurrences is the ice island generation. Because ice islands are generated by calving from the ice shelves, the spatial and temporal distributions of probability for such ice island generation can be quantified by historical statistics on the calving events at the ice shelves, assuming a time-invariant statistical process. A uniform spatial distribution of probability of an ice island shelf calving event can be assumed along the northern coast of Ellesmere and Axel Heiberg Islands, from Clements Markham Inlet west to the mouth of Sverdrup Channel. As an approximation at the present time, one calving event occurring every fourth year can be assumed for the temporal distribution. Sensitivity tests with 3-year and 5-year intervals showed that this interval has no significant influence on the simulation results of ice island recurrence in the Arctic Ocean.

Another important statistical variable for the ice island occurrence in the Arctic Ocean is the numbers of new ice islands calved from ice shelves in one calving event. To overcome the limit of observed data on numbers of ice islands calved at one time, an indirect method was developed in which the number of new ice islands were

automatically produced by deducting the random area of each ice island from the random area of the ice shelf calved at one time. The random area of one ice island can be calculated from the length and length-width ratio which can be randomly generated from their probability distributions.

The dynamic model of ice island movement is distinguished from the sea ice dynamical model by the large water form drag and the pack ice force on the ice island. The ratio of water form drag force and water skin friction force can be approximated as a function of thickness and horizontal dimension of an ice island. For most ice islands known at the present time the water form drag force is greater than the water skin friction drag force. Theoretical analysis showed that the pack ice force has a dependence on the ice island dimensions. Combined with an empirical formula for Hobson's Choice Ice Island (Lu, 1989), a semi-empirical formula of pack ice force has been developed for practical purposes in the ice island dynamic simulation.

A Monte Carlo model for random wind generation has been developed. As the only source of a random driving force on an ice island, the random wind process can be assumed as an approximately Gaussian process, which is determined by the mean wind vector and the wind autocovariance matrix. The mean geostrophic wind vector can be obtained from the surface pressure charts.

The results of probabilities of simulated ice island trajectories show that there are two zones of highest recurrence of ice islands, one near the Canadian Beaufort Sea, and another near the Chukchi Sea. There is a broad area of 1 to 10 year recurrence interval in the central ocean, and a high probability zone near the north end of Greenland, which implies that most of the ice islands are ejected out of the Arctic Ocean through Fram Strait between Greenland and Svalbard. The frequency

of ejection by this route is the highest at 75%, and there is zero probability for ice islands to escape out of the Arctic Ocean by the Bering Strait.

The lifetime of ice islands has a cumulative frequency of 40% for between 5 to 15 years and of 85% for less than 35 years. The distribution of the number of active ice islands in the Arctic Ocean is approximately a Gaussian distribution, with a mean value of 18, excluding ice islands with length less than 1 kilometer.

The ice island motions mainly display two basic patterns. For the first pattern, approximate 14% of ice islands move directly out of the ocean by north Greenland in less than 6 years after generation. About 86% of ice islands fall into the second motion pattern, in which the ice islands circulate clockwise covering the Beaufort Sea in one to four circuits. Among them, 47% of the ice islands complete only one circuit in at least 5 years. There is a common character in both trajectory patterns, in that the large scale trajectory consists of many small loops, either clockwise or counterclockwise.

The sensitivity test of the water current effect near the Chukchi Sea and Alaska Beaufort Sea showed that the dominant effect of the Chukchi Sea currents is to increase the return period from 1-10 years to 10-100 years in the northern Chukchi Sea. A sensitivity test of the annual average pressure chart was run to compare with that using the monthly-averaged pressure charts. Results show that the regions of 1-year return interval of ice islands for that over-simplified case are along the Canadian and Alaskan Beaufort Sea coastline, rather than covering the entire Beaufort Gyre. The influence of the Chukchi Sea current in reducing the frequency of ice islands on the Chukchi Shelf was offset by the over-simplified annual-averaged wind patterns assumed in the calculation.

Although the models presented provide a useful approach to the analysis of probability of ice island trajectories, the present model is limited in that ice island fragments are neglected. Furthermore, the decreasing trend of parent ice shelf area was not considered, because of lack of longterm information. Further observations and study of these phenomena would be useful. In addition to the return periods, the velocity distribution of an ice island in each grid area is also important for determining interactions with a structure when oil production is planned in specific grid areas.

BIBLIOGRAPHY

Albright, M., 1980. "Geostrophic Wind Calculations for AIDJEX," Sea Ice Processes and Models, R.S. Pritchard, ed. University of Washington Press, 402-409.

Banke, E.G., Smith, S.D., 1974. "Measurements of Towing Drag on Small Icebergs," Proc. IEEE Ocean 74, International Conference on Engineering in the Ocean Environment, Vol. 1, Halifax, Canada, 130-132.

Banke, E.G., Smith, S.D., and Anderson, R.J., 1980. "Drag Coefficients at AIDJEX from Sonic Anemometer Measurements," Sea Ice Processes and Models, R.S. Pritchard, ed. University of Washington Press, 430-442.

Brower, W.A. et al., 1977. "Climatic Atlas of the Outer Continental Shelf Waters and Coastal Regions of Alaska, Volume 3: Chukchi-Beaufort Sea," U.S. Dept. of the Interior's Bureau of Land Management and Alaskan Outer Continental Shelf Environmental Assessment Program, 10.

Brown, R.A., 1980. "Planetary Boundary Layer Modeling for AIDJEX," Sea Ice Processes and Models, R.S. Pritchard, ed. University of Washington Press, 387-401.

Browne, I.M. and Crary, A.P., 1958. "The Movement of Ice In the Arctic Ocean," Proceedings of Conference On Arctic Sea Ice, National Academy Sciences and National Research Council, Publication 598, 191-209.

Coachman, L.K., and Aagaard, K., 1988. "Transports through Bering Strait: Annual and Interannual Variability," Journal of Geophysical Research, 93, 15535-

15539.

Colony, R. 1987. Pressure maps over the Arctic Ocean, Personal Communication.

Crary, A.P., 1958. "Arctic Ice Island and Ice Shelf Studies," Part 1, Arctic, 11: 3-42.

De Paoli, S., Morrison, T.B., and Marcellus, R.W., 1982. "Analysis of Interaction Probabilities Between Large Ice Features and Offshore Structures in the Canadian Beaufort Sea," Beaufort E.I.S. Reference Works, 101 pp.

Greenaway, K.R., 1952. "Additional Information from Flights and Air Photographs in the Canadian Arctic," Arctic, Vol. 5, No. 2, 75-82.

Hattersley-Smith, G., 1957. "The Rolls on the Ellesmere Ice Shelf," Arctic, 10, 32-44.

Hattersley-Smith, G., 1963. "The Ward Hunt Ice Shelf: Recent Changes of the Ice Front," Journal of Glaciology, Vol. 4, 415-524.

Hibler III, W.D., 1986. "Ice Dynamics," The Geophysics of Sea Ice, edited by Untersteiner N., New York and London, Plenum Press, 557-640.

Hobson, G., 1989. "Ice Island Field Station," EOS Transactions, American Geophysical Union. Volume 70, No. 37, 833, 835, 838-839.

Hoerner, S., 1965. "Fluid Dynamic Drag," Practical Information on Aerodynamic Drag and Hydrodynamic Resistance, Hoerner, Midland Park, N.J., 11-16.

Holdsworth, G., 1971. "Calving from Ward Hunt Ice Shelf, 1961-1962," Canadian Journal of Earth Science, Vol. 8, 299-305.

Holdsworth, G. and Traetteberg, A., 1973. "The Deformation of An Arctic Ice

Island," Proceedings of the Second International Conference on Port and Ocean Engineering Under Arctic Conditions, University of Iceland, 419-440.

Hunkins, K., 1967. "Inertial Oscillations of Fletcher's Ice Island (T-3)," Journal of Geophysical Research, Vol. 72, No. 4, 1165-1174.

Jeffries, M.O. and Serson, H., 1983. "Recent Changes at the Front of Ward Hunt Ice Shelf, Ellesmere Island, N.W.T.," Arctic, Vol. 36, 289-290.

Jeffries, M.O., Sackinger, W.M., and Shoemaker, H., 1988. "Geometry and Physical Properties of Ice Islands," in Port and Ocean Engineering under Arctic Conditions, Vol.1, W.M. Sackinger and M.O. Jeffries, eds., Geophysical Institute, University of Alaska, 69-83.

Jeffries, M.O., 1989. Personal correspondence.

Jeffries, M.O. and Sackinger, W.M., 1989. "Analysis and Interpretation of an Airborne Synthetic Aperture Radar Image of Hobson's Choice Ice Island," Proceedings of the 10th International Conference on Port and Ocean Engineering under Arctic Conditions (POAC'89), Luleå University of Technology, Luleå, Sweden.

Jeffries, M.O. and Sackinger, W.M., 1990. "Ice Island Detection and Characterization With Airborne Synthetic Aperture Radar," Journal of Geophysical Research, Vol. 95, No. C4, 5371-5377.

Johnson, W.R., 1987. "Physical Oceanography," The Environment and Resources of the Southeastern Chukchi Sea, U.S. Depts. of Commerce and the Interior, 34.

Koenig, L.S., Greenaway, K.R. Dunbar, M. and Hattersley-Smith, G., 1952. "Arctic Ice Island," Arctic, Vol. 5, 67-103.

Kovacs, A., 1977. "Iceberg Thickness and Crack Detection," Iceberg Utilization. Edited by A.A. Husseiny, Iowa State University , Ames, Iowa, USA, 131-144.

Kowalik, Z. and Matthews, J.B., 1982. "The M_2 Tide in the Beaufort and Chukchi Seas," Journal of Physical Oceanography, 12, 743-746.

Langleben, M.P., 1982. "Water Drag Coefficient of First Year Sea Ice," Journal of Geophysical Research, Vol.87(C1), 573-578.

Leavitt, E., 1980. "Surface-based Air Stress Measurements Made during AIDJEX," Sea Ice Processes and Models, R.S. Pritchard ed. University of Washington Press, 419-429.

LeSchack, L.A., 1961. "Arlis II: New Arctic Drift Station," Naval Research Reviews, September, 12-18.

Li, F., Sackinger, W.M., Lu, M., Jeffries, M.O., 1988. "A Probabilistic Study of Ice Island Trajectories," in Proceedings of The 9th International Symposium on Ice, International Association for Hydraulic Research , Committee on Ice Problems, Vol.1, H. Saeki and K. Hirayama, eds., Sapporo, Japan, 405-414.

Lu, M., 1988. "Analysis of Ice Island Movement," M.S. Thesis, Geophysical Institute, University of Alaska Fairbanks, Fairbanks, Alaska.

Martin, S. and Thorndike, A., 1974. "Ice Island Report," AIDJEX Bulletin. No. 27, 108-116.

McBean, G., 1986. "The Atmospheric Boundary Layer," The Geophysics of Sea Ice, Edited by N. Untersteiner, New York and London, Plenum Press, 283-337.

McPhee, M.G., 1979. "The Effect of the Oceanic Boundary Layer on the Mean

Drift of Pack Ice: Application of a Simple Model," Journal of Physical Oceanography, 9: 388-400.

McPhee, M.G., 1980. "An Analysis of Pack Ice Drift in Summer," Sea Ice Processes and Models, R.S. Pritchard, ed. University of Washington Press. 62-75.

McPhee, M.G., 1982. "Sea Ice Drag Laws and Simple Boundary Layer Concepts, Including Application to Rapid Melting," USA Cold Regions Research and Engineering Laboratory, CRREL Report 82-4.

McPhee, M.G., 1986. "The Upper Ocean", The Geophysics of Sea Ice, edited by Untersteiner N., New York and London, Plenum Press, 339-394.

Monin, A.S., and Obukhov A.M., 1954. "Dimensionless Characteristics of Turbulence in the Surface Layer." Trudy Geofiz. Inst., Akad. Nauk SSR, 24: 163-187.

Narod, B.B., Clarke, G.K.C., and Prager, B.T., 1988. "Airborne UHF Radar Sounding of Glaciers and Ice Shelves, Northern Ellesmere Island, Arctic Canada," Canadian Journal of Earth Sciences, Volume 25, No. 1, 95-105.

Nutt, D.C., 1966. "The Drift of Ice Island WH-5," Arctic 19 (3), 244-262.

Paulson, C.A., 1980. "A Review of the AIDJEX Atmospheric Program," Sea Ice Processes and Models, R.S. Pritchard, ed. University of Washington Press, 28-33.

Peary, R., 1907. "Nearest the Pole, A Narrative of the Polar Expedition of the Peary Arctic Club in the S.S. Roosevelt," Hutchinson, London, 1905-1906.

Pease, C.H., Salo, S.A., and Overland, J.E., 1983. "Drag Measurements

for First-Year Sea Ice Over a Shallow Sea," Journal of Geophysical Research, Vol.88(C5), 2853-2862.

Russell, W.E., Riggs, N.P. and Robe, R.Q., 1977. "Local Iceberg Motion - a Comparison of Field and Model Studies," Proc. POAC 77, St. John's, Canada, 784-798.

Sackinger, W.M., Shoemaker, H.D., Serson, H., Jeffries, M.O. and Yan, M., 1985. "Ice Islands as Hazards to Arctic Offshore Production Structures," Proceedings of Offshore Technology Conference, Houston, Texas. 399-408.

Sackinger, W.M., Yan, M., 1987. "Loss, Decay, and Recent Drift of Ice Islands," Workshop On Extreme Ice Features, National Research Council of Canada, Technical Memorandum 141, NRCC 28003, 53-66.

Sackinger, W.M. and Tippens, H., 1988. "Analysis of Ice Island Movement," Port and Ocean Engineering under Arctic Conditions, Vol.1, W.M. Sackinger and M.O. Jeffries, eds., Geophysical Institute, University of Alaska, 269-277.

Sackinger, W.M., Jeffries, M.O., Tippens, H., Li, F., and Lu, M., 1989. "Dynamics of Ice Island Motion Near the Coast of Axel Heiberg Island, Canadian High Arctic," Annals of Glaciology, 12, 152-156.

Sackinger, W.M., Jeffries, M.O., Lu, M. and Li, F., 1990. "Arctic Ice Islands." Final Report, U.S. Department of Energy. 308pp.

Schlichting, H., 1979. "Boundary-Layer Theory." Translated by J. Kestin, Seventh Edition. McGraw-Hill Book Company, 817pp.

Shirasawa, K., Riggs, N.P., and Muggeridge, D.B., 1984. "The Drift of a Number of Idealized Model Icebergs," Cold Regions Science and Technology, Vol.10.

19-30.

Shreider, Y.A., 1962. "The Monte Carlo Method," Pergamon Press.

Smith, D.D., 1964. "Ice Lithologies and Structure of Ice Island Arlis II," Journal of Glaciology, Vol. 5, No. 37, 17-38.

Smith, W.O., Jr., editor, 1990. Polar Oceanography, Part A: Physical Science. Academic Press, Inc. 406pp.

Spedding, L.G., 1977. "Ice Island Count Southern Beaufort Sea 1976," APOA 99, IPRT-13ME-77, Imperial Oil Limited, 50pp.

Stefansson, V., 1922. "The Friendly Arctic," MacMillan, New York.

Sverdrup, H.U., 1926. "Dynamics of Tides on the North Siberian Shelf: Results from the Maud Expedition," Geofysiske Publikajoner, IV (5): 75P.

Thorndike, A.S., 1982. "Statistical Properties of the Atmospheric Pressure Field Over the Arctic Ocean," Journal of the Atmospheric Sciences, Vol. 39, 2229-2338.

Thorndike, A.S., 1986. "Kinematics of Sea Ice," The Geophysics of Sea Ice, edited by Untersteiner N., New York and London, Plenum Press, 489-550.

Thorndike, A.S., Colony, R. and Muñoz, E.A., 1986. "Arctic Ocean Buoy Program, Data Report, 1 January 1980 to 31 December 1985," Polar Science Center, University of Washington.

Walsh, J.E., 1978. "Temporal and Spatial Scales of the Arctic Circulation," Monthly Weather Review, Vol.106, No.11, 1532-1544.

Yan, M., 1986. "The Relationship between Ice Island Movement and Weather Con-

ditions," M.S. Thesis, University of Alaska, Fairbanks.

Zubov, N.N., 1945. "Arctic Ice," Izdatel'stvo Glavsevmorputi, Moscow, Translated for Air Force Cambridge Research Center by U.S. Naval Oceanography Office and American Meteorological Society, 360pp.

Appendix

COMPUTER SIMULATION PROGRAMS

```
C. This program simulates the probabilities of ice island trajectiories
C. with ice island generation model, dynamic model and Monte Carlo method.

      PROGRAM   PROTRA

      COMMON /MOV/ COEFF,Roa,Ca,Row,Cws,Cwf,Omega,MONTH
     &       /COA/ ID1,ID2,PERCO,PARCO
      COMMON /COLAND/ LAND(51,56)
      COMMON ITE
      REAL      RECURRENCY(51,56),PRO(51,56),As(700),
     &          Hi(700),Af(700),Mass(700),X1(700),X2(700),X3(700),
     &          Y1(700),Y2(700),Y3(700),Vix(700),Viy(700),
     &          Mux,Muy,LAT,LONG,LIFE(700)
      INTEGER   BLOCK(51,56),YEAR,YEAR4,OUT   ! OUT=1 out of the ocean.
      COMPLEX   Mu1(9,10),Mu2(9,10),Mu3(9,10),Mu4(9,10),
     &          Mu5(9,10),Mu6(9,10),Mu7(9,10),Mu8(9,10),
     &          Mu9(9,10),Mu10(9,10),Mu11(9,10),Mu12(9,10),
     &      Mu,BOUND1(27),BOUND2(23),BOUND3(7),CURRENT(9,10)
C. Mu1--12 are monthly mean geos. wind(speed in m/s, dir. in degrees).
      COMMON /COCUR/CURRENT
      DATA      BLOCK/2856*0.0/,LAND/2856*0/,RECURRENCY/2856*0/,
     &          LIFE/700*0/
C. input monthly averaged geostrophic wind.
      INCLUDE '[ftf1.pro]WIND.DATA'

C. input boundary data.
      INCLUDE '[ftf1.pro]LAND.DATA'

      INCLUDE '[ftf1.pro]CURRENT.DATA'
      INCLUDE 'PARA.METER'

      OPEN (UNIT=22,FILE='RECURRENCY.DAT',STATUS='NEW')
      OPEN (UNIT=55,FILE='LIVENUMBER.DAT',STATUS='NEW')
      OPEN (UNIT=66,FILE='LIFETIME.DAT',STATUS='NEW')

      Roa=1.3                   ! air density 1.3 kg/(m)3
      Ca =0.00363               ! air drag coefficient
      Row=1032.                 ! water density, 1032 kg/(m)3
      Cws =0.00105              ! water drag coefficient
      Cwf =0.71
      Omega=7.292E-5   ! angular velocity of earth rotation, rad/s.

C  ---------------------------------------------------------------
C. Transform land.data to "land" blocks (land=1).
      LM=0
      DO LN=1,27                ! BOUND1(27)
         I=INT( AIMAG(BOUND1(LN))/50.)
         J=INT( REAL (BOUND1(LN))/50.)
         IF (I.GT.LM) THEN
            LM=LM+1
            DO LI=LM,I
               DO LJ=1,J
                  LAND(LI,LJ)=1
               ENDDO
```

```
          DO LL=1,5                    !COASTAL ZONE 11.
             LAND(LI,J+LL)=11
          ENDDO

       ENDDO
       LM=I
    ENDIF
 ENDDO

 LM=0
 DO LN=1.23              ! BOUND2(23)
    I=INT( AIMAG(BOUND2(LN))/50.)
    J=INT( REAL (BOUND2(LN))/50.)
    IF (J.GT.LM) THEN
       LM=LM+1
       DO LJ=LM,J
          DO LI=I+1,51
             LAND(LI,LJ)=1
          ENDDO

          IF (LJ.LT.43) THEN          ! COASTAL ZONE 22.
             DO LL=I-4,I
                IF (LAND(LL,LJ).EQ.0) LAND(LL,LJ)=22
             ENDDO
          ENDIF

          IF ((LJ.GE.43) .AND. (LJ.LE.52)) THEN  !COASTAL ZONE 55.
             DO LL=I-4,I
                LAND(LL,LJ)=55
             ENDDO
          ENDIF

       ENDDO
       LM=J
    ENDIF
 ENDDO

 DO LI=36,46                          ! COASTAL ZONE 44.
    DO LJ=51,55
       LAND(LI,LJ)=44
       LAND(LI,56)=1
    ENDDO
 ENDDO

 LM=9
 DO LN=1,7                 ! BOUND3(7).
    I=INT( AIMAG(BOUND3(LN))/50.)
    J=INT( REAL (BOUND3(LN))/50.)

    IF (J.GT.LM) THEN
       LM=LM+1
       DO LJ=LM,J
          DO LI=1,I

             LAND(LI,LJ)=1
          ENDDO

          DO LL=1,5              ! COASTAL ZONE 33.
             LAND(I+LL,LJ)=33
          ENDDO

       ENDDO
       LM=J
    ENDIF
 ENDDO

 DO I=7,35
    LAND(I,56)=211           ! for ejecting route:Gr.-Sv.
 ENDDO
```

```
      DO I=36,39                  ! for ejecting route:Bearing Srait
         LAND(I,1 )=222
      ENDDO

      DO I=1,5
         DO J=7,9
            LAND(I,J)=233         ! for ejecting route:Amundsen Gulf
            ENDDO
         ENDDO

         DO J=47,49                 ! for ejecting rout:Nares Strait.
            LAND(2,J)=244
         ENDDO


         DO I=6,11                  ! COASTAL ZONE 66.
            DO J=5,11
               IF (LAND(I,J).NE.1) LAND(I,J)=66
            ENDDO
         ENDDO
         DO J=46,49
            LAND(3,J)=66
         ENDDO
         DO J=46,50
            LAND(4,J)=66
         ENDDO
C-----------------------------------------------------------------------

         YEAR= 0
         YEAR4=4
         NBOUNDARY=0
         NISLAND1 =0
         NISLAND2 =0
         NISLAND3 =0
         NISLAND4 =0
         NMELT    =0
         IS   =0
         NLIFE=0
C-----------------------------------------------------------------------
C. Random ice island dimensions.

50          CALL SHELF(AREA)

100         CALL ISLAND(A)

            AREA=AREA-A

            IF ((AREA.LT.0.).AND.(IS.NE.0)) THEN
               GOTO 150
            ELSE
               IS=IS+1
               IF (AREA.LT.0.) THEN  !if area<a a=area for the last island.
                  As(IS)=AREA+A
               ELSE
                  As(IS)=A
               ENDIF
            ENDIF

            Hi(IS) =42.5
            Af(IS) =0.85*Hi(IS)*SQRT(As(IS))
C.                  form surface area (merged in water),m**2.
            Mass(IS)=As(IS)*Hi(IS)*872.  ! kg. instead of *1.08
C-----------------------------------------------------------------------
C. Random initial ice island positions along Ellesmere Island (km).

            X=RAN(ITE)*420.+1800.
C.
            Y=201.
```

```
            X1(IS)=X                ! set initial position series
            X2(IS)=X
            X3(IS)=X
            Y1(IS)=Y
            Y2(IS)=Y
            Y3(IS)=Y
            Vix(IS)=0.0             ! set initial speed of ice island zero
            Viy(IS)=0.0
            GOTO 100

150         MONTH=INT( RAN(ITE)*12.0 ) +1
            IF (MONTH.GE.13) MONTH=12
            N= (MONTH-1)*15+1

            YEAR4=0

C-------------------------------------------------------------------------
200       N=N+1                                 ! step N increases 1  =2 days.
          INDEX =0                              ! =1 for melted down case.

          IF (N.GE.180) THEN
           N= 1
           YEAR=YEAR+1
           YEAR4=YEAR4+1

           DO M=1,IS
              Hi(M)=Hi(M)-1.0
              Af(M)=SQRT(As(M))*Hi(M)*0.85
              Mass(M)=As(M)*Hi(M)*872.        ! kg
              IF (Hi(M).LE.2.0) THEN
                 INDEX=1
                 Mass(M)=-10.
              ENDIF
              LIFE(M)=LIFE(M)+1.
           ENDDO
          ENDIF
          IF (YEAR4.EQ.4) GOTO 50

C-------------------------------------------------------------------------
C if there is any ice island melted down, rearrange the order.
          IF (INDEX.EQ.1) THEN
             K=0
             DO M=1,IS
                IF (MASS(M).EQ.-10.) THEN
                   K=K+1
                   DO N=M,IS
                      X1(N)=X1(N+1)
                      X2(N)=X2(N+1)
                      X3(N)=X3(N+1)
                      Y1(N)=Y1(N+1)
                      Y2(N)=Y2(N+1)
                      Y3(N)=Y3(N+1)
                      Vix(N)=Vix(N+1)
                      Viy(N)=Viy(N+1)
                      As(N)=As(N+1)
                      Af(N)=Af(N+1)
                      Hi(N)=Hi(N+1)
                      MASS(N)=MASS(N+1)
                      LIFE(N)=LIFE(N+1)
                   ENDDO
                ENDIF
             ENDDO
             IS=IS-K
             NMELT =NMELT+K
          ENDIF
C-------------------------------------------------------------------------

          MONTH=INT( FLOAT(N-1)/15. )+1
```

```
C.calculate each ice island dispalcement during two days.
      INDEX=0                    ! =1 for out of the ocean
250   DO M=1,IS

C.pick up mean wind at individual grids.
        LX=INT(X3(M)/300.)+1
        LY=INT(Y3(M)/300.)+1
        GO TO (1,2,3,4,5,6,7,8,9,10,11,12), MONTH

1       Mu=Mu1( LY,LX )     ! mean geostrophic wind for January at
        GOTO 300            ! block (LX,LY).

2       Mu=Mu2( LY,LX )
        GOTO 300

3       Mu=Mu3( LY,LX )
        GOTO 300

4       Mu=Mu4( LY,LX )
        GOTO 300

5       Mu=Mu5( LY,LX )
        GOTO 300

6       Mu=Mu6( LY,LX )
        GOTO 300

7       Mu=Mu7( LY,LX )
        GOTO 300

8       Mu=Mu8( LY,LX )
        GOTO 300

9       Mu=Mu9( LY,LX )
        GOTO 300

10      Mu=Mu10( LY,LX )
        GOTO 300

11      Mu=Mu11( LY,LX )
        GOTO 300

12      Mu=Mu12( LY,LX )


300     Mux= COSD( AIMAG(Mu) ) *REAL(Mu)
        Muy= SIND( AIMAG(Mu) ) *REAL(Mu)

C.-----------------------------------------------------------------
C. pick up random geostrophic wind in Ug, Vg.(m/s).

301     CALL RANDWIND( X1(M),Y1(M),X2(M),Y2(M),
     &                 X3(M),Y3(M),N,Mux,Muy,Ug,Vg )

C. convert to surface wind: 26 degrees turning angle to the
C. left of geostrophic wind and 0.6 coefficient of modulus.

        SITA= ARCTAN(Vg,Ug)+26.0
        IF (SITA .GT. 360.) SITA=SITA-360.
        Va  = SQRT( Ug**2+Vg**2 )*0.6

        X1(M)=X2(M)
        Y1(M)=Y2(M)
        X2(M)=X3(M)
        Y2(M)=Y3(M)
```

```
          Vax = COSD(SITA)*Va
          Vay = SIND(SITA)*Va

C-----------------------------------------------------------------------
C. compute displacement of ice island for 2 days. input original
C  X,Y(km),Vix, Viy(m/s), and output X48,Y48,Vix48,Viy48 for 48 hrs.
C  later in X3,Y3(km), Vix,Viy(m/s).

       CALL MOVE( X3(M),Y3(M),Vix(M),Viy(M),Vax,Vay,year,
     &          Mass(M),As(M),Af(M),OUT,NBOUNDARY)

C-----------------------------------------------------------------------
C. find the blocks where the ice island passed through in the last 2
C  days with (X2,Y2), (X3,Y3) and step-by-step method. Add 1 to
C  BLOCK(I,J) if it was passed.

       IB= INT(Y2(M)/50.)+1      ! BLOCK location (IB,JB) for (X2,Y2).
       JB= INT(X2(M)/50.)+1
       IF (IB.GT.51) IB=51
       IF (JB.GT.56) JB=56
       IF (IB.LT.1)  IB=1
       IF (JB.LT.1)  JB=1

C. if (X2,Y2) and (X3,Y3) in same block, don't add 1.
       IF ((INT(X3(M)/50.).EQ.INT(X2(M)/50.)) .AND.
     &  (INT(Y3(M)/50.).EQ.INT(Y2(M)/50.))) GOTO 350

C. if in different blocks, check blocks passed and add 1 to them.
       IF (ABS(X3(M)-X2(M)).GE.ABS(Y3(M)-Y2(M))) THEN
           IF (X3(M).GT.X2(M)) THEN      ! if slope < 45 deg. step is dx
              INC=1
           ELSE
              INC=-1
           ENDIF

           DO I=0, INT(X3(M))-INT(X2(M)), INC
              X = X2(M)+I                          ! step-length= 1km
              Y = (Y3(M)-Y2(M))/(X3(M)-X2(M))*
     &            (X-X2(M))+Y2(M)                  ! dy to dx=1km
              ID= INT(Y/50.)+1             ! block location for new (X,Y)
              JD= INT(X/50.)+1
              IF (ID.GT.51) ID=51
              IF (JD.GT.56) JD=56
              IF (ID.LT.1)  ID=1
              IF (JD.LT.1)  JD=1

              IF ((ID .NE. IB) .OR. (JD .NE. JB)) THEN
              BLOCK(ID,JD)=BLOCK(ID,JD)+1 !add 1 if goes into new block
              IB=ID
              JB=JD
              ENDIF
           ENDDO

       ELSE                                    !if slope > 45 deg. dy as step
           IF (Y3(M).GT.Y2(M)) THEN
              INC=1
           ELSE
              INC=-1
           ENDIF

           DO I=0, INT(Y3(M))-INT(Y2(M)), INC
              Y=Y2(M)+I                        ! step length dy=1km
              X=(X3(M)-X2(M))/(Y3(M)-Y2(M))*
     &          (Y-Y2(M))+X2(M)

              ID=INT(Y/50.)+1
```

```
                JD=INT(X/50.)+1
                IF (ID.GT.51) ID=51
                IF (JD.GT.56) JD=56
                IF (ID.LT.1)  ID=1
                IF (JD.LT.1)  JD=1

                IF ((ID .NE. IB) .OR. (JD .NE. JB)) THEN
                   BLOCK(ID,JD)=BLOCK(ID,JD)+1      ! add 1 if goes new
                   IB=ID                            ! block.
                   JB=JD
                ENDIF
             ENDDO
          ENDIF

C-------------------------------------------------------------------------
          IF ( OUT .EQ. 1 ) THEN
             MASS(M)=-10.
             INDEX=1
             NLIFE=NLIFE+1
             WRITE (66,*) NLIFE,LIFE(M)
          IF (NBOUNDARY.EQ.211) NISLAND1=NISLAND1+1
          IF (NBOUNDARY.EQ.222) NISLAND2=NISLAND2+1
          IF (NBOUNDARY.EQ.233) NISLAND3=NISLAND3+1
          IF (NBOUNDARY.EQ.244) NISLAND4=NISLAND4+1
          ENDIF

350       ENDDO                          ! return to 250.

C-------------------------------------------------------------------------
C if there is any ice island going out, rearrange the order.

          IF (INDEX.EQ.1) THEN
             K=0
             DO M=1,IS
                IF (MASS(M).EQ.-10.) THEN
                   K=K+1
                   DO M1=M,IS
                      X1(M1)=X1(M1+1)
                      X2(M1)=X2(M1+1)
                      X3(M1)=X3(M1+1)
                      Y1(M1)=Y1(M1+1)
                      Y2(M1)=Y2(M1+1)
                      Y3(M1)=Y3(M1+1)
                      Vix(M1)=Vix(M1+1)
                      Viy(M1)=Viy(M1+1)
                      As(M1)=As(M1+1)
                      Af(M1)=Af(M1+1)
                      Hi(M1)=Hi(M1+1)
                      MASS(M1)=MASS(M1+1)
                      LIFE(M1)=LIFE(M1+1)
                   ENDDO
                ENDIF
             ENDDO
             IS=IS-K
          ENDIF
C-------------------------------------------------------------------------
400       IF (YEAR .LT. IYEAR) GOTO 200

          SIGMA=0.0
          DO I=1,51
             DO J=1,56
                SIGMA=SIGMA+BLOCK(I,J)    ! sum of events of passing through
             ENDDO
          ENDDO

          IF (SIGMA.GT.1.0E-10) THEN
```

```
      DO I=1,51
         DO J=1,56
            PRO(I,J)=BLOCK(I,J)/SIGMA

            IF (BLOCK(I,J).GE.1) THEN
      RECURRENCY(I,J)=FLOAT(IYEAR)/BLOCK(I,J)
            ELSE
        RECURRENCY(I,J)=100000.
            ENDIF

         ENDDO
      ENDDO

      WRITE (22,*) RECURRENCY
      WRITE (44,*) 'Gr.-Sv.= ',NISLAND1,'B.S.= ',NISLAND2,
     &  'A.G.= ',NISLAND3,'N.S.= ',NISLAND4,'NMELT= ',NMELT

      ELSE

      PRINT *,'!!! SIGMA=0.0'

      ENDIF

500   STOP
      END



C.----------------------------------------------------------------------
C. Subroutine for random geostrophic wind generation.


      SUBROUTINE RANDWIND (X1,Y1,X2,Y2,X3,Y3,N,Mux,Muy,Ug,Vg)
C                 X,Y-- km,  Mu,U,V-- m/s, N-- timestep,2days.

      REAL KEXI(3),Mux,Muy

      R21=SQRT((X2-X1)**2+(Y2-Y1)**2)
      R32=SQRT((X3-X2)**2+(Y3-Y2)**2)
      R31=SQRT((X3-X1)**2+(Y3-Y1)**2)

      DO I=1,2

      IF (I.EQ.1) THEN
         D21=Y2-Y1
         D32=Y3-Y2
         D31=Y3-Y1
      ENDIF
      IF (I.EQ.2) THEN
         D21=X2-X1
         D32=X3-X2
         D31=X3-X1
      ENDIF

C AUTOCOVARIANCE--- (m/s)**2. VARIANCE C11,C22,C33 = 7**2 (m/s)**2
      C21=0.36*(1.0-2.0*(D21/1300.0)**2)*EXP(-(R21/1300.0)**2)*74.0
      C32=0.36*(1.0-2.0*(D32/1300.0)**2)*EXP(-(R32/1300.0)**2)*74.0
      C31=0.36*(1.0-2.0*(D31/1300.0)**2)*EXP(-(R31/1300.0)**2)*46.0

C LINEAR TRANS. COEFFICIENTS.
      A21=C21/7.0
      A22=SQRT(49.0-A21**2)
      A31=C31/7.0
      A32=(C32-A21*A31)/49.0
      A33=SQRT(49.0-A31**2-A32**2)
```

```
C NORMAL RANDOM NUMBER WITH MEAN ZERO AND VARIANCE 1
        DO I1=1,3
         KEXI(I1)=0.0
        ENDDO

        DO J1=1,3
          DO J2=1,12
             KEXI(J1)=KEXI(J1)+ RAN(ITE)
          ENDDO
          KEXI(J1)=KEXI(J1)-6.0
        ENDDO

C JOINT NORMAL RANDOM NUMBERS WITH AUTOCOVARIANCE MATRIX C AND ZERO MEAN
        IF (N.EQ.1) ZETA=7.0*KEXI(1)
        IF (N.EQ.2) ZETA=A21*KEXI(1) +A22*KEXI(2)
        IF (N.GT.2) ZETA=A31*KEXI(1)+A32*KEXI(2)+A33*KEXI(3)

C RANDOM WIND (m/s)
        IF (I.EQ.1) THEN
           Ug= ZETA+Mux
           IF (ABS(Ug).GT.25.) Ug=25.
        ELSE
           Vg= ZETA+Muy
           IF (ABS(Vg).GT.25.) Vg=25.
        ENDIF

        ENDDO

        RETURN
        END


C.-----------------------------------------------------------------------
C. Subroutine of movement of ice island.

        SUBROUTINE MOVE(X,Y,Vix,Viy,Vax,Vay,year,
     &            MASS,As,Af,OUT,NBOUNDARY)

C.  X,Y in km. Vix,Viy,Vax,Vay are in m/s.
C.  input Xo,Yo,Vixo,Viyo and output X48,Y48,Vix48,Viy48 in X,Y,Vix,Viy.
C.  input wind Vax,Vay and output OUT to tell if out of the Arctic Ocean.

        INTEGER OUT          ! out of the Arctic Ocean =1
        REAL MASS,LAT,LONG
        COMPLEX   CURRENT(9,10),Vw
        COMMON /MOV/ COEFF,Roa,Ca,Row,Cws,Cwf,Omega,MONTH
     &         /COA/ ID1,ID2
        COMMON /COLAND/ LAND(51,56) /COCUR/CURRENT

        OUT=0
        NBOUNDARY=0
        hrstep=2.
        DO Ihr=1, 48/hrstep

        DX=Vix*3.6*hrstep   !in km. time-step=1hr.=3600s,3.6=3600/1000
        DY=Viy*3.6*hrstep

C.                          -- coast effect --
        IF (ID2.EQ.1) THEN
           CALL COAST(X,Y,DX,DY)     !input x,y,dx,dy, modified dx,dy
C.                                    outputed in DX,DY.
        ENDIF

C.                          -- modified location every hr. --
           X=X+DX
```

```
      Y=Y+DY

C                  -- check wether or not out of ocean.--
      IL=INT(Y/50.)+1
      JL=INT(X/50.)+1

      IF (IL.GT.51) IL=51
      IF (JL.GT.56) JL=56
      IF (IL.LT.1)  IL=1
      IF (JL.LT.1)  JL=1

      IF (LAND(IL,JL).GT.200) THEN
         OUT=1
         NBOUNDARY=LAND(IL,JL)
         GO TO 10
      ENDIF

      IF (LAND(IL,JL).EQ.1) THEN
         X=X-DX
         Y=Y-DY
         Vix=0.
         Viy=0.
         GO TO 10
      END IF

C                       -- forces in N. --
         V   =SQRT( (Vax-Vix)**2 +(Vay-Viy)**2 )    ! |Va-Vi|

         Fax =Roa*Ca*As/MASS*V*(Vax-Vix)
         Fay =Roa*Ca*As/MASS*V*(Vay-Viy)

         LX=INT(X/300.)+1
         LY=INT(Y/300.)+1

         IF (LX.GT.10) LX=10
         IF (LX.LT.1)  LX=1
         IF (LY.GT.9)  LY=9
         IF (LY.LT.1)  LY=1

         Vw=CURRENT(LY,LX)
         Vwx=COSD(AIMAG(Vw))*REAL(Vw)
         Vwy=SIND(AIMAG(Vw))*REAL(Vw)
         Viwx=Vix-Vwx
         Viwy=Viy-Vwy
         RCWV=Row*Cws*As/MASS*SQRT( Viwx**2+Viwy**2 )
         Fwsx=RCWV*( COSD(204.)*Viwx-SIND(204.)*Viwy )
         Fwsy=RCWV*( SIND(204.)*Viwx+COSD(204.)*Viwy )
C                              ------ turning angle 24 degrees.
         Vi=SQRT(Vix*Vix+Viy*Viy)

         IF (Vi.LT.0.015) THEN
            Fpx=-SQRT(As)*Viy*(51400.-2560000.*Vi)/MASS
            Fpy=SQRT(As)*Vix*(51400.-2560000.*Vi)/MASS
         ELSE IF (Vi.le.0.49) THEN
            Fpx=-SQRT(As)*Viy*(17800.-18000.*Vi)/MASS
            Fpy=SQRT(As)*Vix*(17800.-18000.*Vi)/MASS
         ELSE
            Fpx=-SQRT(As)*8900.*Viy/MASS
            Fpy=SQRT(As)*8900.*Vix/MASS
         ENDIF
         fpx=fpx*coeff1
         fpy=fpy*coeff1

5        CALL CONVER(X,Y,LAT,LONG)
         Fcx = 2*Omega*SIND(LAT)*Viy*COEFF
         Fcy =-2*Omega*SIND(LAT)*Vix*COEFF
```

```
C.              -- acceleration= speed icrease in hrstep hrs. --
          Alfa= 0.5*Cwf*Af/Cws/As                ! ratio of Fwf to Fws
          DVix= (Fax+(1.+Alfa)*Fwsx+Fpx+Fcx) *3600.0*hrstep   ! m/s
          DViy= (Fay+(1.+Alfa)*Fwsy+Fpy+Fcy) *3600.0*hrstep

C.                      -- speed after every hrstep --
          Vix1 = Vix+DVix
          Viy1 = Viy+DViy

C-----------------------------------------------------------------------
C Two false cases for Vix1 and Viy1 are restricted.  One is Vax
C and Vix in same dir. while Vix1 and Vix in opposite dir.,
C another one is Vax zero while Vix1 and Vix in opposite dir.

          IF ((ABS(Vix1).gt.0.0000001).and.(ABS(Vax).gt.
     &                        0.0000001)) THEN
             IF (((Vix/Vax).gt.0.0).and.(((Vix/Vix1).lt.
     &       0.0).OR.(ABS(Vix).gt.ABS(Vix1))))  Vix1=Vix

             IF (((Vix/Vax).lt.0.0).and.(ABS(Vix).LT
     &                        .ABS(Vix1))) Vix1=0.0
             GO TO 8
          ENDIF
          IF ((ABS(Vix1).gt.0.0000001).and.(ABS(Vax).le.
     &                        0.0000001)) THEN
             IF ((Vix/Vix1).lt.0.0) Vix1=0.0
          ENDIF
8         IF ((ABS(Viy1).gt.0.0000001).and.(ABS(Vay).gt.
     &                        0.0000001)) THEN
             IF (((Viy/Vay).gt.0.0).and.(((Viy/Viy1).lt.
     &       0.0).OR.(ABS(Viy).gt.ABS(Viy1))))  Viy1=Viy
             IF (((Viy/Vay).lt.0.0).and.(ABS(Viy).LT.
     &                        ABS(Viy1))) Viy1=0.0
             GO TO 9
          ENDIF
          IF ((ABS(Viy1).gt.0.0000001).and.(ABS(Vay).le.
     &                        0.0000001)) THEN
             IF ((Viy/Viy1).lt.0.0) Viy1=0.0
          ENDIF
C-----------------------------------------------------------------------

9         Vix=Vix1
          Viy=Viy1

        ENDDO

10      RETURN
        END

C-----------------------------------------------------------------------
C This subroutine deals with the conversion from Cartician
C Coordinate X1 Y1 to Latitude SAI and Longitude CITA.

        SUBROUTINE CONVER(X1,Y1,LAT,LONG)
        PARAMETER Re=6371.2       ! Radius of earth in km.
        REAL LAT,LONG

        X= (X1-2350.)*COSD(32.)- (Y1-925.)*SIND(32.)
        Y= (X1-2350.)*SIND(32.)+ (Y1-925.)*COSD(32.)
        LONG= ARCTAN(Y,X)      ! Longitude from 0. to 360. in degree.

        IF ((ABS(X).LT.E-10).AND.(ABS(Y).LT.E-10)) LAT=0
        IF ((LONG.EQ.90.).OR.(LONG.EQ.270.)) THEN
           SINALF=Y/2./Re/SIND(LONG)
        ELSE
```

```
            SINALF=X/2./Re/COSD(LONG)
          ENDIF
          LAT= 90.-2.*ASIND(SINALF)! Latitude from 0. to 90. in degree.

          RETURN
          END


C.-----------------------------------------------------------------
C. ARCTAN(Y/X) in degrees from 0 to 360 in 4 qurtar plane.
C. !!! Y,X must be real numbers for real form name:ARCTAN. integers
C. leads wrong values !

          FUNCTION ARCTAN(Y,X)

          IF (X .EQ. 0.0 .AND. Y .GT. 0.0) ARCTAN=90.0
          IF (X .EQ. 0.0 .AND. Y .LT. 0.0) ARCTAN=270.0
          IF (X .GT. 0.0 .AND. Y .GT. 0.0) ARCTAN=ATAND(Y/X)
          IF (X .GT. 0.0 .AND. Y .LT. 0.0) ARCTAN=360.0+ATAND(Y/X)
          IF (X .LT. 0.0 ) ARCTAN=180.0 +ATAND(Y/X)

          RETURN
          END

C.-----------------------------------------------------------------
C. This subroutine deals with the effect of coast on ice island movement.

          SUBROUTINE COAST(X,Y,DX,DY)
C                                 in km. input and output dx,dy in DX,DY.

          COMMON /COA/ ID1,ID2,PERCO,PARCO
     &           /COLAND/LAND(51,56)

          I=INT(Y/50.)+1
          IF (I.GT.51) I=51
          IF (I.LT.1)  I=1
          J=INT(X/50.)+1
          IF (J.GT.56) J=56
          IF (J.LT.1)  J=1


          IF ((LAND(I,J).NE.1).AND.(X.LE.500.).AND.(Y.GE.1950.)) THEN
             DX=0.

             IF (DY.GE.0.) THEN
                DY=0.
             ELSE
                DY=PERCO*DY
             ENDIF

             GO TO 10
          ENDIF

          IF ((LAND(I,J).NE.1).AND.(X.LT.450.).AND.(Y.GT.1700.)) THEN
             DY=DY*PERCO
             IF (DX.LT.0.) DX=DX*PERCO
C            IF (DX.GT.0.) DX=DX*PARCO
             GO TO 10
          END IF

          IF (LAND(I,J).EQ.11) THEN
             DY=PARCO*DY
             IF (DX.LT.0) DX=PERCO*DX*0.5
             GO TO 10
          ENDIF
```

```
      IF (LAND(I,J).EQ.22) THEN
         DX=PARCO*DX
         IF ((DY.GT.0) .OR. (J.LT.6))  DY=PERCO*DY
         GO TO 10
      ENDIF

      IF (LAND(I,J).EQ.55) THEN
         DX=PERCO*DX
         DY=PERCO*DY
         GO TO 10
      ENDIF

      IF (LAND(I,J).EQ.44) THEN
         DY=PARCO*DY
         IF (DX.GT.0) DX=PERCO*DX
         GO TO 10
      ENDIF

      IF (LAND(I,J).EQ.33) THEN
         DX=PARCO*DX
         IF (DY.LT.0) DY=PERCO*DY
         GO TO 10
      ENDIF

      IF (LAND(I,J).EQ.66) THEN
         DX=PERCO*DX
         DY=PERCO*DY
      ENDIF

10    RETURN
      END

C-----------------------------------------------------------------------
C Random area of ice shelf lost.
      SUBROUTINE SHELF(AREA)       ! area in m**2
      COMMON ITE
      RN=RAN(ITE)
      IF ((RN.GE.0.0).AND.(RN.LE.0.8)) THEN
         AREA=(RAN(ITE)*262.+15.)*1000000.
      ELSE
         AREA=(RAN(ITE)*262.+277.)*1000000.
      ENDIF
      RETURN
      END

C-----------------------------------------------------------------------
C Random dimensions of ice island and area.

      SUBROUTINE ISLAND(A)
      COMMON ITE

      RN=RAN(ITE)
      IF ((RN.GE.0.0).AND.(RN.LE.0.607)) THEN
         XLENGTH=(RAN(ITE)*9.+1.)*1000.
      ELSE IF ((RN.GT.0.607).AND.(RN.LE.0.928)) THEN
         XLENGTH=(RAN(ITE)*10.+10.1)*1000.
      ELSE
         XLENGTH=(RAN(ITE)*10.+20.1)*1000.
      ENDIF

      RN=RAN(ITE)
      IF ((RN.GE.0.0).AND.(RN.LE.0.491)) THEN
         RATIO=RAN(ITE)+1.
      ELSE IF ((RN.GT.0.491).AND.(RN.LE.0.793)) THEN
         RATIO=RAN(ITE)+2.0
      ELSE IF ((RN.GT.0.793).AND.(RN.LE.0.944)) THEN
```

```
      RATIO=RAN(ITE)+3.0
   ELSE IF ((RN.GT.0.944).AND.(RN.LE.0.972)) THEN
      RATIO=RAN(ITE)+4.0
   ELSE
      RATIO=RAN(ITE)+5.0
   ENDIF

   A=XLENGTH**2/RATIO

   RETURN
   END


C. IN UNIT OF M/S.
      DATA   ((CURRENT(I,J),J=1,10),I=1,9)/
     &  (0.,0.),(0.,0.),(0.,0.),(0.,0.),(0.,0.),
     &  (0.,0.),(0.,0.),(0.,0.),(0.,0.),(0.,0.),
     &  (.0,0.),(.0,0.),(.0,0.),(0.,0.),(0.,0.),
     &  (0.,0.),(0.,0.),(0.,0.),(0.,0.),(0.,0.),
     &  (.0,0.),(.0,0.),(.0,0.),(0.,0.),(0.,0.),
     &  (.0,0.),(0.,0.),(0.,0.),(0.,0.),(0.,0.),
     &  (.0,0.),(.0,0.),(0.,0.),(0.,0.),(0.,0.),
     &  (0.,0.),(0.,0.),(0.,0.),(0.,0.),(0.,0.),
     &  (.2,320.),(.2,320.),(.05,330.),(0.,0.),(0.,0.),
     &  (0.,0.),(0.,0.),(0.,0.),(0.,0.),(0.,0.),
     &  (.25,330.),(.2,330.),(.05,330.),(0.,0.),(0.,0.),
     &  (0.,0.),(0.,0.),(0.,0.),(0.,0.),(0.,0.),
     &  (.15,30.),(.2,300.),(0.1,310.),(0.,0.),(0.,0.),
     &  (0.,0.),(0.,0.),(0.,0.),(0.,0.),(0.,0.),
     &  (0.,0.),(0.,0.),(0.,0.),(0.,0.),(0.,0.),
     &  (0.,0.),(0.,0.),(0.,0.),(0.,0.),(0.,0.),
     &  (0.,0.),(0.,0.),(0.,0.),(0.,0.),(0.,0.),
     &  (0.,0.),(0.,0.),(0.,0.),(0.,0.),(0.,0.)/



C. Boundaries = 32 m water depth contours.
C. Boundary 1 (left).
      DATA      (BOUND1(I),I=1,27)/
     &  (300.,250.),(300.,400.),(250.,400.),(250.,450.),
     &  (200.,450.),(200.,550.),(100.,550.),(100.,600.),
     &  (150.,600.),(150.,750.),(200.,750.),(200.,950.),
     &  (250.,950.),(250.,1050.),(300.,1050.),(300.,1100.),
     &  (350.,1100.),(350.,1400.),(300.,1400.),(300.,1550.),
     &  (250.,1550.),(250.,1600.),(200.,1600.),(200.,1650.),
     &  (150.,1650.),(150.,1750.),(0.,1750.)/

C. Boundary 2 (top).
      DATA      (BOUND2(I),I=1,23)/
     &  (0.,1950.),(100.,1950.),(100.,2050.),(450.,2050.),
     &  (450.,1950.),(700.,1950.),(700.,2100.),(950.,2100.),
     &  (950.,2150.),(1200.,2150.),(1200.,2250.),(1700.,2250.),
     &  (1700.,2150.),(2000.,2150.),(2000.,2250.),(2100.,2250.),
     &  (2100.,2500.),(2600.,2500.),(2600.,2300.),(2750.,2300.),
     &  (2750.,2000.),(2800.,2000.),(2800.,1750.)/

C. Boundary 3 (bottum).
      DATA      (BOUND3(I),I=1,7)/
     &  (450.,250.),(450.,300.),(1150.,300.),(1150.,200.),
     &  (2550.,200.),(2550.,300.),(2800.,300.)/
```

C. monthly averaged geostrophic wind

```
      DATA       ((Mu1(I,J),J=1,10),I=1,9 )/
     &  (0.,0.),(0.,0.),(2.,190.),(2.5,210.),(3.3,220.),
     &  (4.,220.),(4.2,220.),(4.2,230.),(3.,230.),(2.5,270.),
     &  (2.,116.),(2.,116.),(2.,175.),(2.5,193.),(3.2,220.),
     &  (3.4,230.),(3.,242.),(3.,265.),(2.8,270.),(3.2,305.),
     &  (2.5,120.),(2.5,120.),(3.,120.),(0.,0.),(0.,0.),
     &  (0.,0.),(2.8,270.),(3.,290.),(4.,300.),(4., 310.),
     &  (2.7,120.),(2.7,120.),(4.,120.),(0.,0.),(0.,0.),
     &  (0.,0.),(2.8,300.),(4.,305.),(4.1,305.),(3.8,305.),
     &  (0.,0.),(1.,110.),(1.,105.),(0.,0.),(0.,0.),
     &  (0.,0.),(3.,330.),(4.,305.),(4.,305.),(3.8,305.),
     &  (0.,0.),(1.2,105.),(1.,100.),(0.,0.),(0.,0.),
     &  (0.,0.),(3.2,320.),(3.4,310.),(3.4,300.),(3.7,300.),
     &  (0.,0.),(1.,140.),(1.,120.),(0.,0.),(0.,0.),
     &  (0.,0.),(2.4,295.),(2.8,285.),(3.1,275.),(3.6,270.),
     &  (0.,0.),(4.,140.),(0.,0.),(0.,0.),(0.,0.),
     &  (0.,0.),(2.3,270.),(2.3,270.),(3.4,250.),(0.,0.),
     &  (0.,0.),(0.,0.),(0.,0.),(0.,0.),(0.,0.),
     &  (0.,0.),(2.6,255.),(2.8,250.),(3.1,240.),(0.,0.)/

      DATA     ((Mu2(I,J),J=1,10),I=1,9)/
     &  (0.,0.),(0.,0.),(3.,275.),(3.,275.),(2.,265.),
     &  (1.6,260.),(1.6,260.),(2.9,270.),(2.9,270.),(2.,305.),
     &  (0.,0.),(0.,0.),(1.5,280.),(2.1,270.),(2.,260.),
     &  (1.6,260.),(1.6,270.),(2.5,300.),(3.4,300.),(3.,305.),
     &  (0.,0.),(0.,0.),(0.,0.),(1.8,275.),(1.7,270.),
     &  (1.6,260.),(2.2,290.),(3.,305.),(3.8,305.),(3.5,300.),
     &  (0.,0.),(0.,0.),(0.,0.),(1.6,260.),(1.6,260.),
     &  (1.9,270.),(3.,280.),(3.8,300.),(3.8,300.),(3.3,2.8),
     &  (0.,0.),(0.,0.),(1.,230.),(1.6,230.),(1.8,245.),
     &  (2.4,270.),(2.8,285.),(3.6,290.),(3.6,285.),(3.1,275.),
     &  (0.,0.),(0.,0.),(1.,230.),(1.5,230.),(2.,240.),
     &  (3.4,280.),(3.6,285.),(3.4,275.),(3.1,260),(2.3,265),
     &  (0.,0.),(0.,0.),(0.,0.),(0.,0.),(1.,260.),
     &  (2.6,280.),(3.,285.),(3.4,285.),(3.,270.),(3.1,240.),
     &  (0.,0.),(0.,0.),(0.,0.),(0.,0.),(0.,0.),
     &  (3.,285.),(3.,270.),(3.3,270.),(3.,250.),(3.,230.),
     &  (0.,0.),(0.,0.),(0.,0.),(0.,0.),(0.,0.),
     &  (2.,245.),(3.,255.),(3.4,250.),(3.3,230.),(3.4,220.)/

      DATA       ((Mu3(I,J),J=1,10),I=1,9)/
     &  (0.,0.),(1.,170.),(2.2,240.),(3.,240.),(2.9,240.),
     &  (2.4,215.),(2.2,210.),(2.2,230.),(2.5,260.),(2.,290.),
     &  (1.,150.),(1.,170.),(2.4,230.),(3.4,240.),(3.6,235.),
     &  (3.,230.),(2.8,210.),(2.2,240.),(2.5,270.),(2.7,290.),
     &  (1.5,110.),(1.5,130.),(1.9,180.),(3.,220.),(3.6,230.),
     &  (3.2,230.),(2.5,230.),(2.3,270.),(2.6,275.),(2.7,280.),
     &  (3.6,115.),(3.6,120.),(3.,150.),(1.,220.),(3.,230.),
     &  (3.4,235.),(3.,250.),(3.1,270.),(2.8,270.),(2.7,270.),
     &  (4.,100.),(4.2,115.),(4.,120.),(0.,0.),(0.,0.),
     &  (1.,260.),(3.,270.),(3.,280.),(2.8,270.),(2.8,270.),
     &  (1.,120.),(1.1,115.),(1.,110.),(0.,0.),(0.,0.),
     &  (0.,0.),(3.,280.),(3.,280.),(2.6,270.),(2.5,270.),
     &  (1.,130.),(1.,140.),(1.2,120.),(0.,0.),(0.,0.),
     &  (0.,0.),(2.,300.),(2.6,295.),(2.1,280.),(2.2,275.),
     &  (0.,0.),(2.,130.),(1.,110.),(1.,85.),(0.,0.),
     &  (0.,0.),(2.2,295.),(2.2,300.),(1.9,290.),(1.8,270.),
     &  (0.,0.),(0.,0.),(1.,110.),(1.,90.),(1.,60.),
     &  (1.,0.),(1.8,320.),(1.8,300.),(1.3,290.),(0.,0.)/

      DATA      ((Mu4(I,J),J=1,10),I=1,9)/
     &  (1.,120.),(2.5,130.),(2.,150.),(1.7,180.),(1.7,210.),
```

```
&  (1.8,220.),(1.5,220.),(2.5,230.),(2.5,275.),(2.5,300.),
&  (1.5,115.),(3.8,130.),(2.,140.),(1.7,180.),(1.7,210.),
&  (1.8,220.),(1.5,260.),(1.5,270.),(3.,290.),(3.2,300.),
&  (2.,120.),(3.4,120.),(2.4,135.),(2.4,165.),(.5,210.),
&  (1.7,220.),(1.6,270.),(1.6,280.),(3.4,295.),(3.3,300.),
&  (2.,110.),(5.,110.),(2.8,115.),(0.,0.),(0.,0.),
&  (0.,0.),(1.8,300.),(1.8,300.),(3.7,300.),(3.3,300.),
&  (1.,110.),(5.2,100.),(3.,100.),(2.7,90.),(0.,0.),
&  (2.1,320.),(2.1,320.),(3.,320.),(3.6,320.),(3.7,310.),
&  (0.,0.),(1.,100.),(1.3,95.),(2.7,75.),(2.1,60.),
&  (2.1,340.),(2.1,340.),(3.5,330.),(3.6,320.),(3.,320.),
&  (0.,0.),(0.,0.),(1.,80.),(2.8,60.),(2.1,30.),
&  (2.1,0.),(3.3,340.),(3.4,330.),(3.6,330.),(3.,320.),
&  (0.,0.),(0.,0.),(0.,0.),(3.,60.),(3.,40.),
&  (3.,20.),(3.1,340.),(3.4,330.),(2.8,330.),(3.,330.),
&  (0.,0.),(0.,0.),(1.,60.),(2.,40.),(2.7,30.),
&  (3.,20.),(3.,0.),(2.5,340.),(2.7,330.),(0.,0.)/


   DATA      ((Mu5(I,J),J=1,10),I=1,9)/
&  (1.,100.),(1.6,120.),(.8,140.),(.6,180.),(.6,200.),
&  (1.,180.),(1.1,180.),(1.4,190.),(1.2,270.),(1.4,320.),
&  (1.,120.),(2.7,120.),(.7,150.),(.7,150.),(.6,180.),
&  (.7,200.),(1.,160.),(0.,0.),(1.5,320.),(2.3,320.),
&  (3.,110.),(3.2,110.),(.8,120.),(.8,120.),(.6,170.),
&  (0.,0.),(0.,0.),(1.4,330.),(1.7,330.),(2.3,330.),
&  (1.,90.),(3.5,100.),(.9,100.),(.9,90.),(.5,70.),
&  (0.,0.),(0.,0.),(1.4,340.),(2.3,330.),(2.4,330.),
&  (2.5,70.),(4.,90.),(2.5,80.),(.9,60.),(1.,50.),
&  (1.2,30.),(1.4,0.),(2.3,350.),(2.4,340.),(2.5,330.),
&  (0.,0.),(1.,90.),(1.0,80.),(2.1,50.),(2.,40.),
&  (2.,10.),(2.5,40.),(2.5,0.),(2.5,340.),(2.5,320.),
&  (0.,0.),(1.,90.),(1.,50.),(2.5,40.),(2.,30.),
&  (2.5,10.),(3.,10.),(3.,0.),(2.5,0.),(2.4,350.),
&  (0.,0.),(1.,40.),(2.,40.),(3.2,40.),(3.2,20.),
&  (3.2,10.),(3.2,10.),(3.1,10.),(3.1,10.),(2.4,10.),
&  (0.,0.),(0.,0.),(3.,30.),(3.,30.),(3.,30.),
&  (3.,20.),(3.,10.),(3.1,20.),(3.1,20.),(0.,0.)/

   DATA      ((Mu6(I,J),J=1,10),I=1,9)/
&  (0.,0.),(0.,0.),(0.,0.),(0.,0.),(1.1,280.),
&  (1.,270.),(0.,0.),(0.,0.),(0.,0.),(1.,350.),
&  (1.,80.),(0.,0.),(0.,0.),(0.,0.),(2.4,310.),
&  (1.5,330.),(0.,0.),(1.,20.),(1.5,0.),(2.,0.),
&  (1.,70.),(0.,0.),(0.,0.),(0.,0.),(1.1,330.),
&  (1.1,340.),(1.,10.),(1.1,30.),(1.9,0.),(2.3,350.),
&  (1.,70.),(1.5,90.),(0.,0.),(1.6,330.),(1.8,340.),
&  (1.6,350.),(1.4,0.),(1.6,10.),(1.7,0.),(2.,350.),
&  (1.,80.),(1.8,80.),(1.3,30.),(1.5,340.),(1.7,340.),
&  (1.4,340.),(1.,350.),(1.,0.),(1.5,350.),(0.,0.),
&  (1.5,35.),(2.,40.),(2.,25.),(2.6,340.),(1.3,330.),
&  (1.3,330.),(.8,310.),(.9,330.),(0.,0.),(0.,0.),
&  (1.,40.),(1.8,35.),(1.9,25.),(1.5,20.),(.8,340.),
&  (.8,310.),(.8,290.),(.8,280.),(0.,0.),(0.,0.),
&  (0.,0.),(2.,50.),(1.8,40.),(1.5,40.),(1.,30.),
&  (.8,350.),(.6,280.),(.6,270.),(.5,250.),(0.,0.),
&  (0.,0.),(0.,0.),(1.7,50.),(1.7,40.),(1.5,40.),
&  (1.,30.),(.5,0.),(.4,320.),(.4,270.),(0.,0.)/

   DATA      ((Mu7(I,J),J=1,10),I=1,9)/
&  (.5,210.),(1.,220.),(1.2,230.),(2.,280.),(2.,270.),
&  (.8,270.),(0.,0.),(.5,150.),(.5,120.),(.5,120.),
&  (.5,200.),(1.,200.),(1.3,260.),(1.7,270.),(1.7,280.),
&  (1.5,270.),(0.,0.),(0.,0.),(0.,0.),(.6,100.),
&  (0.,0.),(0.,0.),(1.5,280.),(1.5,280.),(1.5,280.),
&  (1.2,270.),(1.,270.),(0.,0.),(0.,0.),(1.,120.),
```

```
&  (1.,60.),(.5,80.),(1.,320.),(1.1,290.),(1.4,270.),
&  (1.3,270.),(1.2,260.),(1.1,250.),(1.,210.),(1.2,160.),
&  (.8,60.),(1.,60.),(.7,30.),(.3,0.),(1.,260.),
&  (1.4,260.),(1.2,250.),(1.1,230.),(1.1,210.),(1.1,180.),
&  (1.,60.),(1.3,50.),(.7,40.),(0.,0.),(0.,0.),
&  (1.,250.),(1.,250.),(1.,230.),(.9,210.),(.9,300.),
&  (1.,60.),(1.7,60.),(1.5,60.),(1.5,60.),(0.,0.),
&  (0.,0.),(1.,260.),(1.,260.),(0.,0.),(0.,0.),
&  (0.,0.),(1.7,60.),(1.5,60.),(1.5,70.),(1.6,70.),
&  (1.,60.),(1.,20.),(0.,0.),(0.,0.),(0.,0.),
&  (0.,0.),(0.,0.),(1.5,60.),(3.,70.),(3.,70.),
&  (2.5,50.),(1.,30.),(.5,10.),(.5,10.),(0.,0.)/

   DATA      ((Mu8(I,J),J=1,10),I=1,9)/
&  (0.,0.),(0.,0.),(0.,0.),(2.4,320.),(2.8,320.),
&  (1.5,330.),(1.1,40.),(1.5,90.),(1.2,100.),(.5,120.),
&  (0.,0.),(0.,0.),(1.,320.),(2.4,320.),(2.8,330.),
&  (1.6,340.),(1.1,30.),(1.5,90.),(1.7,110.),(1.,120.),
&  (0.,0.),(0.,0.),(2.2,320.),(2.4,320.),(2.4,320.),
&  (1.5,310.),(0.,0.),(1.4,120.),(1.8,120.),(2.,130.),
&  (0.,0.),(0.,0.),(2.,310.),(2.2,300.),(2.2,270.),
&  (1.5,260.),(1.5,180.),(2.,170.),(2.4,150.),(2.5,140.),
&  (0.,0.),(0.,0.),(1.4,270.),(2.,260.),(2.,240.),
&  (2.5,220.),(2.7,210.),(2.4,180.),(2.6,170.),(2.7,180.),
&  (0.,0.),(0.,0.),(1.,260.),(2.,230.),(2.5,220.),
&  (2.8,220.),(3.1,210.),(3.1,190.),(1.9,180.),(1.6,180.),
&  (0.,0.),(0.,0.),(0.,0.),(1.,220.),(1.5,210.),
&  (2.,210.),(2.3,200.),(2.3,190.),(2.,190.),(0.,0.),
&  (0.,0.),(0.,0.),(0.,0.),(0.,0.),(1.,180.),(0.,0.),
&                  (0.,0.),(0.,0.),(0.,0.),(0.,0.),
&  (0.,0.),(0.,0.),(0.,0.),(0.,0.),(0.,0.),(0.,0.),
&                  (0.,0.),(0.,0.),(0.,0.),(0.,0.)/

   DATA      ((Mu9(I,J),J=1,10),I=1,9)/
&  (0.,0.),(1.,180.),(1.,190.),(1.,240.),(1.3,270.),
&  (1.3,300.),(0.,0.),(0.,0.),(0.,0.),(0.,0.),
&  (0.,0.),(0.,0.),(0.,0.),(1.5,300.),(1.4,290.),
&  (1.3,300.),(0.,0.),(0.,0.),(0.,0.),(0.,0.),
&  (0.,0.),(0.,0.),(0.,0.),(1.4,300.),(1.5,290.),
&  (1.3,290.),(0.,0.),(0.,0.),(0.,0.),(0.,0.),
&  (0.,0.),(0.,0.),(0.,0.),(1.,300.),(1.2,290.),
&  (1.3,270.),(1.,260.),(0.,0.),(0.,0.),(0.,0.),
&  (0.,0.),(0.,0.),(0.,0.),(1.,290.),(1.1,290.),
&  (1.1,270.),(1.1,250.),(1.,250.),(0.,0.),(0.,0.),
&  (0.,0.),(0.,0.),(0.,0.),(.5,280.),(.8,270.),
&  (1.,250.),(1.,240.),(1.1,230.),(1.2,230.),(1.,240.),
&  (0.,0.),(0.,0.),(0.,0.),(0.,0.),(.5,230.),(1.,240.),
&           (.9,240.),(.8,240.),(1.,240.),(1.2,260.),
&  (0.,0.),(0.,0.),(0.,0.),(0.,0.),(0.,0.),(0.,0.),
&           (.8,270.),(.6,280.),(.6,280.),(1.,270.),
&  (0.,0.),(0.,0.),(0.,0.),(0.,0.),(0.,0.),(0.,0.),
&           (.6,280.),(.6,280.),(.6,280.),(0.,0.)/

   DATA      ((Mu10(I,J),J=1,10),I=1,9)/
&  (0.,0.),(1.,140.),(2.,140.),(1.5,150.),(1.2,210.),
&  (2.,230.),(1.7,230.),(0.,0.),(0.,0.),(0.,0.),
&  (0.,0.),(2.2,140.),(2.3,140.),(1.8,150.),(1.2,210.),
&  (1.2,210.),(1.,280.),(0.,0.),(0.,0.),(0.,0.),
&  (0.,0.),(2.8,140.),(2.8,140.),(2.,160.),(1.2,210.),
&  (1.2,210.),(2.,280.),(2.,290.),(1.8,310.),(1.9,320.),
&  (0.,0.),(3.,130.),(2.4,140.),(2.,160.),(1.2,210.),
&  (1.2,220.),(2.6,260.),(2.8,270.),(2.5,290.),(2.,300.),
&  (0.,0.),(1.,130.),(2.,130.),(1.,150.),(0.,0.),
&  (0.,0.),(2.8,270.),(3.,270.),(3.2,270.),(2.6,270.),
&  (1.,150.),(1.,150.),(1.,130.),(0.,0.),(0.,0.),
&  (0.,0.),(1.5,280.),(2.5,270.),(3.,270.),(2.8,270.),
```

```
&  (1.,160.),(1.,180.),(1.,130.),(0.,0.),(0.,0.),
&  (0.,0.),(1.,310.),(2.,300.),(2.6,280.),(2.8,270.),
&  (0.,0.),(0.,0.),(0.,0.),(0.,0.),(0.,0.),(0.,0.),
&           (1.2,330.),(1.6,320.),(1.8,300.),(2.,280.),
&  (0.,0.),(0.,0.),(0.,0.),(0.,0.),(0.,0.),(1.,350.),
&           (1.4,320.),(1.4,310.),(1.5,310.),(0.,0.)/

   DATA      ((Mul1(I,J),J=1,10),I=1,9)/
&  (0.,0.),(0.,0.),(2.,170.),(3.,200.),(3.,210.),
&  (3.,220.),(3.,220.),(2.8,220.),(1.7,250.),(3.6,310.),
&  (2.,110.),(2.6,120.),(3.,160.),(2.7,180.),(3.1,210.),
&  (2.7,220.),(2.6,230.),(1.7,260.),(2.,300.),(3.6,310.),
&  (3.7,110.),(3.7,110.),(3.6,130.),(0.,0.),(0.,0.),
&  (0.,0.),(2.5,260.),(2.7,280.),(2.7,290.),(3.6,310.),
&  (3.7,100.),(5.,100.),(4.5,120.),(0.,0.),(0.,0.),
&  (0.,0.),(0.,0.),(3.,280.),(3.8,300.),(4.,300.),
&  (1.,100.),(1.,100.),(1.,100.),(3.,90.),(2.,90.),
&  (1.6,320.),(1.6,300.),(3.2,300.),(4.,300.),(4.,300.),
&  (0.,0.),(1.,110.),(1.,100.),(3.5,90.),(2.,60.),
&  (1.6,0.),(2.,320.),(2.5,310.),(3.6,300.),(4.,300.),
&  (0.,0.),(1.,110.),(1.,100.),(1.,80.),(3.,70.),
&  (1.8,30.),(1.8,350.),(2.5,330.),(2.8,300.),(3.2,300.),
&  (0.,0.),(2.8,110.),(3.,100.),(2.8,90.),(2.,70.),
&  (2.,30.),(2.1,350.),(2.1,320.),(2.5,320.),(2.6,300.),
&  (0.,0.),(0.,0.),(1.5,110.),(2.,90.),(1.,70.),(1.,40.),
&           (1.,350.),(1.6,330.),(1.6,310.),(0.,0.)/

   DATA      ((Mul2(I,J),J=1,10),I=1,9)/
&  (0.,0.),(1.5,220.),(2.,230.),(3.5,230.),(4.6,230.),
&  (4.2,230.),(4.2,230.),(4.2,230.),(3.,230.),(3.,270.),
&  (1.,160.),(2.,180.),(3.1,210.),(3.5,220.),(3.5,230.),
&  (4.,230.),(4.2,230.),(4.2,230.),(3.,260.),(2.5,290.),
&  (0.,0.),(1.5,140.),(1.4,160.),(2.,210.),(2.4,210.),
&  (3.,230.),(3.8,240.),(3.8,270.),(3.5,280.),(4.,300.),
&  (0.,0.),(1.4,120.),(1.4,140.),(1.4,180.),(2.,220.),
&  (2.4,240.),(3.,270.),(3.7,280.),(4.1,290.),(4.,300.),
&  (1.,70.),(1.,90.),(1.,90.),(2.,90.),(0.,0.),
&  (2.2,330.),(2.5,320.),(4.,310.),(4.2,310.),(5.,300.),
&  (0.,0.),(1.,90.),(1.,80.),(2.4,50.),(2.2,20.),
&  (2.2,0.),(3.5,340.),(4.,330.),(4.8,320.),(5.,310.),
&  (0.,0.),(0.,0.),(1.,70.),(2.8,50.),(2.2,30.),
&  (3.,350.),(4.,340.),(3.8,340.),(3.7,320.),(3.7,310.),
&  (0.,0.),(0.,0.),(1.,80.),(2.2,50.),(2.2,30.),
&  (2.2,350.),(3.,330.),(3.,330.),(2.2,330.),(2.5,310.),
&  (0.,0.),(0.,0.),(0.,0.),(0.,0.),(0.,0.),(0.,0.),
&           (2.,310.),(3.6,300.),(2.2,270.),(0.,0.)/
```

```
IYEAR= 1000       ! control number of computation time.
coeff1=0.03
COEFF= 0.05       !reduction of Coriolis force due residue force
ID1=   0          ! 0- no cosideration of loose effect. 1- yes
ID2=   1          ! 0- no cosideration of coast effect, 1- yes
PERCO= 0.5        ! for reduction of move. toward coast.
PARCO= 1.0        ! for reduction of move. parallel to coast
ITE=   44100      ! Set random integer for random generation.
```

```
C. This program plot probability contours of ice island
C. trajectories with file RECURRENCY.DAT.
      PROGRAM PROPLOT
      REAL RC(51,56),PA(51,56),LGRC(56,51),CX(2),CY(2),
     &     X2(2),Y2(2),X3(2),Y3(2),X4(2),Y4(2),X5(2),Y5(2),
     &     X1(1),Y1(1)
      COMMON  WORK(10000)       ! necessary for contour plot.
      INTEGER LAND(51,56)
      COMPLEX BOUND1(27),BOUND2(23),BOUND3(7)
      DIMENSION ZARAY(5)
      DATA    LAND/2856*0/
      DATA    ZARAY /0.0,1.,1.7,2.,3./
      OPEN (UNIT=22,FILE='RECURRENCY.DAT',STATUS='OLD')
C-----------------------------------------------------------------------
C. Transform land.data to "land" blocks (land=1).
      INCLUDE '[FTFL.PRO]LAND.DATA'
      LM=0
      DO LN=1,27                  ! BOUND1(27)
         I=INT( AIMAG(BOUND1(LN))/50.)
         J=INT( REAL (BOUND1(LN))/50.)
         IF (I.GT.LM) THEN
            LM=LM+1
            DO LI=LM,I
               DO LJ=1,J
                  LAND(LI,LJ)=1
               ENDDO
            ENDDO
            LM=I
         ENDIF
      ENDDO

      LM=0
      DO LN=1,23              ! BOUND2(23)
         I=INT( AIMAG(BOUND2(LN))/50.)
         J=INT( REAL (BOUND2(LN))/50.)
         IF (J.GT.LM) THEN
            LM=LM+1
            DO LJ=LM,J
               DO LI=I,51
                  LAND(LI,LJ)=1
               ENDDO
            ENDDO
            LM=J
         ENDIF
      ENDDO

      DO LI=36,46
         DO LJ=51,55
            LAND(LI,56)=1
         ENDDO
      ENDDO

      LM=9
      DO LN=1,7                  ! BOUND3(7).
         I=INT( AIMAG(BOUND3(LN))/50.)
         J=INT( REAL (BOUND3(LN))/50.)

         IF (J.GT.LM) THEN
            LM=LM+1
            DO LJ=LM,J
               DO LI=1,I+1
                  LAND(LI,LJ)=1
               ENDDO
            ENDDO
            LM=J
         ENDIF
```

```
      ENDDO

      DO I=1,6
        DO J=6,10
           LAND(I,J)=1
        ENDDO
      ENDDO

C-----------------------------------------------------------------------
      READ (22,*) RC

      DO I=1,51
         DO J=1,56
            IF  (RC(I,J) .LE. 0.)  THEN
               LGRC(J,I)= 1E-10
            ELSE
               LGRC(J,I)= ALOG10 (RC(I,J))
            ENDIF

            IF (LGRC(J,I).GT.3.) LGRC(J,I)=3.3
            IF (LAND(I,J).EQ.1)  LGRC(J,I)=3.3
      IF ((LAND(I,J).EQ.1).AND.(I.LT.8).AND.(J.GT.8))
     &     LGRC(J,I)=0.5
            IF ((J.GE.54).AND.(I.GE.37).AND.(I.LE.43))
     &     LGRC(J,I)=3.3
            IF ((J.GE.51).AND.(I.GE.46)) LGRC(J,I)=3.3

         ENDDO
      ENDDO
C-----------------------------------------------------------------------

      PRINT *,'ENTER PRINT OPTION, 0=COMPRS, 1=PLNTK'
      READ  *,OPTION
      IF (OPTION .EQ. 0) THEN
         CALL COMPRS
      ELSE
         CALL PLNTK
      ENDIF

      CALL NOBRDR
      CALL PAGE (8.5,8.5)
      CALL PHYSOR (.0,0.0)
           CALL BANGLE (123.3)
           CALL BSHIFT (8.75,2.70)
           CALL AREA2D (5.74,5.32)
           CALL GRAF   (.05,500.,2800., 0.05,500.,2550.)

           CALL THKCRV (.015)
           CALL THKRND (0.)

           CALL HEIGHT (0.05)

           CALL BCOMON (10000)
           CALL ZRANGE (-0.3,3.3)
           CALL CONLVS (ZARAY,5,'DATA')
           CALL CONMAK (LGRC,56,51,1.)
           CALL CONLIN (0, 'MYCNLN', 'NOLABELS',3,10)
           CALL CONANG (90.)
           CALL RASPLN (5.)
           CALL CONTUR ( 1,'NOLABELS','DRAW')
           CALL RESET ('BANGLE')
           CALL RESET ('BSHIFT')
           CALL ANGLE (90.)
```

```
      CALL HWSHD
      CALL SWISSL
      CALL CHRPAT(16)
CALL HEIGHT (0.15)
CALL MESSAG ('CONTOURS OF RETURN PERIOD (YEARS)$',100,0.2,2.0)
CALL BANGLE (90.)
CALL RESET('ANGLE')
CALL BSHIFT (8.5,0.)
CALL HEIGHT(0.11)
CALL MESSAG ('E90$',100,5.8,7.8)
CALL MESSAG ('W180$',100,0.2,4.1)
CALL MESSAG ('W90$',100,5.9,0.05)
CALL MESSAG ('N$',100,5.8,4.1)
CALL MESSAG ('1 YEAR$',100,0.2,7.7)
CALL MESSAG ('10 YEARS$',100,0.2,7.4)
CALL MESSAG ('50 YEARS$',100,0.2,7.1)
CALL MESSAG ('100 YEARS$',100,0.2,6.8)
CALL MESSAG ('1000 YEARS$',100,0.2,6.5)

CALL ENDGR(0)
X1(1)=180.
Y1(1)=90.

CALL OREL    (.0,0.,)
      CALL AREA2D (5.74,8.)
      CALL GRAF    (.05,500.,2800., 0.05,500.,3200.)
CX(1)=40.
CX(2)=700.
CY(1)=3050.
CY(2)=3050.
Y2(1)=2930.
Y2(2)=2930.
Y3(1)=2810.
Y3(2)=2810.
Y4(1)=2690.
Y4(2)=2690.
Y5(1)=2570.
Y5(2)=2570.
CALL THKCRV (.01)
CALL THKRND (0.)
CALL RESET ('CHNDSH')
CALL CURVE(CX,CY,2,0)
CALL CHNDOT
CALL CURVE (CX,Y2,2,0)
CALL RESET ('CHNDOT')
CALL DOT
CALL CURVE (CX,Y3,2,0)
CALL RESET ('DOT')
CALL DASH
CALL CURVE (CX,Y4,2,0)
CALL RESET ('DASH')
CALL CHNDSH
CALL CURVE (CX,Y5,2,0)
CALL RESET ('CHNDSH')
CALL RESET ('BANGLE')
CALL RESET ('BSHIFT')
CALL RESET ('THKCRV')
CALL RESET ('THKRND')
CALL ENDGR(0)

CALL PROJCT ('LAMBERT EQ/AREA')
CALL OREL    (.5,0.)
CALL MAPOLE (0.,90.)
CALL AREA2D (8.,8.)
CALL FRAME
CALL THKFRM (.02)
```

```
CALL MAPGR  (90.,90.,270.,65.,25.,100.)
CALL RESET  ('DOT')
CALL RESET  ('DASH')
CALL MAPFIL ('MAPDTA')
CALL LBLANK ('WATER',4000)
CALL DASH
CALL GRID   (1,1)
CALL RESET  ('DASH')
CALL RESET  ('LBLANK')
CALL MARKER (3)
CALL CURVE  (X1,Y1,1,1)

CALL ENDPL(0)
CALL DONEPL
STOP
END

SUBROUTINE MYCNLN(RARAY,IARAY,CHARA)
DIMENSION  RARAY(1),IARAY(4)
CHARACTER*20 CHARA

Z=RARAY(1)
IF(Z.EQ.0.) THEN
CALL RESET ('CHNDOT')
IARAY(3)=1
CHARA='1'
ENDIF

IF (Z.EQ.1.) THEN
CALL RESET ('SOLID')
CALL CHNDOT
IARAY(3)=2
CHARA='10'
ENDIF

IF (Z.EQ.1.7) THEN
CALL RESET ('CHNDSH')
CALL DOT
IARAY(3)=2
CHARA='50'
ENDIF

IF (Z.EQ.2.) THEN
CALL RESET ('DOT')
CALL DASH
IARAY(3)=3
CHARA='100'
ENDIF

IF (Z.EQ.3.) THEN
CALL RESET('DASH')
CALL CHNDSH
IARAY(3)=4
CHARA='1000'
ENDIF
RETURN
END
```